

The applicability of the cellular automata model DUBEVEG on an anthropogenic shore

Thesis

University of Twente
Master Civil Engineering and Management
Water Engineering and Management

20-03-2019

Author: Jan Willem van Dokkum

Student number: s1758470

Supervisors:

Prof.dr. Kathelijne M. Wijnberg

Ir. Daan W. Poppema

Filipe Galiforni Silva, Msc

Abstract

A relatively new type of beach nourishment to combat the hydrodynamical erosion is the mega-nourishment where large amounts of sand are placed in a relatively small area. The pilot project called The Sand Motor is a mega-nourishment of 21 Mm³, which was constructed in 2011 at the coast near Ter Heijde in the Netherlands. The objectives of the Sand Motor mega-nourishment are to maintain coastal safety and nature development.

This research is focused on modelling dune formation pattern development at this out-of-equilibrium anthropogenic shore like the Sand Motor. Gaining knowledge about the dune growth patterns on this type of nourishment may influence decision making for the shape and elevation of future mega-nourishments projects all over the world increasing coastal safety and nature development.

To get understanding which processes are influencing the dune growth at the Sand Motor the cellular model DUBEVEG (DUne BEach VEGetation) is used in this research. Advances of the DUBEVEG model is that complex processes (hydrodynamic erosion, aeolian sediment transport and vegetation development) are partly replaced by stochastic parameters decreasing the computation time significantly compared to computational fluid dynamic (CDF) models. The DUBEVEG is very flexible since many rules in the model can be easily adapted.

The DUBEVEG model has not been applied previously for an out-of-equilibrium anthropogenic shore like the Sand Motor and needs adjustments to model this area. To implement the fast-changing coastline, a reference surface elevation map, measured at the Sand Motor, is used to force the changing coastline by hydrodynamical erosion or deposition. Furthermore, a new method for determining the areas that are sheltered from the hydrodynamics is implemented.

The model is not able to correctly simulate the observed dune formation patterns at the Sand Motor with the standard model settings. The model results show different dune development, aeolian deposition locations and vegetation locations compared to the LIDAR measurements of actual dune development. The model simulates rows of dunes perpendicular to the wind direction while the LIDAR measurements at the coast do not show these dune patterns. The observed vegetation occurs mainly near the foredune and around the lake, while the model simulates vegetation all over the Sand Motor.

A sensitivity analysis is to be performed to get insight into the effect of model parameters on dune development. The parameters used in the sensitivity analysis are the aeolian probability of erosion and deposition ($P_e P_d$), the groundwater depth and the pioneer vegetation expansion rate. The sensitivity analysis for the combined $P_e P_d$ shows that more dunes, but of similar elevation, develop at a higher $P_e P_d$. The effect of $P_e P_d$ for the number of dunes is relatively small compared to the groundwater level. The sensitivity analysis for the groundwater level shows that increasing the groundwater level results in a decrease in the number and elevation of dunes. The effect on dune elevation is relatively small compared to the pioneer vegetation expansion rate. The sensitivity analysis for the pioneer vegetation expansion rate shows that increasing the pioneer vegetation expansion rate results in an increase in the height of the dunes but the locations of these dunes are similar and not influenced.

Furthermore, two model revisions are tested for their influence on the dune development on the Sand Motor. The first model revision is multidirectional wind and the second model revision is beach armouring. In the standard model, unidirectional wind (one aeolian transport direction) is applied. Beach armouring is relevant for this area because large parts of the Sand Motor are elevated above the storm surge level. The lack of hydrodynamic erosion causes the beach armouring to limit the sediment supply available for aeolian erosion.

In the first model revision, including multidirectional wind in the DUBEVEG model (two aeolian transport directions) results in different dune patterns and vegetation that is more spread over the Sand Motor area compared to simulation with the unidirectional wind. The dunes, simulated by the model with the multidirectional wind, are smaller and closer together compared to the model results with the unidirectional wind. The results of the simulation with multidirectional wind are more realistic because the dune patterns are closer to observations than the rows of dunes simulated by the model with the unidirectional wind.

In the second model revision, including beach armouring in the DUBEVEG model decreases the probability for aeolian erosion for armoured cells. In the model, beach armouring occurs only at the high elevated areas of the Sand Motor resulting in fewer dunes to develop on these highly elevated areas with larger distances between the dunes and fewer vegetated cells.

This research shows that it is possible to implement a forced coastline by hydrodynamics, beach armouring and multidirectional wind in the DUBEVEG model, but improvements can be made in future research. The DUBEVEG model in the current form is not applicable for the out-of-equilibrium anthropogenic shores like the Sand Motor because processes are missing. However, Including multidirectional wind (aeolian transport directions) and beach armouring in the model result in a better approach to the observed dunes. Assumed is that improvements in these processes would further increase the approach of the observed dune patterns and increase the applicability of the DUBEVEG model for out-of-equilibrium anthropogenic shores.

Preface

This document is the results of the final project of my study at the University of Twente. During this period I have learnt a lot about dune development and dune modelling. I am thankful for my supervisors that helped me during my thesis. Every time I had a question my supervisors were always there to help me out, which I really appreciated. First of all, I thank Daan, my daily supervisor, for his good feedback and suggestions during all parts and all subjects of this period. I thank Filipe for helping me with the modelling part. My knowledge of modelling and Matlab has enormously increased during this period. I thank Kathelijne for her ideas and feedback that helped me further.

Furthermore, I was happy to be of help during the field experiments Daan and Kathelijne performed on Terschelling and the Sand Motor during this period. It was a really good opportunity to get an understanding of what is behind field work on dune development and to experience the Sand Motor in real instead of only the model.

I like to thank Kelly, my friends, family and all the 'afstudeerkamergenoten' for their support during the thesis.

Table of content

Abstract	2
Preface.....	4
1 Introduction.....	8
1.1 Background.....	8
1.2 Knowledge gap and objective	9
1.3 Research questions.....	10
1.4 Reading guide	10
2 Methodology	11
2.1 Study site	11
2.1.1 Elevation	11
2.1.2 Water levels.....	12
2.1.3 Vegetation	12
2.1.4 Wind data used for the orientation of the model grid.....	12
2.2 Model description	13
2.2.1 The aeolian transport module	13
2.2.2 The hydrodynamic module.....	14
2.2.3 The biotic module.....	15
2.2.4 Adaptations to the model for an out-of-equilibrium anthropogenic shore.....	16
2.3 Model settings.....	18
2.3.1 Model parameters.....	18
2.3.2 Parameter settings	20
2.4 Areas of interest and the quantification of the elevation and vegetation.....	21
2.5 Method for comparing the observed and modelled dune formation patterns.....	22
2.6 Method for determining the dominant model parameters.....	23
2.6.1 Model parameters used in the sensitivity analysis	23
2.6.2 Method for comparing the modelled dune formation patterns for the sensitivity analysis	25
2.7 Method for including the additional model revisions.....	25
2.7.1 Multidirectional wind	25
2.7.2 Beach armouring	26
2.8 Method for comparing the modelled dune formation patterns for the additional physical processes	27
3 Results	28
3.1 Results of the model adapted for an out-of-equilibrium anthropogenic shore	28
3.2 Results of the sensitivity analysis	30

3.2.1	The probability of erosion and deposition	30
3.2.2	The groundwater level	32
3.2.3	The pioneer vegetation expansion rate	34
3.3	Results of including additional model revisions to the model	36
3.3.1	Multidirectional wind	36
3.3.2	Beach armouring	38
4	Discussion	40
4.1	Discussion of the model adapted for an out-of-equilibrium anthropogenic shore	40
4.2	Discussion of the sensitivity analysis	42
4.2.1	The probability of aeolian erosion and deposition	42
4.2.2	The groundwater level	43
4.2.3	The pioneer vegetation expansion rate	45
4.3	Discussion of including additional model revisions to the model	45
4.3.1	Multidirectional wind	45
4.3.2	Beach armouring	47
4.4	General discussion	47
5	Conclusions	49
5.1	The extend that the observed dune formation patterns at an out-of-equilibrium anthropogenic shore like the Sand Motor can be simulated by the model	49
5.2	The dominant parameters explaining modelled dune formation patterns at the Sand Motor	49
5.3	Conclusions of including additional physical processes to the model	50
5.4	The applicability of the DUBEVEG model for out-of-equilibrium anthropogenic shores like the Sand Motor	50
6	Recommendations	51
	References	52
	Appendix A: An extensive description of the calculation steps in the DUBEVEG model	54
A.1.	Aeolian transport module	54
A.2.	Hydrodynamic module	58
A.3.	Biotic module	60
	Appendix B: Elevation plots and stacked bar plots of the adapted probability of erosion and deposition ($P_e P_d$)	62
	Appendix C: Vegetation plots and stacked bar plots of the adapted probability of erosion and deposition ($P_e P_d$)	64
	Appendix D: Elevation plots and stacked bar plots of the adapted groundwater level (GW)	66
	Appendix E: Vegetation plots and stacked bar plots of the adapted groundwater level (GW)	68

Appendix F: Elevation plots and stacked bar plots of the adapted vegetation expansion rates (Veg rate) 70

Appendix G: Vegetation plots and stacked bar plots of adapted vegetation expansion rates (Veg rate) 72

1 Introduction

1.1 Background

The sandy Dutch coastline is moving landwards due to increased hydrodynamical erosion caused by sea level rise endangering the strength of the dunes protecting the low elevated hinterlands (Essink & Bierkens, 2016; Luijendijk et al., 2017). Nearly 9 million people, which are more than half of the Dutch population, live in the hinterlands of this coastal defence (Stive et al., 2013). To stop the structural coastline-moving trend, the Dutch government defined in 1990 the coastline position of 1990 as the reference coastline that should be maintained using sand nourishments (Mulder & Tonnon, 2011; Stive et al., 2013).

Traditional nourishments since the '70s were mostly beach and dune nourishments. Since the '90s shoreface nourishment, sand that is placed underwater around the outer breaker bar was widely used. This type of nourishment is as effective as the beach/dune nourishments, but cheaper and less hindrance for the public. To maintain the coastline location in the 1990 position the Dutch coast need to be nourished with increasing capacity and frequency. Traditional nourishment, both beach/ dune and shoreface, needs to be executed every 2-5 years. A relatively new type of nourishment is the mega-nourishment where very large amounts of sand are placed. Marine and aeolian processes distribute the nourished sand in cross-shore and longshore direction. (Stive et al., 2013)

The pilot project called The Sand Motor is a mega-nourishment of 21 Mm³, which was constructed in 2011 at the coast near Ter Heijde in the Netherlands. This project consists of the main part, the peninsula-shaped extension of the beach, and two flanking shoreface nourishments (De Schipper et al., 2016). This type of nourishment is large enough to give at least sufficient coastal reinforcements for the coming 20 years (Stive et al., 2013).

The objectives of the Sand Motor mega-nourishment are to maintain long term coastal safety and nature development (Mulder & Tonnon, 2011). Long term coastal safety is obtained by the hydrodynamical distribution of sand by longshore transport to feed a large stretch of the neighbouring beach (Arriaga, Rutten, Ribas, Falqués, & Ruessink, 2017) in a more natural way than more frequently smaller nourishments (Tonnon, Huisman, Stam, & van Rijn, 2018).

Before construction, estimates of dune development on the Sand Motor were performed by an empirical relation between beach width and dune foot migration (Mulder & Tonnon, 2011). An increase in dunes enhances coastal safety against flooding (Mulder & Tonnon, 2011). Understanding more about the dune formation patterns at the Sand Motor mega-nourishment and the neighbouring stretches is important for multiple reasons. First, the Sand Motor is a nourishment that is never executed before and knowledge of dune growth on the Sand Motor, except the estimations by the empirical relation between beach width and dune foot migration, is unknown (Puijenbroek, 2017). Second, gaining knowledge about the dune growth patterns on this type of nourishment may influence decision making for the shape and elevation of future mega-nourishments projects all over the world increasing coastal safety and nature development.

Currently, there are no dune simulation models assessed or adapted for anthropogenic shores like the Sand Motor. This research is focussed on the applicability of a cellular automata model for this type of coastline.

1.2 Knowledge gap and objective

The Sand Motor is different compared to normal coasts as shown in Figure 1. The coastline is out of equilibrium and the longshore spatially different hydrodynamical erosion and deposition will bring back the coast to its equilibrium profile over time; a straight coastline. The longshore spatially different hydrodynamical erosion and deposition cause the nourished coastline to change very fast compared to normal coastlines.



Figure 1, a picture of the Sand Motor after completion (September 2011) (Stive et al., 2013)

Large parts of the Sand Motor are elevated above the maximum water level and are not influenced by hydrodynamic processes. Hydrodynamic processes influence vegetation distribution and sediment availability for aeolian transport. The lack of waves and currents result in reduced transport of vegetation (seeds and rhizomes) compared to normal coasts (Hoonhout & de Vries, 2017b). In this area, seeds and rhizomes can only be transported by wind. Furthermore, waves and current do not wash away large particles like shells and cobbles. Smaller particles are sheltered below the beach armoring of shells and cobbles which limits the available sediment for aeolian transport (Hoonhout & de Vries, 2017b).

On the Sand Motor, the dune growth for the first five years is less than expected (Zandmotor, 2016). There is little dune growth on the Sand Motor itself but the foredune is actively growing with rates that are normal for nourished Dutch coasts (Nolet, van Puijenbroek, Suomalainen, Limpens, & Riksen, 2017).

To get an understanding of which processes are influencing the dune growth at the Sand Motor the cellular model DUBEVEG (DUne BEach VEGetation) is used in this research. The model is developed by the Wageningen University to gain an understanding of ecological valuable swales (dune valleys). The model uses aeolian sand transport, hydrodynamic and biotic processes to update the beach-dune area in a probabilistic rule-based approach (Silva, Wijnberg, de Groot, & Hulscher, 2017).

The DUBEVEG is largely based on the DECAL algorithm used by Nield and Baas (2008) for exploring relationships between ecological and morphological processes (Nield & Baas, 2008). Keijsers, De Groot, and Riksen (2016) used the DUBEVEG model to study the effects of climate change on coastal dune development on the Dutch islands Terschelling and Ameland. Furthermore, the DUBEVEG model is used by Silva et al. (2017) and Silva, Wijnberg, de Groot, and Hulscher (2018) to simulate coastal dunes on sandflats close to inlets.

The DUBEVEG model is not used before for an out-of-equilibrium anthropogenic shore like the Sand Motor. It is unknown how the model performs on this type of shores. Processes related to out-of-equilibrium anthropogenic shores might be missing and need to be implemented in the model.

The objective of this research is:

‘To assess and improve the applicability of the DUBEVEG model for an out-of-equilibrium anthropogenic shore’

1.3 Research questions

Three research questions are formed to guide the study towards the objective:

1. To what extent can the observed dune formation patterns at an out-of-equilibrium anthropogenic shore like the Sand Motor be simulated by the DUBEVEG model?
2. What are the dominant parameters explaining modelled dune formation patterns at the Sand Motor?
3. How can including additional model revisions improve the model applicability for the Sand Motor?

1.4 Reading guide

The research methodology is written in chapter 2 and includes information about the study site, the model description, model settings and the methods for answering the three research questions. Chapter 3 includes the results for the model adapted for an out-of-equilibrium anthropogenic shore, results of the sensitivity analysis and the results of including additional model revisions to the model. The discussion is written in chapter 4 and the conclusions in chapter 5. The recommendations for further research are written in chapter 6. Furthermore, Appendix A includes an extensive model description and appendix B - G consist of model results of the sensitivity analysis.

2 Methodology

This chapter includes the description of the study site, the model description, the model settings and the areas of interest and the quantification of the elevation and vegetation. Furthermore, the method for comparing the observed and modelled dune formation patterns, the method for determining the dominant model parameters and the method for including the additional model revisions are described in this chapter.

2.1 Study site

Multiple types of data from the Sand Motor area are needed to model dune development. The data that is needed is the elevation data, the water levels, the locations of the initial vegetation and the wind data.

2.1.1 Elevation

There are two types of elevation data used in this research, namely LIDAR data acquired from Rijkswaterstaat (2016) and elevation data obtained by combined jetski, quad and walking measurements acquired from Shoremonitoring (2017). LIDAR is a surveying method that measures the reflection time of a send laser light on a surface (Oceanservice, 2013). There are no LIDAR measurements below the mean sea level (MSL). The first LIDAR image (2m grid resolution) is interpolated and used as the initial elevation profile for the model and the final LIDAR image (1m grid resolution) is interpolated and used to compare dune development with the model outcomes. The used grid size for the model in this research is 1.25m (described in chapter 2.3.1). The LIDAR map for the initial profile (2m grid resolution) is the highest resolution map available. The final LIDAR map (1m grid resolution) is detailed enough to compare observed dune development and the model results. More detailed LIDAR maps, which are available for the final situation, do not increase accuracy because the model grid is 1.25 by 1.25m.

For the Sand Motor area, the reference surface consists of elevation data gathered once or twice every two months by combined jet ski, quad and walking measurements. This data is more frequently measured than LIDAR data (once a year) and has elevation values under water. The elevation data obtained by combined jet ski, quad and walking (Figure 2) is interpolated and used to (I) give a bathymetry to the initial elevation profile and (II) to make the reference surface, which is described in chapter 2.2.

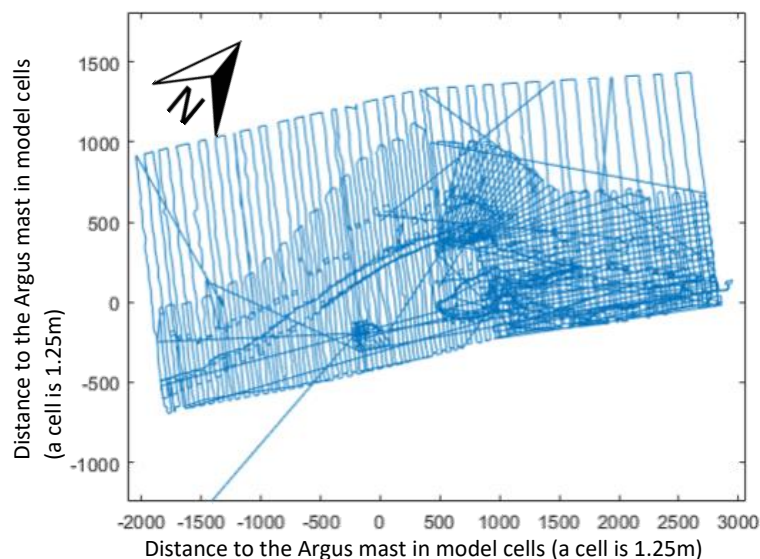


Figure 2, an example of a measuring pattern for obtaining elevation data by combined jet ski, quad and walking. The axis are the number of cells (1.25 by 1.25m) measured from the Argus mast (measuring station at the Sand Motor) at location 0.0.

2.1.2 Water levels

The maximum observed water level of two weeks (spring-neap cycle) is used by the model to inundate the low lying area of the beach which may cause hydrodynamic erosion or deposition. The maximum water levels every two weeks are obtained from measurements in Scheveningen which is close by the Sand Motor area (approximately eight kilometre north).

2.1.3 Vegetation

At the start of the model simulations, the Sand Motor is bare and the foredunes are assumed to be covered with vegetation. Google satellite images show that the area landwards of the foredune is almost fully vegetated. At the moment it is not possible to include hard structures in the DUBEVEG model. The buildings and roads behind the dunes are assumed not to be there and instead, that area is modelled fully vegetated.

2.1.4 Wind data used for the orientation of the model grid

Observed wind measurements were obtained at the closest measuring location (Hoek van Holland) and started after the Sand Motor was built in 2011 and ended in 2017 at the end of the model time. The wind direction (average of the last 10 minutes of each hour) and the wind speed (in m/s) of each hour are considered.

In the DUBEVEG model, sand slab transport can only occur towards neighbouring cells and not diagonal or in a different angle than 0, 90, 180, 270 degrees. In the field, the observed wind direction and sand transport change over time, but there is an average transport direction. The most reasonable direction for slab transport in the model is the average observed wind direction of the period of multiple years. The grid needs to be orientated so that an above-mentioned angle of 0, 90, 180 or 270 degrees is reached.

Based on observed wind directions of wind speeds where aeolian transport is possible, the slab transport direction in the model is assumed 230 degrees. The wind speed threshold for aeolian transport on the Dutch coast is around 7 m/s (Puijenbroek, 2017). Therefore, only wind directions for wind speed larger than 6, 7, 8 or 9 m/s are shown in Figure 3 (left). The orientation of the model grid is conform the blue line in Figure 3 (right).

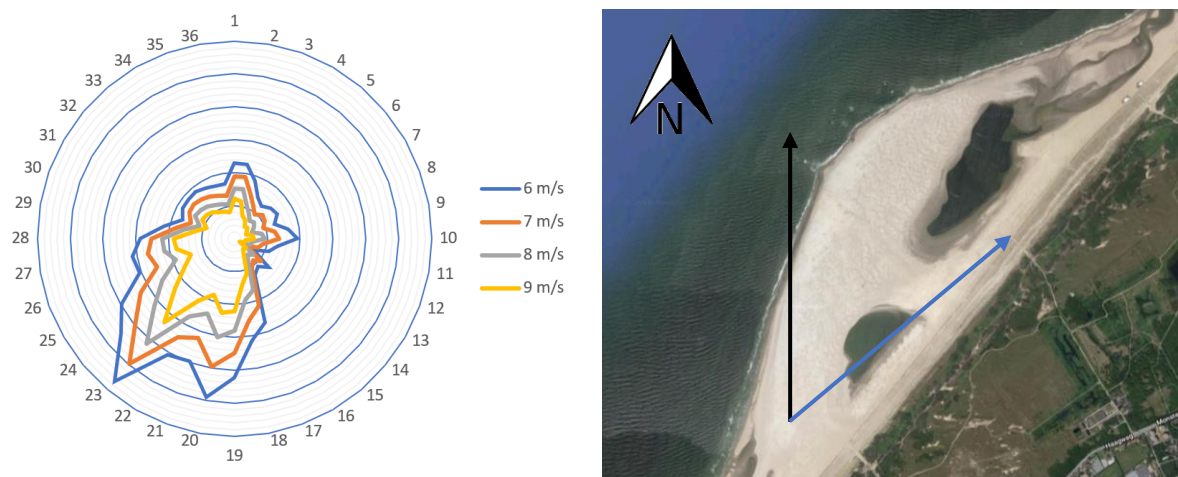


Figure 3, (left) wind directions for wind speed larger than 6, 7, 8 and 9 m/s. Measuring location Hoek van Holland. Timespan 02-2011 until 05-2017. Units are in degrees divided by 10. (right) Map of the sand motor including (I) a black arrow which shows the North and (II) a blue arrow which shows the orientation of the grid (230 degrees) based on the average wind direction for winds speeds of 6 m/s and stronger.

2.2 Model description

The DUBEVEG model is a cellular automata model developed by the Wageningen University to gain an understanding of ecological valuable swales (dune valleys) and is assessed in this research for the applicability for out-of-equilibrium anthropogenic shores. The model uses aeolian sand transport, hydrodynamic and biotic processes to update the beach-dune area in a probabilistic rule-based approach (Silva et al., 2017). The model outline is displayed in Figure 4 and consists of an aeolian transport module, a hydrodynamic module and a biotic module. Appendix A presents an extensive model description of the calculation steps. In this subchapter, the aeolian, hydrodynamic and biotic modules are described followed by the adaptations needed for modelling an out-of-equilibrium anthropogenic shore like the Sand Motor.

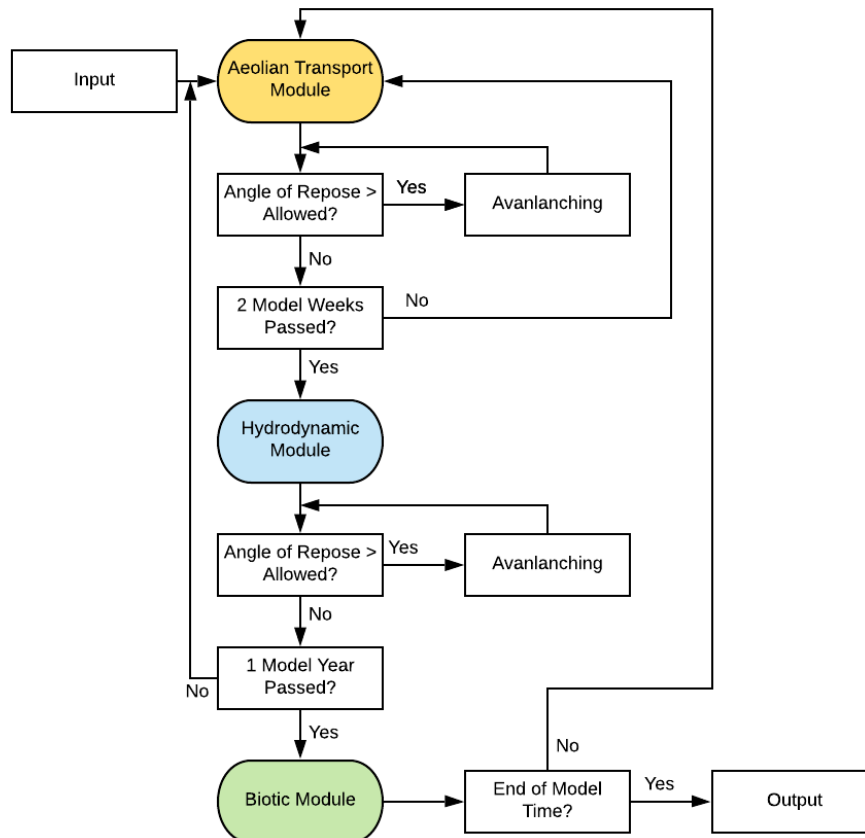


Figure 4, the DUBEVEG model outline.

2.2.1 The aeolian transport module

The wind is the forcing factor that initiates the sand particles to move when a certain threshold is exceeded (Du Pont, 2015; Puijtenbroek, 2017). The model mimics all wind effects causing aeolian transport with a probability of aeolian erosion. Individual blocks of sand (slabs) are picked up stochastically with chance p_e (probability of aeolian erosion), move downwind with a slab jump length (J) of 1 and are stochastically deposited with chance p_d (probability of deposition) or move further downwind with chance $1-p_d$ (Keijsers et al., 2016) as shown in Figure 5. During an iteration, the wind direction is constant.

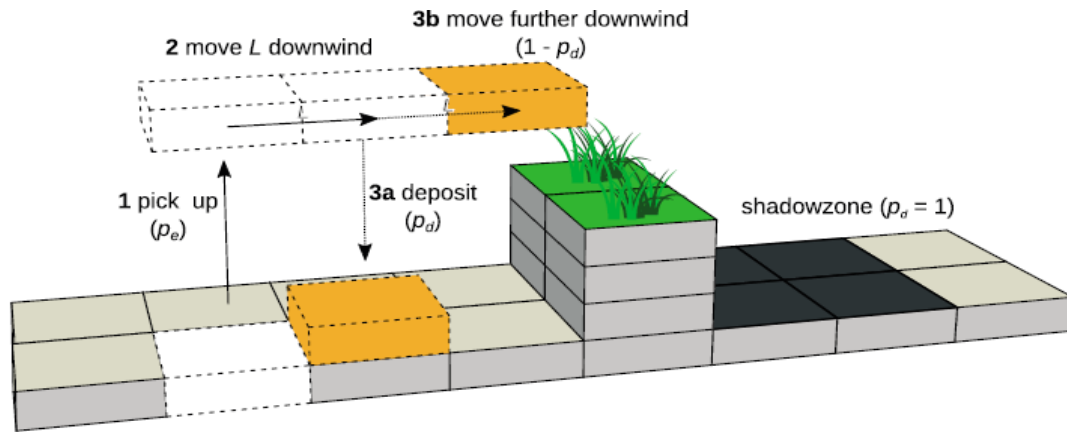


Figure 5, a schematic representation of the DUBEVEG-model (Keijsers et al., 2016). A slab of sand is picked up with chance p_e (1) and is moved in the direction of the wind (2) and is deposited with chance p_d (3a) or moves further downwind with chance $1 - p_d$ (3b).

Aeolian erosion and deposition probabilities are influenced by the vegetation grade, the shadow zones, the groundwater level and the mean sea level (MSL). Aeolian erosion cannot take place when at least a certain vegetation grade (C_{lim}) is present in a cell (Keijsers et al., 2016). A denser vegetated area increases the probability of aeolian deposition. Next to vegetation, the aeolian probability of erosion and deposition is influenced by shadow zones. Shadow zones occur when multiple neighbouring cells in the direction of the wind have a larger difference in elevation than the threshold (β_s) as shown in Figure 5. Cells in the shadow zone have a probability of aeolian erosion of 0 and a probability of aeolian deposition of 1. Furthermore, the aeolian probability of erosion is 0 below the groundwater level and the MSL.

The model includes an avalanching module. When the angles between neighbouring or diagonal cells are equal or larger than the angle of repose, slabs are transported from the high elevated cell to the lowest neighbouring or diagonal cell. In case of multiple equal lowest elevated neighbouring or diagonal cells, one cell is arbitrarily chosen. The angle of repose for bare cells (θ_b) is smaller than the angle of repose for vegetated cells (θ_v) allowing steeper slopes for vegetated cells (Keijsers et al., 2016). The stability of the sand is increased by the vegetation. Cells with a vegetation grade smaller than the threshold (T_{veg}) are calculated with the angle of repose for bare cells and cells with a vegetation grade equal or larger than the threshold are calculated with the angle of repose for vegetated cells. In the model, the avalanching takes place after the aeolian transport module and after the hydrodynamic model.

2.2.2 The hydrodynamic module

The hydrodynamic module covers the marine processes and represents the forcing of the sea in the beach-dune system. Roughly every two model weeks the module is called which is approximately after a full neap-spring cycle (Keijsers et al., 2016). The number of hydrodynamic iterations each model year (n_{hydro}) is 25.

For calculating the maximum water level in the model, the highest water level recorded the period of two weeks is used (Keijsers et al., 2016) combined with the empirical formula for wave runup of Stockdon, Holman, Howd, and Sallenger Jr (2006). The maximum water level is used in the model to determine which cells are inundated.

The hydrodynamic erosion of cells is stochastic and only inundated cells can erode by hydrodynamics (Silva et al., 2017). The DUBEVEG model includes wave dissipation as a function of the water depth (Silva et al., 2017) reducing the hydrodynamical erosion probability of cells in shallow water. The

maximum erosive strength of waves (h_{max}) is 1. Lower elevated areas behind cells with an elevation higher than the maximum water level are sheltered from the hydrodynamic forces, which reduces the probability of hydrodynamic erosion to zero (Silva et al., 2017).

Cells that are not sheltered and erode hydrodynamically are brought back to the reference surface which is defined beforehand (Silva et al., 2017). The reference surface is an elevation map used to give hydrodynamically eroded cells a new elevation. This can be an increase in elevation, which mimics sediment input from the sea, or a decrease in elevation, which is hydrodynamic erosion. Marine processes can reduce or completely remove vegetation (Keijsers et al., 2016).

Furthermore, the reference surface is used to determine the groundwater depth (G). The groundwater depth is a unitless value which indicates the groundwater level which is a portion between the MSL and the reference surface. The minimum groundwater level (0) is equal to MSL and the maximum groundwater level (1) is equal to the reference surface. The unitless value of 0.8 is assumed the standard groundwater depth conform to Keijsers et al. (2016). In the sensitivity analysis of this research, the groundwater depth is increased (0.9 and 0.95) and decreased (0.6 and 0.7) and the effect on dune development is compared with the dune development of the standard groundwater depth.

2.2.3 The biotic module

The biotic module includes the vegetation processes in the model. The vegetation grade in a cell is a dimensionless number between 0 (no vegetation) and 1 (fully vegetated). The number of biotic iterations per model year (n_{biotic}) is 1 (Keijsers et al., 2016).

Two vegetation species are in the model, namely a pioneer species and a stabilizer species. The pioneer species has an optimal growth when the plant is buried for a certain extent, while extreme burial or erosion causes mortality (Hesp, 1989; Keijsers et al., 2016). The stabilizer species have optimal growth when there is no sedimentation. This plant can survive with little erosion, but extreme erosion or sedimentation cause mortality (Keijsers et al., 2016). The growth curves of both vegetation species are shown in

Figure 6. The values of the vertices of the pioneer species ($a_{pioneer} - e_{pioneer}$) and the stabilizer species ($a_{stabilizer} - e_{stabilizer}$) are included in Table 1. The optimal growth for species 1 ($peak_{pioneer}$) is 0.2 and the optimal growth for species 2 ($peak_{stabilizer}$) is 0.05 (Keijsers et al., 2016).

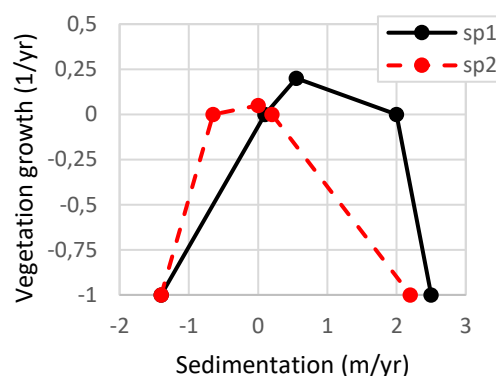


Figure 6, growth function to burial or erosion for the pioneer species (sp1) and the stabilizer species (sp2).

Vegetation expands by pioneer and lateral growth. Bare cells can become vegetated with pioneer species by pioneer expansion. Pioneer expansion is vegetation that starts to grow with equal probability on any unvegetated cell on the map. New stabilizer vegetation can only establish on cells with already pioneer species vegetation on it. The probability of pioneer expansion ($p_{establish}$) is 0.05.

Furthermore, both species can establish in neighbouring bare cells by lateral expansion (Keijsers et al., 2016). The probability of lateral expansion (p_{lateral}) is 0.2 (Keijsers et al., 2016). Due to the vegetation establishment, the stability of the sand increases which allows steeper slopes (Keijsers et al., 2016).

2.2.4 Adaptations to the model for an out-of-equilibrium anthropogenic shore

The Sand Motor area is not a straight coastline and has processes that do not occur on normal beaches like a fast-changing coastline. The DUBEVEG model is developed for straight coastlines (Silva et al., 2017) and needs adaptations to model out-of-equilibrium anthropogenic shores like the Sand Motor.

The reference surface used for the hydrodynamical erosion and the groundwater level has different requirements for the Sand Motor area compared to the straight coastline used in Keijsers et al. (2016) or the Hors area used in Silva et al. (2017). Keijsers et al. (2016) used a plane as a reference surface that crosses the initial beach profile. This profile was moved landwards and upwards over the model years to mimic sea level rise. Silva et al. (2017) used the initial elevation map as a reference surface. The coastline of Silva et al. (2017) did barely change, resulting in no need for more than one reference surface. The Sand Motor area has a fast-changing coastline and multiple reference surfaces are needed to force the coastline in the model to change similarly to the observed coastline. To smoothly change the forced deformation of the coastline in the model, each hydrodynamic model run has an updated reference surface conform to the observed coastline.

Hydrodynamic erosion forces the eroded cells to the elevation of the reference surface and therefore the reference surface should have no dunes. The initial elevation map Silva et al. (2017) used as a reference surface which was smoothed with a Gaussian low-pass filter to erase the dunes. Similar to Silva et al. (2017), all reference surfaces used for the Sand Motor area are smoothed with a Gaussian low-pass filter. The foredunes and the dune field behind the foredune on the Sand Motor's reference surface are too large to level with the Gaussian low-pass filter and are levelled by a constant elevation value characterising the surrounding area (Figure 7).

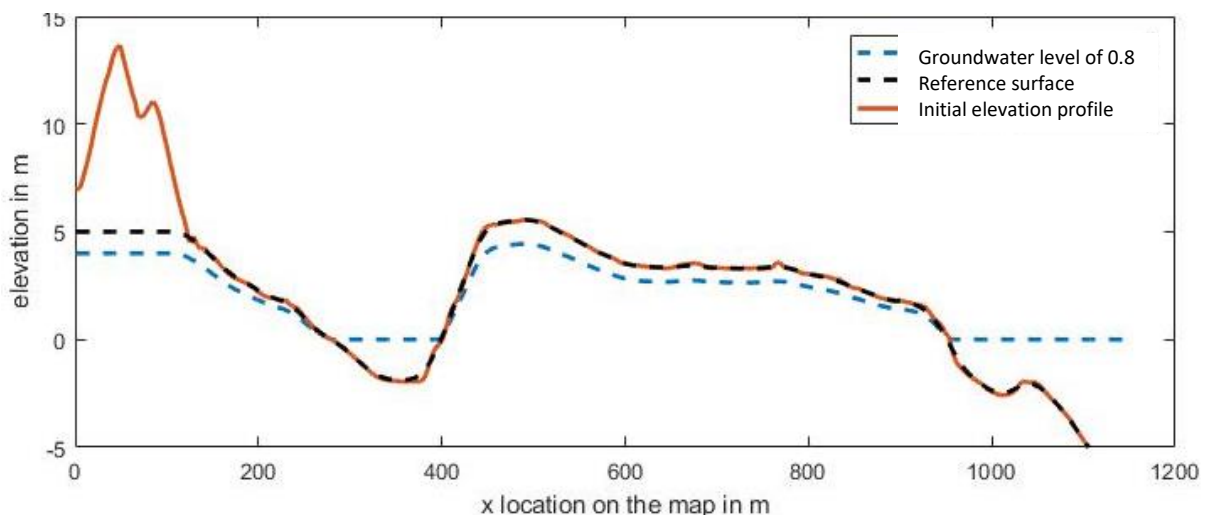


Figure 7, Cross section of the Sand Motor including the groundwater level, the reference surface and the initial elevation profile.

The method to determine model cells that are sheltered from the hydrodynamic forces used in the previous DUBEVEG model by Keijsers et al. (2016) cannot be used for out-of-equilibrium anthropogenic shores like the Sand Motor. Keijsers et al. (2016) searched each row of cells in the model (in the direction seaward to landward) for the first cell which has a higher elevation than the maximum water level. All cells landwards of this first cell with a higher elevation than the maximum water level were sheltered. This approach is correct for straight coastlines but does not work for the Sand Motor area

because of the lagoon. Using this approach, the lagoon area is sheltered because there is in certain rows of cells a more seaward located cell with a higher elevation than the maximum water level (Figure 8, left). The lagoon area is subject to hydrodynamic forces and should not be sheltered.

A new approach to determine which model cells are sheltered is applied in the DUBEVEG model, shown in a flowchart in Figure 9. The first logical question is if the area (or cell) is higher elevated than the maximum water level. A positive answer leads always to a sheltered area for hydrodynamic forces as shown in Figure 8 middle. A negative answer leads to the question if the cell is in direct connection to the sea. In other words, can seawater flow to this cell? A positive answer leads to an exposed cell because hydrodynamic forces can reach this cell. A negative answer means that the area is sheltered even the fact that the area is below the maximum water level as shown in Figure 8 right.

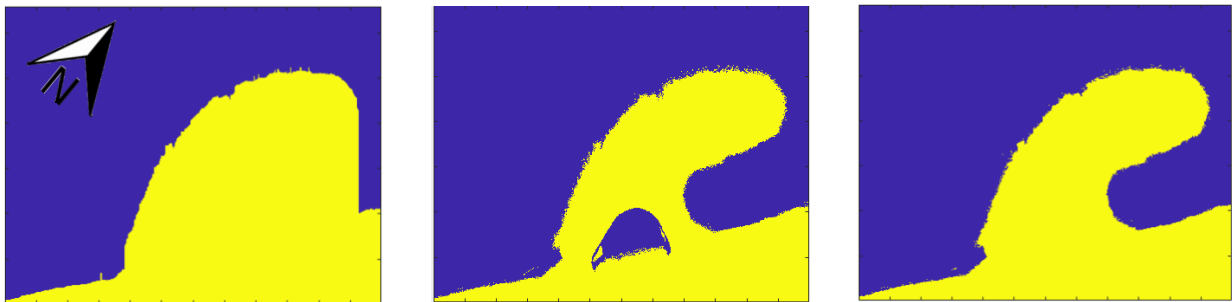


Figure 8, original sheltering method (left), elevation of land higher than the maximum water level (middle) and the sheltered area (right). The yellow area is sheltered from hydrodynamic forces and the blue area is exposed to hydrodynamic forces.

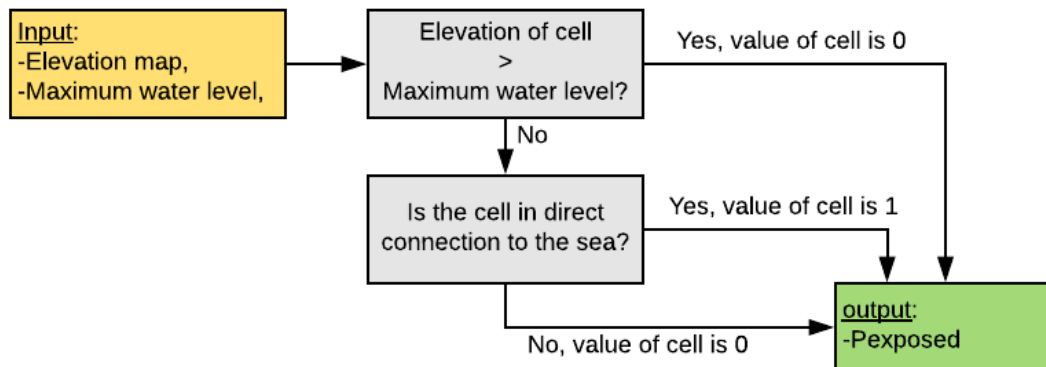


Figure 9, a flowchart of how the model determines the exposed/ sheltered map. Value 0 means sheltered and value 1 means not sheltered.

The calculation method for the dissipation in previous versions of the DUBEVEG model is not suitable for the Sand Motor area and needs to be adapted. In the previous DUBEVEG model, the dissipation was calculated with a similar method as the sheltering of cells by hydrodynamic forces, namely by rows of cells in the direction offshore to landwards. The total dissipation in a cell is the total dissipation in the previous (offshore) cell plus the dissipation in the current cell. It was assumed that the main wind direction is in a cross-shore direction to the beach. In the case of the Sand Motor, the main wind direction is not cross-shore to the beach but almost align with the beach. The total dissipation cannot be calculated with this method which results in unrealistic dissipation values. In the case of the Sand Motor, it is assumed that the dissipation is calculated by the rows of cells perpendicular to the average wind direction in the direction offshore to landwards (in other words, from the top to the bottom of Figure 10). This method for calculating the dissipation is used because the direction of the waves influenced by diffraction is now better approached.

Due to very shallow water depths near de beaches and in the lagoon the dissipation strength is very high resulting in zero hydrodynamic erosion chance in these areas (Figure 10, left) which is not correct. Hydrodynamic erosion or deposition does happen in these areas because the topography is changing over time caused by hydrodynamic forces. To adapt the model a minimum erosive strength of waves ($P_{\text{wave_min}}$) is added for areas that (I) have a smaller probability of erosion due to waves than the $P_{\text{wave_min}}$ and (II) have a lower elevation than the maximum water level and (III) are not sheltered. The $P_{\text{wave_min}}$ value has overwritten the probability of erosion due to waves in the areas near the beach and the lagoon (Figure 10, **Fout! Verwijzingsbron niet gevonden.** right). Hydrodynamic erosion is now possible in these areas. This method to determine the hydrodynamic erosion probability results in a strong increase in dissipation values for the most offshore parts of the Sand Motor (where the slope of the beach is steep), a more graduate increase for the beaches near the sand Motor (with a less steep slope) and a lagoon with constant dissipation values (Figure 10, right).

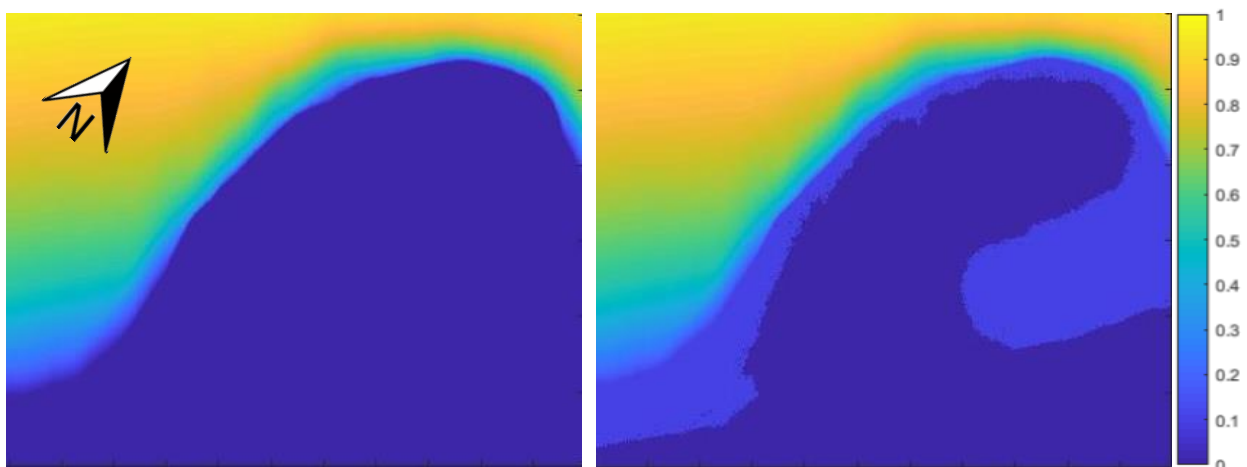


Figure 10, the probability of hydrodynamic erosion due to waves without $P_{\text{wave_min}}$ (left) and with $P_{\text{wave_min}}$ (right). The value 1 means always erodes, the value 0.2 is the minimum hydrodynamic erosion probability for areas under the maximal water level (excluding the lake) and the value 0 means no hydrodynamic erosion possible.

2.3 Model settings

This subchapter describes the remaining parameters used in the model.

2.3.1 Model parameters

The Sand Motor has been built in 2011 and the latest available elevation data is from 2017 resulting in a model time (N) of 6 years. This model time is relatively short compared to Nield and Baas (2008) with at least multiple model decades, Keijsers et al. (2016) with at least 10 model years and Silva et al. (2017, 2018) with 15 model years. However, 6 years should be enough to witness embryo dune development.

The sand slab represents the aeolian sand transport in the model and is used to change the elevation in the landscape. The slab has an aeolian erosion and deposition probability influenced by vegetation or shadow zones. This probability replaces the complex interacting forces of wind, sediment and water (Silva et al., 2018). The accretion of multiple slabs in the same area will result in new dunes or increase the height of existing dunes.

The annual observed aeolian transport needs to be equal to the aeolian transport in the model, which depends on the slab height (h_s), the cell size (L), the probability of aeolian erosion (p_e) and deposition (p_d) and the number of aeolian iterations each model year (n_{aeolian}). Equation 1 of Nield and Baas (2008) is used.

$$Q = h_s * L * \left(\frac{P_e}{P_d}\right) * n_{aeolian} \quad [1]$$

The observed annual aeolian transport (Q) is 20 m³/m/yr (Puijenbroek, 2017). In the model, this value is applied for the complete area and during all model years.

The cell size and slab height must meet certain requirements. Small grid sizes (<1m) result in a fundamental change in the dynamics of the vegetation growth and individual vegetation elements resulting in different unexpected landforms (Nield & Baas, 2008). Increasing the cell size decreases the resolution of the grid and sediment-covered cells in a 5 or 10m grid are isolated from each other having a dune on a single grid cell (Nield & Baas, 2008). Furthermore, Realistic ranges for slab heights divided by the cell size are between 1/7.5 and 1/13 (Nield & Baas, 2008).

The probability of aeolian erosion and deposition are assumed 0.5 and 0.1 conform to Silva et al. (2018) and Keijsers et al. (2016). In the sensitivity analysis in this research, the effect of increasing (125%) and decreasing (25%, 50%, 75%) both the aeolian erosion and deposition probability is compared to the standard parameter settings of aeolian erosion and deposition of 0.5 and 0.1.

The preferred model parameter values for the slab height, cells size and amount of aeolian iterations must fulfil the requirements of Nield and Baas (2008) and should not result in a major increase in calculation time. The Sand Motor is a very large area and a decrease in cell size and an increase in the number of aeolian iterations results in a major increase in computation time. The amount of aeolian transport iterations in the model is assumed 25 per model year and the cell size is estimated at 1.25 m conform to the standard grid of Nield and Baas (2008). Decreasing the number of aeolian iterations to the minimum of 25, which is similar to the number of hydrodynamic iterations, reduces the calculation time considerably. A model run with a cell size of 1.25m instead of 1m reduces the number of cells and the calculation time. The cells size is larger and the amount of aeolian iterations is smaller than used in Keijsers et al. (2016) and Silva et al. (2017) but result in a realistic slab height conform equation 1. Keijsers et al. (2016) and Silva et al. (2017) used both a cell size of 1m and 52 and 50 aeolian iterations per year respectively. In the model, the slab height is 0.128m, calculated with equation 1, and is in the realistic range of Nield and Baas (2008).

2.3.2 Parameter settings

The parameters used in the model are listed in Table 1. Values that are based on Keijsers et al. (2016) have a '*' in the reference column of Table 1.

Table 1, Model parameters of the DUBEVEG model of the Sand Motor area

Symbol	Parameter	Value	Units	Reference
<i>General model parameters</i>				
N	Model years	6	year	-
L	Cell size	1.25	m	Equation 1
h_s	Slab height or thickness	0.128	m	Equation 1
<i>Aeolian model parameters</i>				
$n_{aeolian}$	Aeolian transport iterations	25	year ⁻¹	Equation 1
Q	Annual aeolian transport	20	m ³ /m/yr	Puijenbroek (2017)
p_d	Aeolian deposition probability	0.1	-	*
p_e	Aeolian erosion probability of a cell without vegetation	0.5	-	*
β_s	Shadow angle	15	°	Baas (2002)
Θ_b	Angle of repose of a bare cell	20	°	*
Θ_v	Angle of repose of a vegetated cell	30	°	*
T_{veg}	Vegetation threshold for repose vegetated cells	0.3	-	*
J	Slab jump length	1	cell	Nield and Baas (2008)
<i>Hydrodynamic model parameters</i>				
n_{hydro}	Hydrodynamic iterations	25	year ⁻¹	*
G	Groundwater depth below the reference surface	0.8	-	*
$P_{wave-min}$	Minimum erosive strength of waves	0.2	-	*
h_{max}	Maximum erosive strength of waves	1	-	*
<i>Biotic model parameters</i>				
n_{biotic}	Biotic iterations	1	year ⁻¹	*
C_{lim}	Minimum value of vegetation that completely prevents aeolian erosion	0.5	-	*
$a_{pioneer}$ – $e_{pioneer}$	Vegetation parameters (vertices locations on the x-axis on the growth curves) for species 1	-1.4, 0.1, 0.55, 2, 2.5	-	*
$a_{stabilizer}$ – $e_{stabilizer}$	Vegetation parameters (vertices locations on the x-axis on the growth curves) for species 2	-1.4, -0.65, 0, 0.2, 2.2	-	*
$peak_{pioneer}$	Optimal growth species 1	0.2	year ⁻¹	*
$peak_{stabilizer}$	Optimal growth species 2	0.05	year ⁻¹	*
$p_{lateral}$	Probability of lateral expansion	0.2	-	*
$p_{establish}$	Probability of pioneer expansion	0.05	-	*

2.4 Areas of interest and the quantification of the elevation and vegetation

To quantify the model outcomes for elevation and vegetation, multiple areas of interest are chosen that are representing the different areas of the Sand Motor. Interesting areas for this study are the areas of the Sand Motor where dunes develop, which includes the higher elevated part, the lake, the old beach and the foredune. Areas which are mainly shaped by the hydrodynamic forces are not of interest in this study because no dunes do develop here. These areas are the edges of the Sand Motor, the lagoon and the accreted areas in front of the old beaches on both sides. Furthermore, the dunes behind the foredune are not of interest in this study. The area of interest stops in the south at the location where the Sand Motor starts and in the North around half the lagoon.

The Sand Motor area is classified in nine areas of 150 · 250 m or 24000 cells in the model which represent the Sand Motor his different areas (Figure 11). The classified areas are large enough for multiple dune rows to emerge which reduces the chance that the area contains only one dune or is located between dunes, influencing the results.

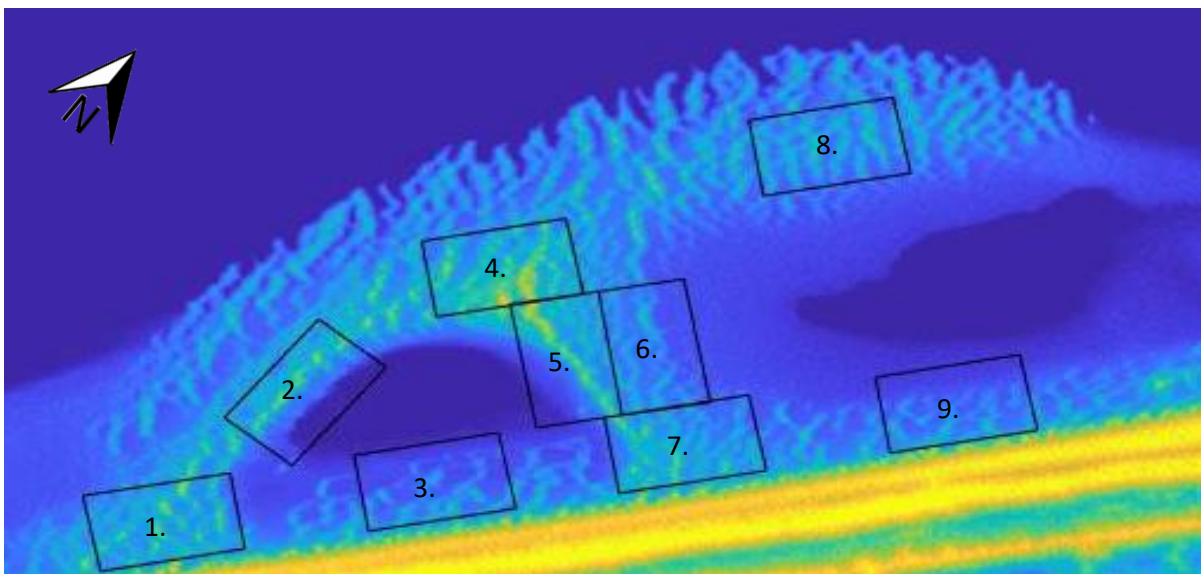


Figure 11, areas of interest.

Each area of interest is subject to different combinations of factors influencing dune development. The factors influencing dune development that are area-dependent are the elevation, the type of terrain, the influence of the lake and influence of the sea. Table 2 shows to what extent area-dependent factors are influencing dune development.

The elevation of an area is directly connected to the groundwater level by the reference surface influencing the amount of sediment available for aeolian transport. In the model, no sediment can erode by wind below the groundwater level.

Although the model does not include different probabilities of aeolian erosion or deposition for uphill or downhill areas, the shadow zone threshold (certain elevation difference between neighbouring cells in the direction of the wind) is reached with less sediment for downhill zones. An increase or decrease in the number of shadow zones in an area might influence dune development because sediment is trapped ($P_e = 0$, $P_d = 1$) in shadow zones, enhancing the dune development. There are flat, uphill and downhill areas of interest chosen.

The dune development in the areas nearby the lake is influenced by the lake. Aeolian sediment is trapped in the lake instead of developing dunes. Furthermore, the aeolian sediment inflow of areas

behind the lake is reduced because no aeolian sediment can erode below the water level of the lake. In the model, the hydrodynamic erosion of the lake is neglected because of the relative low wave strength due to the shallow water and the absence of tidal currents. The areas around the lake experience no hydrodynamical erosion in the model.

Areas that do experience hydrodynamical erosion are the areas that are not sheltered from the hydrodynamics and can be reached by the maximum water level. Similar to the lake influence, the aeolian sediment inflow of areas behind the zone that is influenced by the sea is reduced because no aeolian sediment can erode below the water level.

Table 2, the extent that area-dependent factors are influencing dune development.

Area number	Elevation of the area	Terrain type of the area	Lake influence	Sea influence
1	high	flat	no	no
2	high and low	downhill	yes	no
3	low	flat	yes	no
4	high	uphill and downhill	no	no
5	high and low	uphill	yes	no
6	high and low	downhill	no	yes
7	high	flat	yes	no
8	high	flat	no	no
9	low	flat	no	yes

The quantification of the elevation for each area of interest is done by summing the number of cells that are higher than the threshold. The threshold is an elevation of 0.5 m above the smoothed final reference surface map. This map is the final LIDAR map (2017) with a Gaussian filter that results in a map without dunes. The 0.5 m threshold is chosen so that the elevation at least needs to be 4 sand slabs higher than the final LIDAR map. Very small height differences (<4 slabs) are not taken into account because they might consist of a smoothing error or a slab of sand that has landed by coincidence on a certain location which cannot be called a dune. Multiple gradations in elevation are made by summing the number of cells elevated between an upper and lower threshold.

The quantification of the vegetation for each cell of interest is done by summing the number of cells with vegetation on it. Similar to the elevation, multiple gradations in vegetation density are quantified by summing the number of cells between an upper and lower threshold.

2.5 Method for comparing the observed and modelled dune formation patterns

To find out to what extent the observed dune formation patterns at an out-of-equilibrium anthropogenic shore like the Sand Motor can be simulated by the DUBEVEG model, the modelled topography and vegetation is compared with the observed topography and vegetation. The comparison between observed and modelled topography and vegetation takes place after 6 years. The Sand Motor is built in 2011 and the LIDAR maps of 2017 are used for comparison. The available observed vegetation map for comparison is of 2018. However this map is one year later than 2017, it is not expected that the vegetation patterns are fundamentally different.

A figure of the modelled topography and a figure of the observed topography are compared for dune patterns development. The dune pattern development comparison includes the elevation and direction of the dunes. Furthermore, the modelled and observed elevation of the coastal area and the

lake are compared by subtracting the elevation of modelled topography by the observed topography. Furthermore, a figure of the modelled vegetation and a figure of the observed vegetation are compared. The (difference between the) areas of modelled and observed vegetation are described.

Because the model includes multiple stochastic processes that may cause different outcomes for model runs with equal parameter settings, multiple model runs with equal settings are performed to find out the deviation in the model results. The stochastic elements in the model are aeolian erosion and deposition, hydrodynamic erosion, pioneer and lateral vegetation expansion rate and avalanching for two or more cells lower than the threshold with an equal elevation. The mean and standard deviation of the percentage of cells in an area of interest larger than the reference (described in subchapter 2.4) and the percentage of cells in an area of interest with vegetation are calculated. Five model runs with equal model parameters settings are performed.

2.6 Method for determining the dominant model parameters

To find out the dominant parameters explaining modelled dune formation patterns at the Sand Motor area, a sensitivity analysis is performed. In the sensitivity analysis, one model parameter is changed while the other model parameters are kept constant.

2.6.1 Model parameters used in the sensitivity analysis

Parameters related to aeolian transport are useful and suitable to change in the sensitivity analysis, while general model parameters or hydrodynamic parameters are not useful and suitable to change. General parameters, for example, the number of model years, the number of iterations, shadow angle and the angle of repose are fixed parameters. The number of model years cannot be extended because there are no future maps for comparing and the reference surface, increasing the amount of iterations results in a major increase in calculation time and the shadow angle and angles of repose are fixed. Furthermore, changing parameters related to hydrodynamics will not result in different dune development in most areas of the Sand Motor because most parts of the Sand Motor are not influenced by the hydrodynamics.

The first model parameter used in the sensitivity analysis is the combined probability of aeolian erosion and deposition (P_e and P_d). If the probability of erosion is changed, and the amount of aeolian transport (Q) is kept the same, the probability of deposition needs to change as well conform formula 1. The flux of sediment does not change when increasing or decreasing the amount of aeolian erosion and deposition with the same percentage. Decreasing both aeolian erosion and deposition results in less sediment that is transported further distance and increasing both aeolian erosion and deposition results in more sediment that is transported shorter distance. The changes in both aeolian erosion and deposition probability are 125%, 100%, 75%, 50% and 25% of the normal probability of aeolian erosion and deposition.

The probability of aeolian erosion is chosen because results of Keijsers et al. (2016) showed that the probability of aeolian erosion influenced among other things the dune volume and the vegetation cover on a normal beach and Nield and Baas (2008) showed that different probabilities of aeolian erosion resulted in different dune patterns for a flat area.

For the probability of aeolian deposition, it is assumed that, at the Sand Motor location, the eroded sand slabs are transported further in reality than in the model. Theoretically, with the current model parameter settings, the travel distance for 50% of the aeolian eroded slabs of sand over non-vegetated cells and cells without shadow zones in one iteration is 8m (Figure 12). In the model, relative less sediment is reaching the foredunes or the lake and a dune is developed from sediment within its

surroundings (Silva et al., 2017). Field measurements show that more sand is transported to the foredunes that are growing with 15 to 20 m³/m/year (Puijenbroek, 2017) and fill in the lake (Van der Weerd & Wijnberg, 2016).

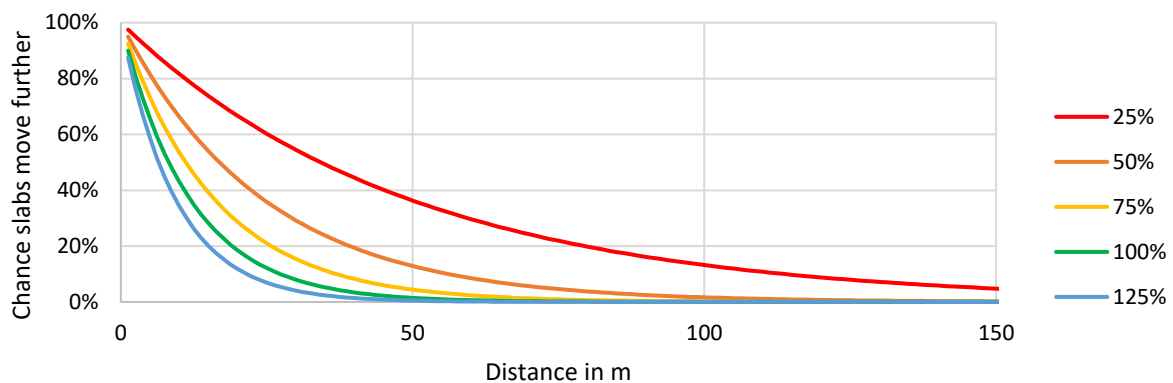


Figure 12, travel distance for eroded slabs of sand over non-vegetated cells and cells without shadow zones in one iteration. Probability of erosion (P_e) 100% = 0.5 and probability of deposition (P_d) 100% = 0.1.

The second model parameter used in the sensitivity analysis is the groundwater level (G) because the groundwater level limits the available sediment for aeolian transport. The effect of groundwater depth on dune development has been studied by Silva et al. (2017) and Silva et al. (2018) for the Hors area with the DUBEVEG model. The Hors is roughly a 3km² sand flat above the mean spring tide but is flooded during storms (Silva et al., 2018). The Sand Motor is a different area compared to the Hors area because it has very highly elevated areas. Model runs with different groundwater depths will clarify if the groundwater depth in the Sand Motor area is important for (the type of) dune development. The changes in the dimensionless groundwater level are 60%, 70% 80% 90% and 95% of the total elevation of the reference surface (explained in chapter 2.2.2), wherein 80% is the standard groundwater level in the model. Lower values of groundwater depth had a minor influence on the Hors area (Silva et al., 2018) and therefore model runs with lower groundwater levels than 60% are not applied to the Sand Motor area.

The third model parameter used in the sensitivity analysis is the probability of pioneer expansion of pioneer vegetation ($p_{lateral}$) because vegetation influences the probability of aeolian and hydrodynamic erosion, aeolian deposition and the angle of repose. Pioneer expansion is the major distributor of vegetation influencing dune development compared to the lateral expansion of vegetation. The Sand Motor is completely bare at the start and lateral vegetation expansion can vegetate 6 cells away (7,5m) from the initial vegetated cell (1 cell each year) at optimal conditions while the pioneer vegetation expansion can reach the whole area.

The hypotheses are that $p_{lateral}$ is smaller than 0.05 chance every year on every cell above MSL because on normal beaches seeds and plants are transported by wind and water (Hesp, 1989; Puijenbroek, 2017). Large areas of the Sand Motor cannot be reached by water, which differs from most regular beaches, and thus seeds and plants distribution are depended on wind only. Model runs are performed for a $p_{lateral}$ of 0%, 20%, 50%, 100% and 200% of the normal $p_{lateral}$.

2.6.2 Method for comparing the modelled dune formation patterns for the sensitivity analysis

The modelled elevation and vegetation results of the sensitivity analysis (for each different parameter type) are visually and numerically compared. This comparing method is similar for all three parameter types. The visual comparison is between the final model results for the lowest and highest parameter value for elevation and vegetation. Differences in dune patterns and areas with vegetation are compared for the whole Sand Motor area. Furthermore, all areas of interest for all values of the parameters are visually displayed. When a parameter is changed, the difference in results of the elevation and the vegetation is visible for each area of interest.

The numerical comparison is based on the number of cells higher than the threshold as described in chapter 2.4. The percentage of cells above the threshold (for vegetation and elevation) in an area of interest is displayed in a 2D line figure for all areas of interest for all values used in the sensitivity analysis. The difference in elevation results or vegetation cover results when changing the parameters used in the sensitivity analysis is shown for all areas of interest.

2.7 Method for including the additional model revisions

Two model revisions are tested for their influence on dune development on the Sand Motor.

2.7.1 Multidirectional wind

One wind direction in the model results in mainly dune rows perpendicular to the wind which are not observed at the Sand Motor. The first model revision is the multidirectional wind. In the model, the slab transport is only in the direction of the main wind direction influencing the orientation of the dunes. Only one wind direction is used in the researches of Keijsers et al. (2016), Silva et al. (2017) and Silva et al. (2018) that resulted in mainly dune rows perpendicular to the wind direction.

At the Sand Motor, the wind is coming from multiple directions (subchapter 2.1.4) and adding a second wind direction in the DUBEVEG model area might influence the orientation and the type of the dunes. Multiple (slab transporting) wind directions have been modelled in bare sand models, previous to the DUBEVEG model, by adding two components by moving a certain amount (1/3 for example) of eroded cells in a direction and 2/3 in the perpendicular direction (Nield & Baas, 2008).

In the DUBEVEG model, a wind direction of +/- 90 or 180 degrees can be easily made. The quadrant with the second largest average wind speeds is the 320 degrees direction as shown in Figure 13. The wind direction enabling aeolian transport is 2/3 of the time 230° and 1/3 of the time 320°, neglecting the wind directions outside the two quadrants. The calculation is based on the summed percentage of time the wind comes from a direction for the wind speeds 6, 7, 8 and 9 m/s in a quadrant.

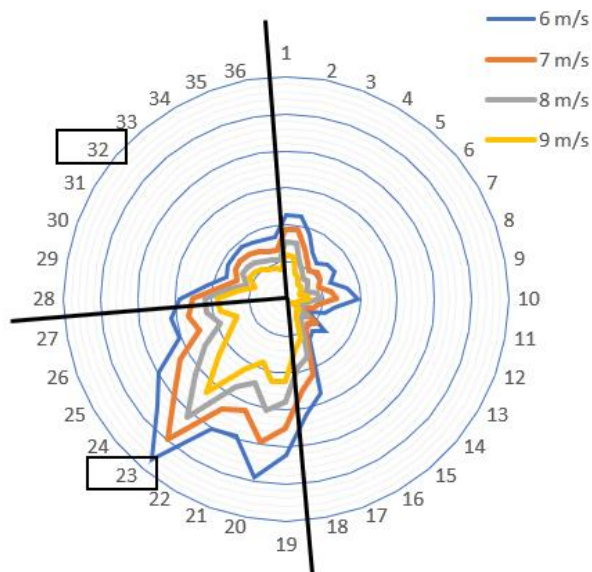


Figure 13, wind directions for wind speed larger than 6, 7, 8 and 9 m/s. Measuring location Hoek van Holland. Timespan 02-2011 until 05-2017. Units are in degrees divided by 10. The values in the black squares are the wind directions representing the average quadrant values. The quadrant values are all wind occurrences measured between the black lines (the representing value +/- 45°).

2.7.2 Beach armouring

The aeolian erosion of sand can be significantly reduced when a beach armouring layer is present (Hoonhout & de Vries, 2017b). On normal beaches, the armouring is washed away after a certain period which is not the case at the Sand Motor's higher elevated areas. In the previous versions of the DUBEVEG model, there was no beach armouring incorporated and the aeolian erosion has no spatial differences, which is not the case for the areas of the Sand Motor with beach armouring.

The second model revision is including beach armouring by spatially reducing the probability of aeolian erosion for areas that fulfil certain conditions. Next to beach armouring, the probability of aeolian erosion in the model is influenced by vegetation density, shadow zones, the MSL and the groundwater level. Data of the locations of beach armouring and the effect of it on aeolian erosion is not available. The beach armouring effectiveness changes in time due to very strong winds. Because of the lack of data, in the model, assumptions are made of the locations and effectiveness of the armouring.

The effect of armouring changes spatially and over time but is assumed constant in this model revision. This assumption is a simplification but will result in insight if armouring effects dune development on the Sand Motor. Hoonhout and de Vries (2017b) found a reduction of 42% of aeolian transport at the aeolian zone (part of the Sand Motor that is elevated above 3m+MSL). In the model, the probability of aeolian erosion for areas without beach armouring is 0.5 (Keijsers et al., 2016). The probability of aeolian erosion for armoured cells in the model should be lower than 42% of 0.5 because not all cells of the aeolian zone are armoured. Therefore it is assumed that cells with beach armouring have a probability of aeolian erosion of 0.125 (25% of 0.5).

The first assumption for the location of beach armouring in the model is that a cell can only have armouring when it is elevated above 3m+MSL, which is not reached by hydrodynamics 99% of the time. The armouring layer is likely to be removed by hydrodynamic erosion and therefore lower elevated cells in the model should have no armouring.

The second assumption for the location of beach armouring in the model is that the elevation of a cell is equal or smaller than the reference surface (described in chapter 2.2.2). Dunes that grow above the

3m+MSL threshold should not become armoured. If sediment is deposited by aeolian transport it is not covered by beach armouring and should not have a reduced probability of aeolian erosion. This is incorporated by the rule that armouring cannot exist if the elevation is larger than the reference surface elevation.

The third assumption for the location of beach armouring in the model is that the elevation of a cell needs to be equal or smaller than the elevation of the initial elevation (elevation at $t = 0$ years). Although the reference surface is smoothed with a Gaussian low pass filter removing the dunes, the elevation of certain areas (for example the lake infill and foredune growth) in the reference surface is increasing over time. An increase of the reference profile elevated 3m+MSL or higher is always caused by aeolian transport which should not be armoured.

An aeolian erosion probability map at $t = 6$ years is shown in Figure 14 (left) for normal model settings and (right) including armouring at areas larger than 3m+MSL and lower or equal than the reference surface elevation and extended with no armouring at locations larger than the initial profile at.

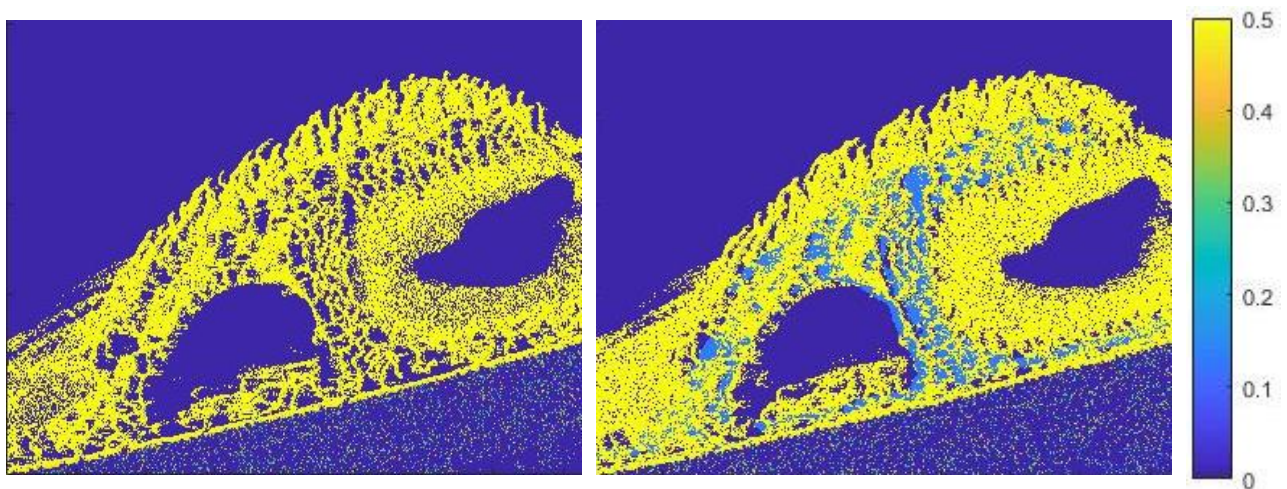


Figure 14, Map of the probability of erosion at $t = 6$ years with a maximum probability of erosion of 0.5 and a minimum of 0 (left). A map with a reduced probability of erosion caused by armouring of shells (assumed to be 0.125 which is 25% of the maximum probability of erosion) for areas larger than 3m MSL, smaller or equal than the reference surface and smaller or equal to the initial profile ($t = 0$ years) (right).

2.8 Method for comparing the modelled dune formation patterns for the additional physical processes

The modelled elevation and vegetation of the model revisions (for the multidirectional wind and the beach armouring) are visually and numerically compared. The comparing method is similar for both model revisions. The visual comparison is between the final model results for a model revision and the results of the standard DUBEVEG model for vegetation and elevation. Differences in dune patterns and areas with vegetation are compared for the whole Sand Motor area.

The numerical comparison is based on the number of cells higher than the threshold as described in chapter 2.4. The percentage of cells above the threshold (for vegetation and elevation) in an area of interest is displayed in a stacked bar plot for the standard DUBEVEG outcomes and the outcomes of the concerning model revision.

3 Results

In this chapter, the results of the model adapted for an out-of-equilibrium anthropogenic shore, results of the sensitivity analysis and results of including additional physical processes to the model are shown and described.

3.1 Results of the model adapted for an out-of-equilibrium anthropogenic shore

Figure 15 shows an elevation map of the Sand Motor area in 2017 (after 6 model years). The model elevation outcomes are shown on the left and the LIDAR elevation measurements on the right for elevation magnitudes larger than MSL. The model outcomes show complete rows of dunes perpendicular on the wind direction on the Sand Motor. The LIDAR measurements do not show these dune rows.

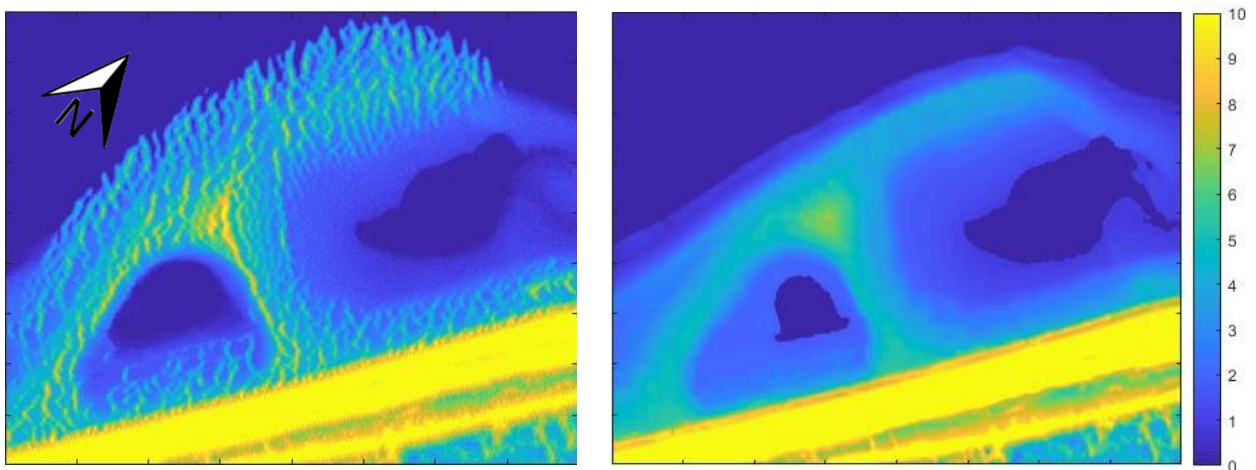


Figure 15, Model elevation results at $t = 6$ year (left) and LIDAR map (right) in February 2017 in m.

The difference in elevation between the model outcomes and the LIDAR map is shown in Figure 16 (left). Positive values mark the areas where the elevation of the model results is higher than the elevation of the LIDAR measurements and visa-versa. The most seaward part of the Sand Motor is higher elevated in the model than the LIDAR measurements while the inner lake and area seaward of the foredune are lower elevated. Furthermore, the dune rows on the Sand Motor itself in the model elevation results are not on the LIDAR measurements. The lagoon area has similar elevation levels.

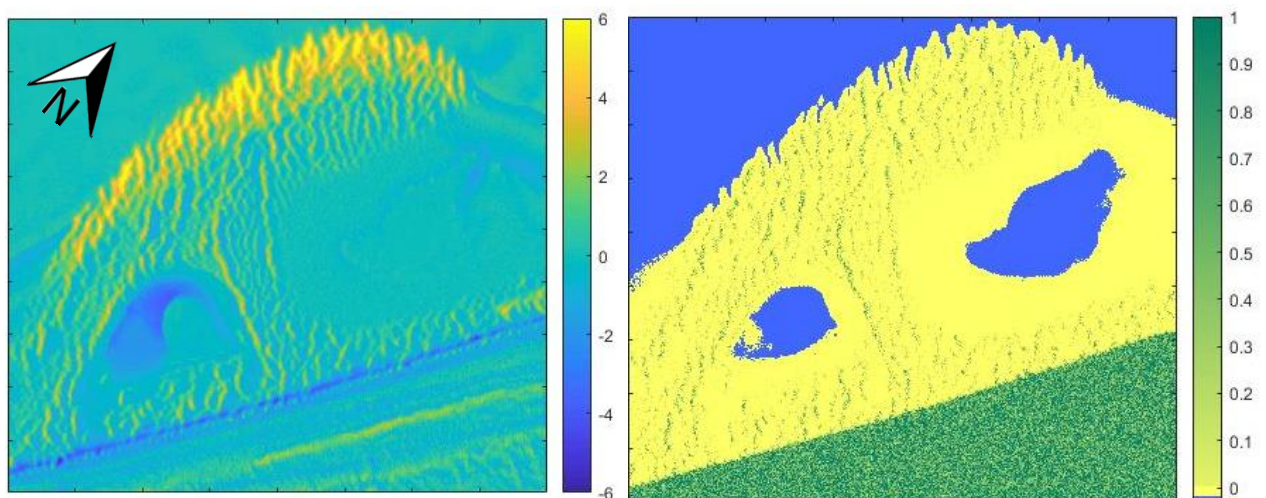


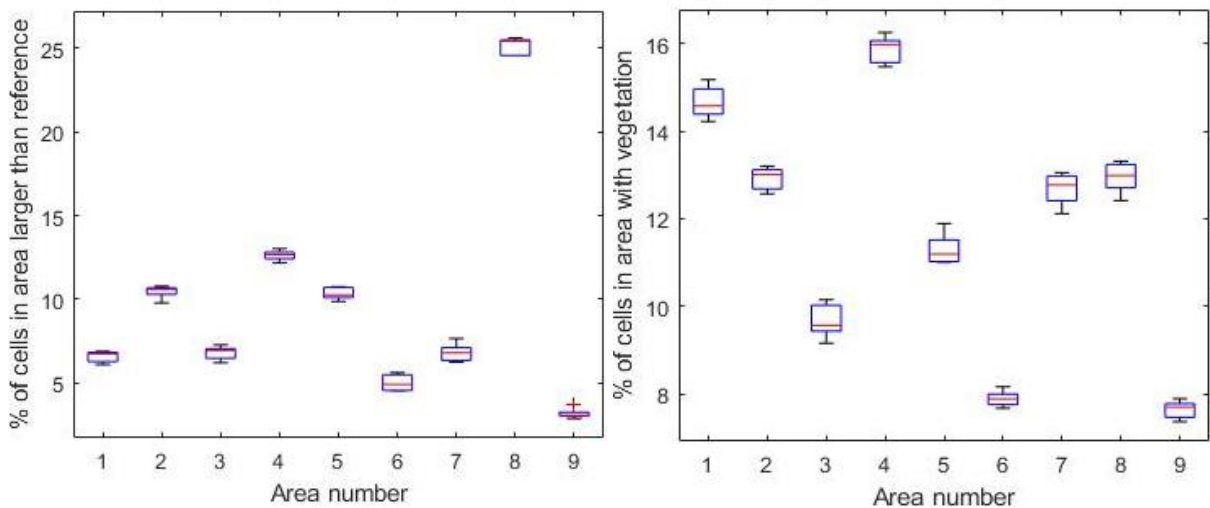
Figure 16, a map of difference in elevation (elevation of model results minus the elevation of the LIDAR map) (left). The final model locations of vegetation (right). The blue colour is the area below MSL. Value one (green) means a fully vegetated cell and a value 0 (yellow) means a cell without vegetation.



Figure 17, 12-images-merged-rectified picture of the Sand Motor 27-10-2018. The pictures are made from the Argus station at the centre of the Sand Motor. The black area on this picture is outside the range of the cameras. The green dots on the picture is vegetation growing on the Sand Motor.

The model results of the final vegetation on the Sand Motor is shown in Figure 16 right. At the start of the model, the foredune and the area behind it were assumed completely vegetated. At the end of the model time, this area is still densely vegetated. In the model, the low elevated areas (around the inner lake and the lagoon) have both a low vegetation grade. Vegetation is present at the dune rows all over the Sand Motor area. Figure 17 shows a 12-images-merged-rectified picture of the Sand Motor made from the Argus station in 2018. The area close to the foredune, around the lake and west of the lake, has the most vegetation, while the most offshore parts of the Sand Motor are mostly bare. Both the model and the picture have little vegetation around the lagoon area.

Five model runs with equal parameter settings are performed to find out the deviation in model results caused by the stochastic elements. The results are quantified by the percentage of cells in each area of interest that are larger than the threshold (Figure 18, left) and have vegetation on it (Figure 18, right) as described in chapter 2.4. For both elevation and vegetation, the deviation between the areas is larger (percentages) than the deviation in the area of interest itself (tenths of percentages).



Area of interest	1	2	3	4	5	6	7	8	9
Mean elevation	6.58	1.05	6.80	1.26	1.04	5.02	6.80	2.51	3.16
Stdev elevation	0.30	0.04	0.37	0.03	0.03	0.45	0.50	0.05	0.29
Mean vegetation	14.66	12.92	9.68	15.86	11.30	7.89	12.68	12.95	7.64
Stdev vegetation	0.34	0.24	0.35	0.29	0.33	0.17	0.34	0.32	0.19

Figure 18, boxplot with the percentage of cells larger than the threshold for each area of interest (upper left). Boxplot with the percentage of cells with vegetation on it for each area of interest (upper right). The mean and standard deviation (Stdev) for the percentage of cells larger than the threshold and percentage of cells with vegetation on it for each area of interest (lower).

3.2 Results of the sensitivity analysis

In this subchapter, the results of the sensitivity analysis are described. First, the change in the probability of aeolian erosion and deposition is described followed by the change in groundwater level and the change in pioneer vegetation expansion rates.

3.2.1 The probability of erosion and deposition

Including the standard situation, there are five model runs performed with different probabilities of erosion (P_e) and deposition (P_d). The standard probability of erosion is 0.5 and the standard probability of deposition is 0.1. These values have been changed to 125%, 75%, 50% and 25% of the standard situation. Appendix B shows the elevation map and stacked bar plots of each area of interest for all model runs with a changed probability and deposition. The elevation results of the standard run are shown in Figure 15 left. Figure 19 shows the elevation map for the probability of erosion and deposition 25% (left) and 125% (right) of the standard value.

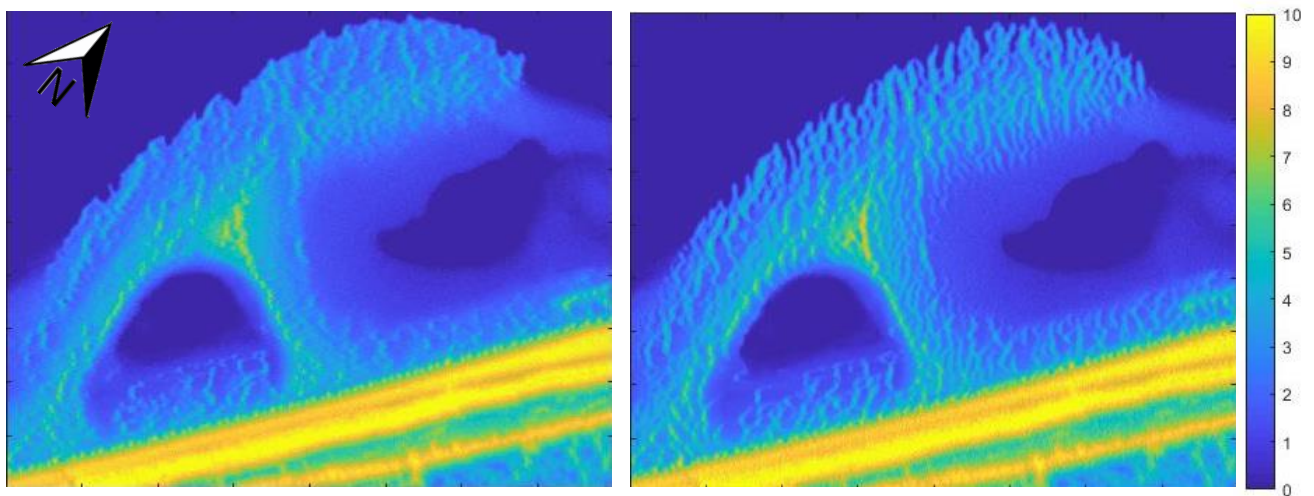


Figure 19, Model elevation result at $t = 6$ years for P_e & P_d is 25% (left) and P_e & P_d is 125% (right).

The pictures in Figure 19 shows that the P_e and P_d do influence the number of dunes to develop. A large value of $P_e P_d$ results in more and longer dune rows than a low value of $P_e P_d$.

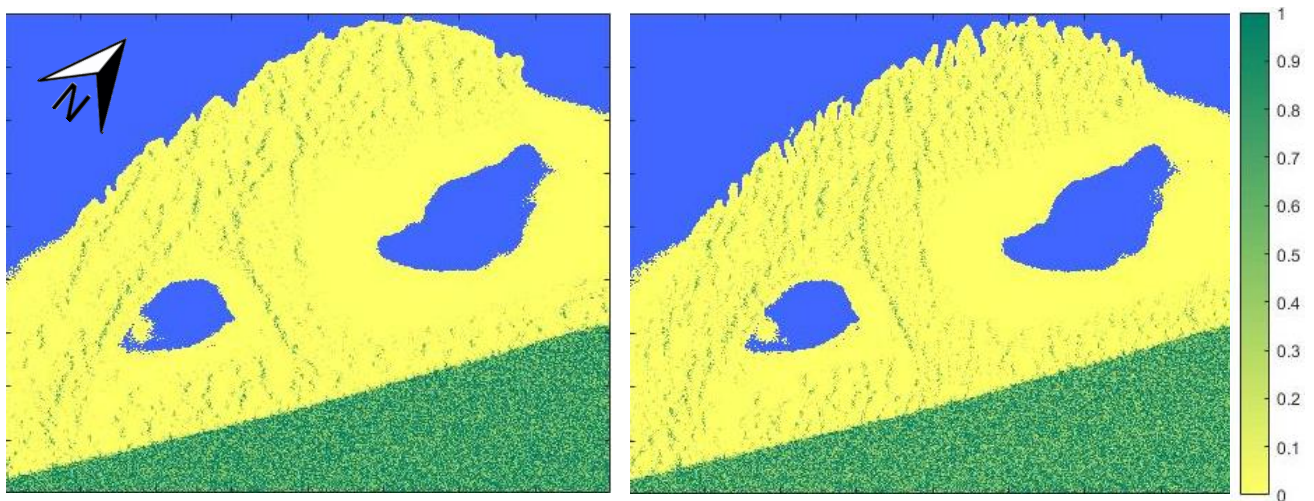


Figure 20, Model locations of vegetation at $t = 6$ years for P_e & P_d is 25% (left) and P_e & P_d is 125% (right). The blue colour is the area below MSL. Value one (green) means a fully vegetated cell and a value 0 (yellow) means a cell without vegetation.

Figure 20 shows the results of the modelled final vegetation on the Sand Motor. Appendix C shows the vegetation map and stacked bar plots of each area of interest for all model runs with a changed probability and deposition. Similar to the dune patterns, the vegetation is more scattered across the

area in the large $P_e P_d$ vegetation map compared with the low $P_e P_d$ vegetation map. Both maps do not have vegetation in the intertidal areas.

Figure 21 shows the number of cells larger than the threshold (left) and the number of cells with vegetation on it (>0) (right) in each area of interest (as described in chapter 2.4) for the five different $P_e P_d$ values. Area 8 has the most cells above the threshold and area 9 the least. All areas experience growth in a number of cells above the threshold between the smallest and largest $P_e P_d$. A fast increase for the lower $P_e P_d$ values (25%-75%) is witnessed at area 1, 4, 5 and 8. Area 9 increases most at the standard and increased $P_e P_d$ while area 5 and 7 experience a decay. Area 8 has the largest increase and area 3 the smallest increase. The results for area 7 are different compared to the other areas which do not increase and decrease twice. Area 5 seems to have a maximum percentage of cells larger than the threshold at 75% of the $P_e P_d$.

The number of cells larger than the threshold and the number of cells with vegetation on it is not linear dependent. For example, area 8 has many cells above the threshold and relative less vegetation on it while area 1 has fewer cells above the threshold and many vegetated cells. Area 3 experiences the least difference in vegetated cells for the different $P_e P_d$ values. All areas have a maximum percentage of vegetated cells mostly for the lower $P_e P_d$ values than the standard.

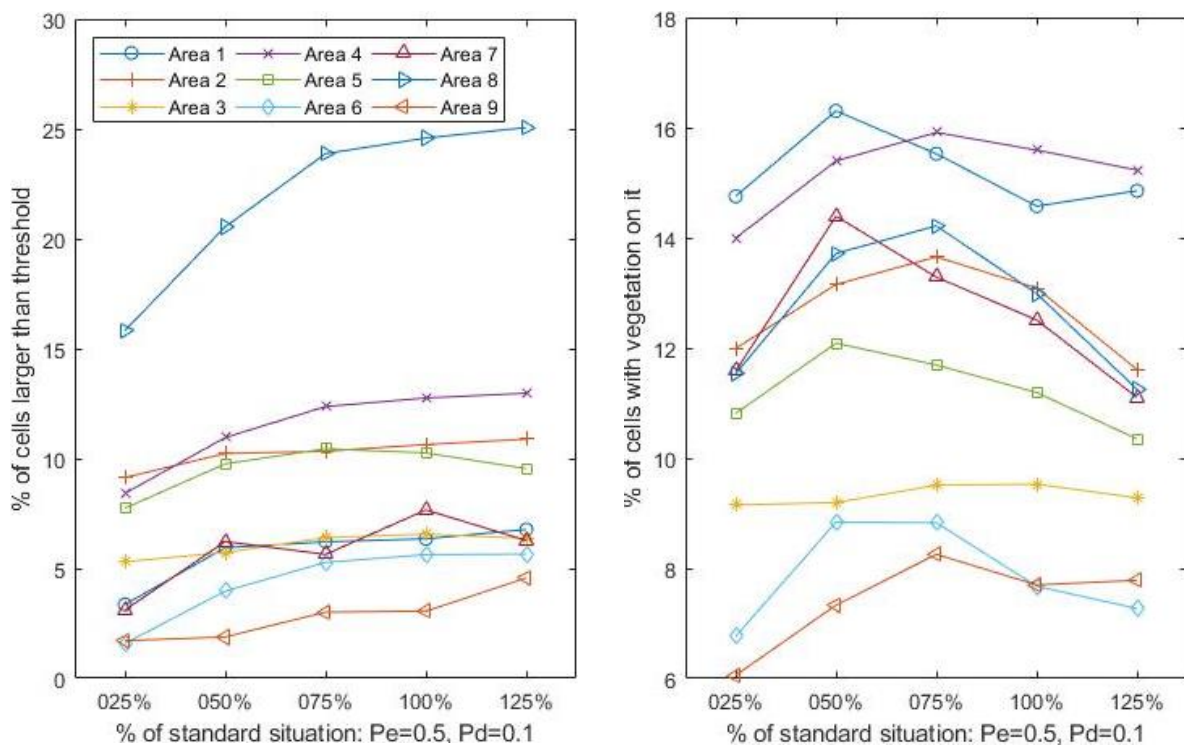


Figure 21, left: Number of cells larger than the threshold in each area of interest for the five different $P_e P_d$ values. Right: Number of cells with vegetation on it (>0) in each area of interest for the five different $P_e P_d$ values.

3.2.2 The groundwater level

Including the standard situation, there are five model runs performed with different groundwater levels. The standard groundwater level (a fraction between the reference surface and MSL as described in chapter 2.2.2) is 0.8. This value has been changed to 0.6, 0.7, 0.9 and 0.95. Appendix D shows the elevation map and stacked bar plots of each area of interest for all model runs with a changed groundwater level. The elevation results of the standard run are shown in Figure 15 left. Figure 22 shows the elevation map for groundwater level 0.6 (left) and 0.95 (right).

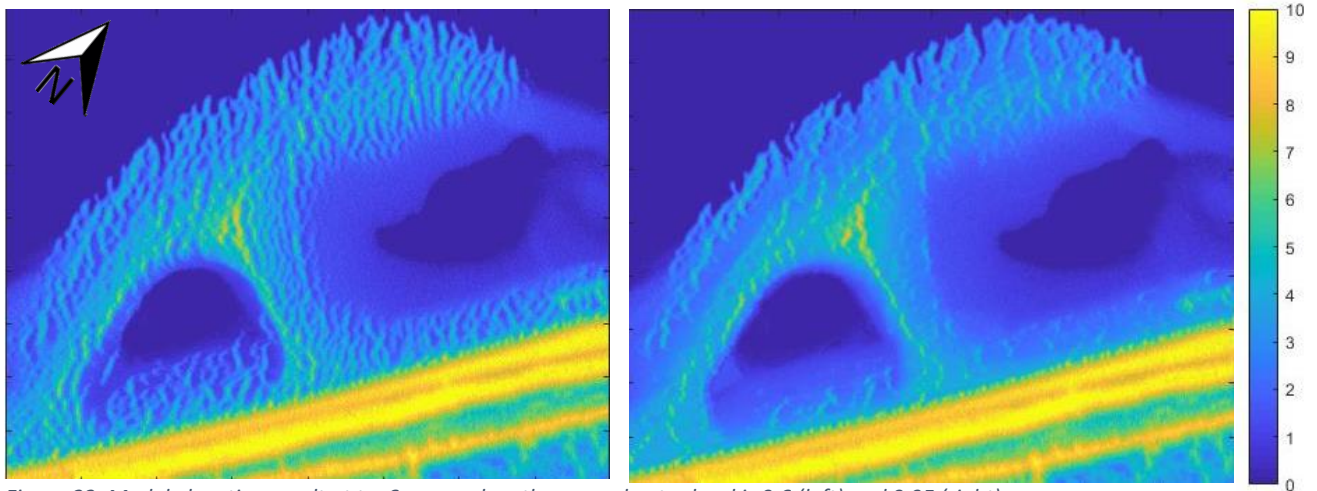


Figure 22, Model elevation result at $t = 6$ years when the groundwater level is 0.6 (left) and 0.95 (right)

The pictures in Figure 22 shows that the groundwater level does influence the number of dunes to develop. More dunes develop when the groundwater level is low.

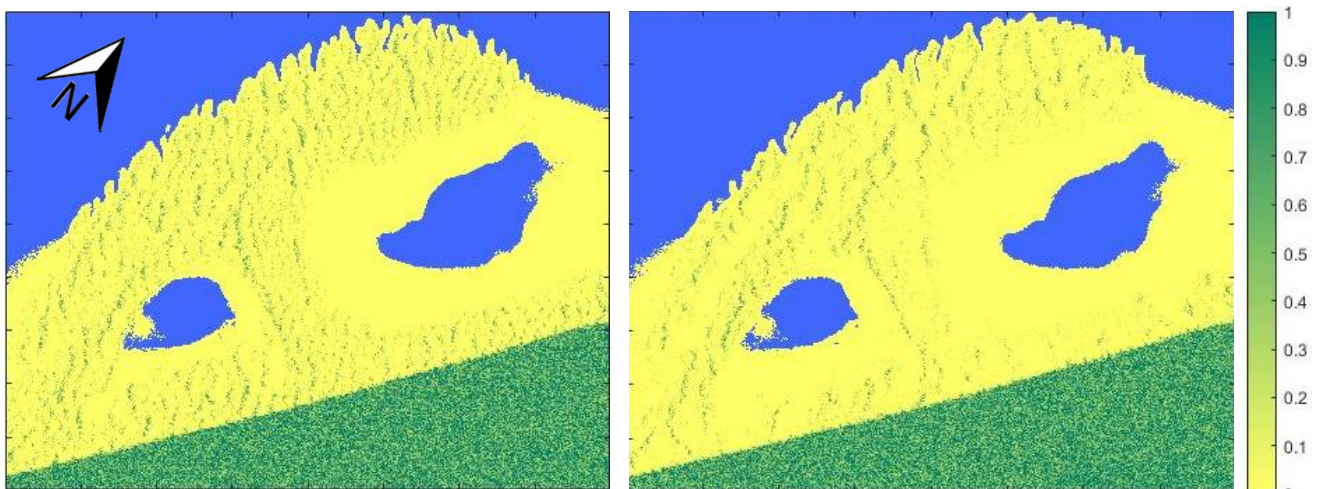


Figure 23, Model locations of vegetation at $t = 6$ years for groundwater level 0.6 (left) and 0.95 (right). The blue colour is the area below MSL. Value one (green) means a fully vegetated cell and a value 0 (yellow) means a cell without vegetation.

Figure 23 shows the results of the final vegetation on the Sand Motor. Appendix E shows the vegetation map and stacked bar plots of each area of interest for all model runs with a changed groundwater level. Similar to the dune patterns, the vegetation is more scattered in the low groundwater level vegetation map compared with the high groundwater level vegetation map. Both maps do not have vegetation in the intertidal areas.

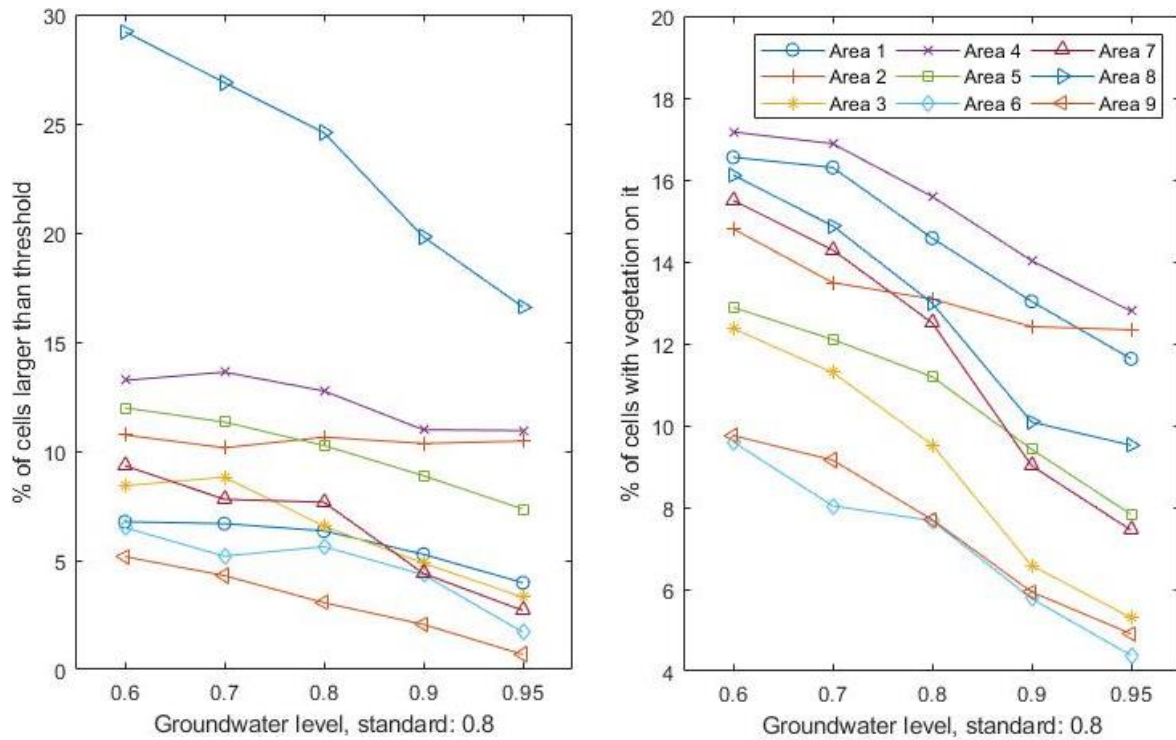


Figure 24, left: Number of cells larger than the threshold in each area of interest for the five different groundwater levels. Right: Number of cells with vegetation on it (>0) in each area of interest for the five different groundwater levels.

Figure 24 shows the number of cells larger than the threshold (left) and the number of cells with vegetation on it (>0) (right) in each area of interest (as described in chapter 2.4) for the five different groundwater level values. Area 8 has the most cells above the threshold and area 9 the least, similar to the $P_e P_d$ results. All areas experience a decrease in a number of cells above the threshold between the smallest and largest $P_e P_d$, except area 2. Area 8 has the largest decrease in cells above the threshold while area 2 has little change in the percentage of cells larger than the threshold for changing groundwater levels.

The number of cells larger than the threshold and the number of cells with vegetation on it is not linear dependent. For example, area 8 has many cells above the threshold and relative less vegetation on it while area 1 has fewer cells above the threshold and many vegetated cells. All areas seem to experience a decrease in vegetated cells when the groundwater level increases.

3.2.3 The pioneer vegetation expansion rate

Including the standard situation, there are five model runs performed with different pioneer vegetation expansion rates. The standard pioneer vegetation expansion rate is 0.05 (100%). This value has been changed to 0 (0%), 0.01 (20%), 0.025 (50%) and 0.1 (200%). Appendix F shows the elevation map and stacked bar plot of each area of interest for all model runs with a changed pioneer vegetation expansion rate. The elevation results of the standard run are shown in Figure 15 left. Figure 25 shows the elevation map for pioneer vegetation expansion rate 0% (left) and 200% (right).

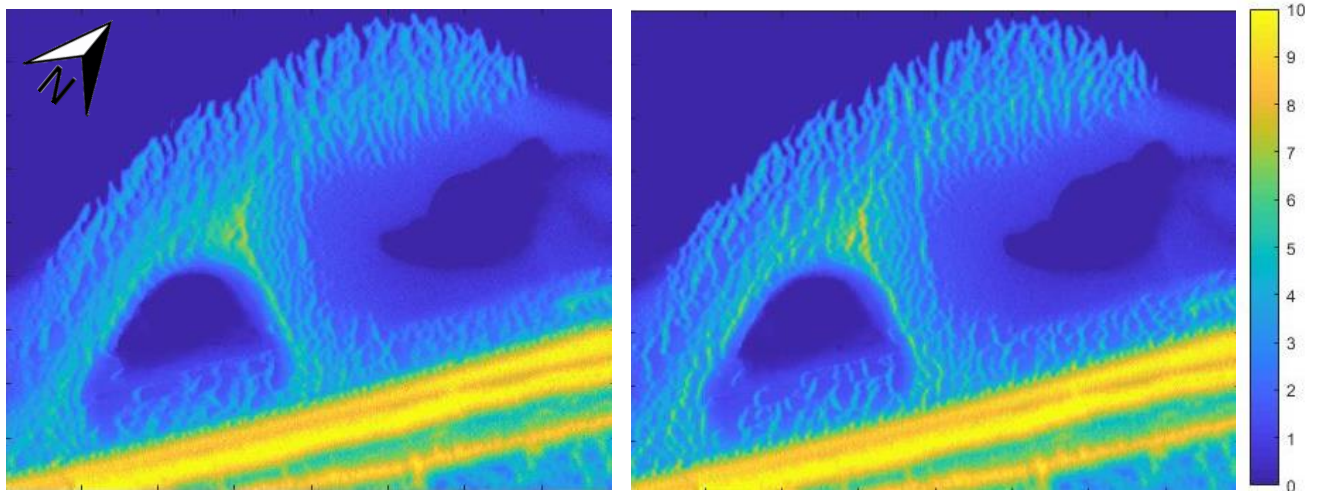


Figure 25, Model elevation result at $t = 6$ years when the pioneer vegetation expansion rate is 0% (left) and is 200% (right)

The pictures in Figure 25 shows that the vegetation expansion rate does influence the dune development. The amount of dunes and dune rows is similar but the dunes in the increased pioneer expansion rate elevation map are steeper.

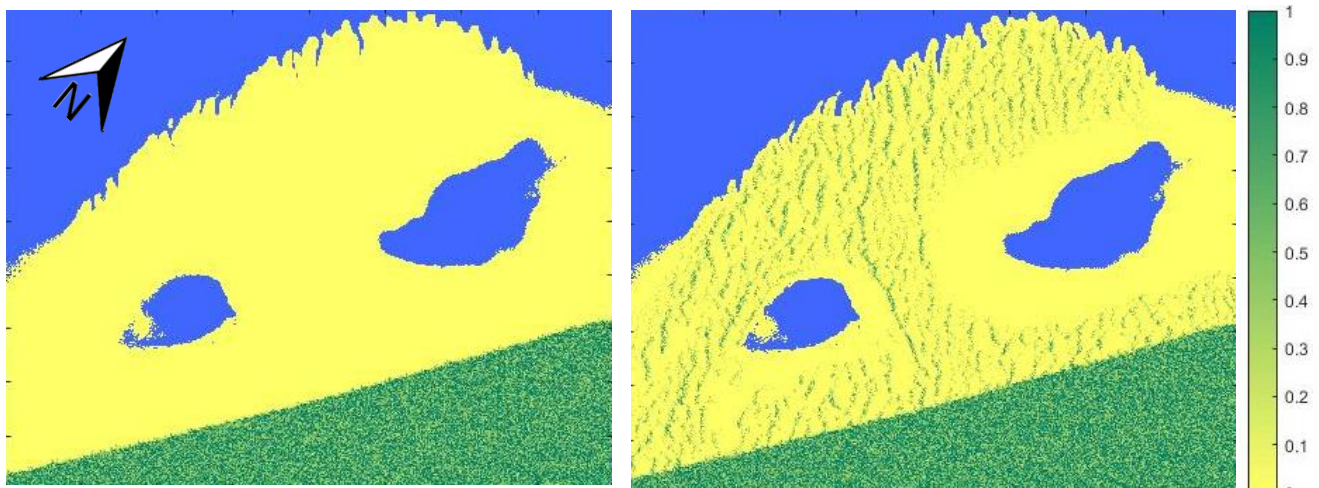


Figure 26, Model locations of vegetation at $t = 6$ years for pioneer vegetation expansion rate of 0% (left) and 200% (right). The blue colour is the area below MSL. Value one (green) means a fully vegetated cell and a value 0 (yellow) means a cell without vegetation.

Figure 26 shows the results of the final vegetation on the Sand Motor. Appendix G shows the vegetation map and stacked bar plots of each area of interest for all model runs with a changed pioneer vegetation expansion rate. Figure 26 (left) shows that a pioneer vegetation expansion rate of 0% results in no vegetation on the Sand Motor. Figure 26 (right) shows that a double pioneer vegetation expansion rate (200%) has vegetation all over the area except the tidal area of the lagoon.

Figure 27 shows the number of cells larger than the threshold (left) and the number of cells with vegetation on it (>0) (right) in each area of interest (as described in chapter 2.4) for the five different pioneer vegetation expansion rates. Area 8 has the most cells above the threshold and area 9 the least, similar to the previous results of the sensitivity analysis.

All areas experience an increase in the number of cells above the threshold when increasing the pioneer vegetation expansion rate. Area 4 experiences the largest increase and area 5 the smallest. Area 6 and 7 have a drop in the number of cells above the threshold at 50% pioneer vegetation expansion rate and area 2, 3, 8 and 9 do not increase in a number of cells above the threshold at the 50% pioneer vegetation expansion rate compared to lower pioneer vegetation expansion rates.

The amount of vegetated cells increases strongly at higher pioneer vegetation expansion rates and are not linear dependent with the number of cells larger than the threshold. Area 1 and 4 have the most vegetation and area 6 and 7 the least for all 5 different pioneer expansion rate values.

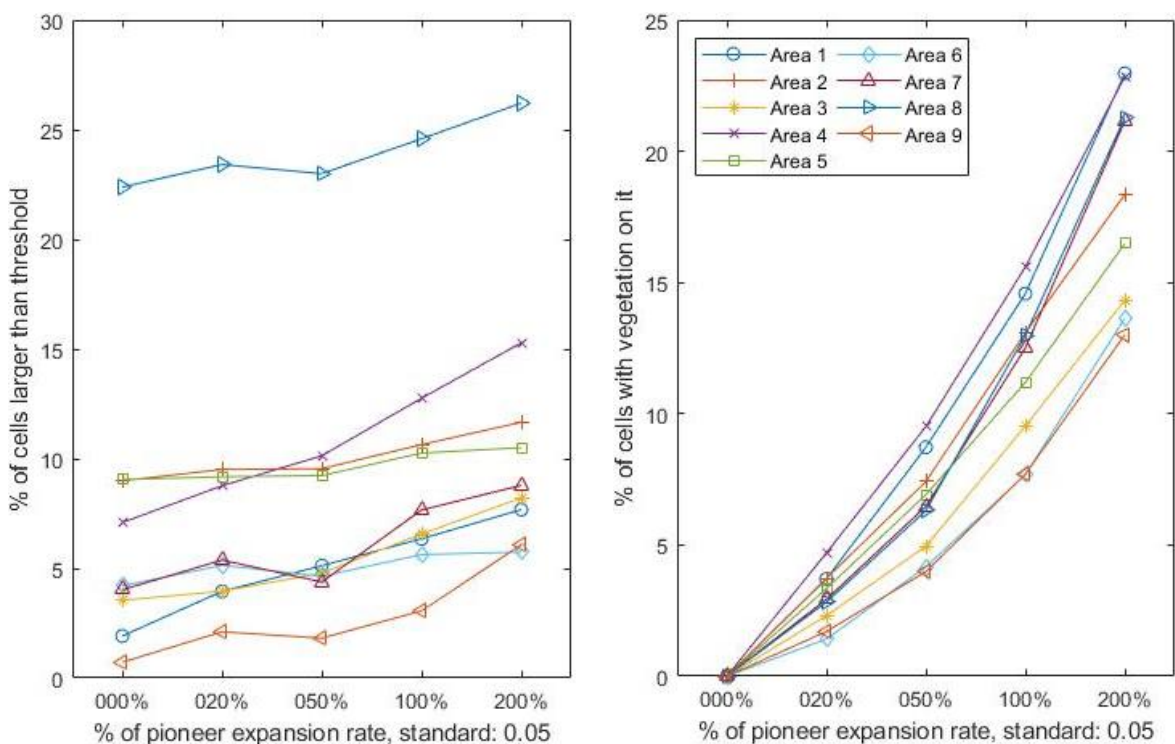


Figure 27, left: Number of cells larger than the threshold in each area of interest for the five different pioneer vegetation expansion probabilities. Right: Number of cells with vegetation on it (>0) in each area of interest for the five different pioneer vegetation expansion probabilities.

3.3 Results of including additional model revisions to the model

The results of the two model revisions are separately compared to the model results obtained with the model results without revisions.

3.3.1 Multidirectional wind

In the first model revision, including multidirectional wind in the DUBEVEG model (two aeolian transport directions) results in different dune patterns. The dunes, simulated by the model with the multidirectional wind, are smaller and closer together as shown in Figure 28 (left). Furthermore, Figure 28 (right) shows the difference in elevation (elevation of model results with multidirectional wind minus the elevation of the model results with the unidirectional wind). The foredune is receiving more aeolian sediment due to the second wind direction which is the yellow line (at least 4m elevation difference) at the bottom of Figure 28 (right).

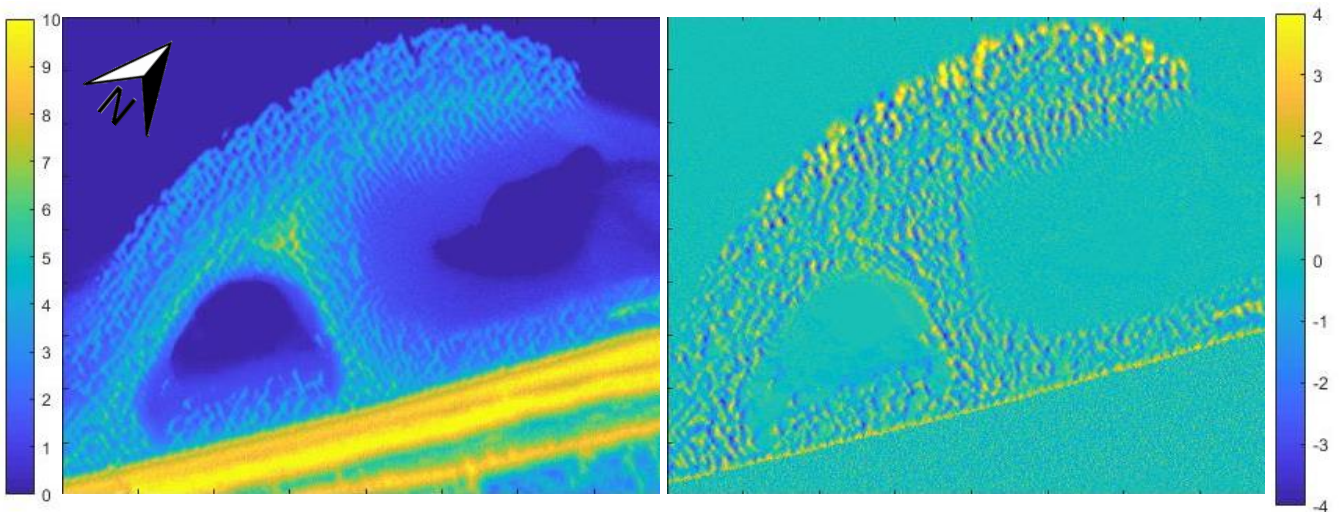


Figure 28, (left) model elevation results at $t = 6$ years with different wind directions and (right) a map of difference in elevation (elevation of model results with multidirectional wind minus the elevation of the model results with the unidirectional wind).

Furthermore, the vegetation is more spread over the Sand Motor area instead of densely vegetated rows of vegetation, which are simulated by the model with the unidirectional wind (aeolian transport in one direction). Figure 29 (left) are the locations of vegetation for multidirectional wind and Figure 29 (right) are the locations of vegetation for unidirectional wind (similar to Figure 16 (right)).

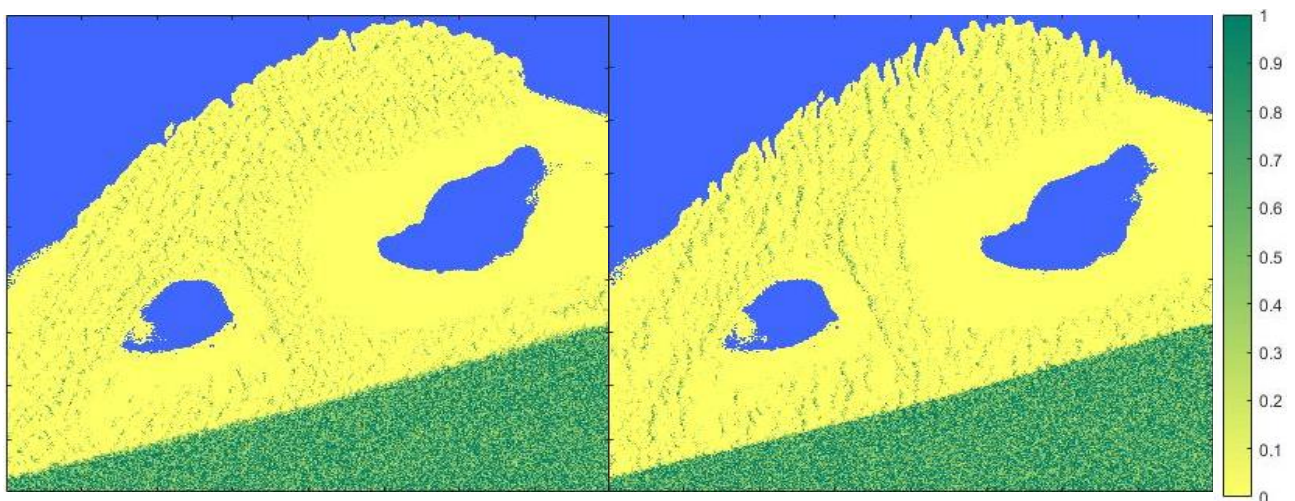


Figure 29, (left) modelled locations of vegetation at $t=6$ years for multidirectional wind and (right) the modelled locations of vegetation at $t=6$ years for unidirectional wind (similar with Figure 16 (right)). The blue colour is the area below MSL. Value one (green) means a fully vegetated cell and a value 0 (yellow) means a cell without vegetation.

All areas experience a decrease in the number of cells higher than the threshold when a second wind direction is included. Figure 30 shows the stacked bar plots for all areas of interest as described in chapter 2.4. The largest decrease in cells above the threshold due to the second wind direction is 48% for area 6. The smallest decrease, 11%, is for area 8. Furthermore, for all areas, the number of cells above the threshold is decreasing except the low dunes (0.5 - 1m) in area 5 which is increasing by 16% compared to the standard model results.

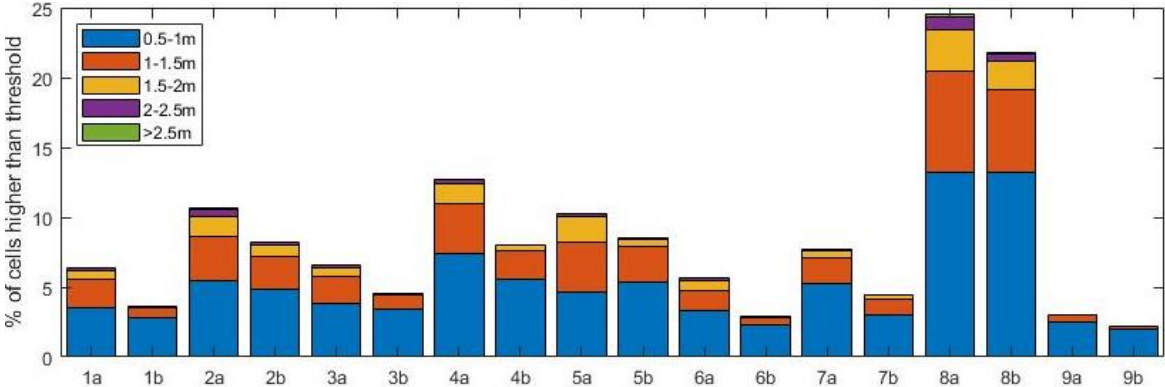


Figure 30, Stacked bar plot with results of the dune counting method for all areas (1-9). The letter 'a' is the final topography for standard model settings and the letter 'b' means the final topography for model settings including multidirectional wind.

Some areas experience a decrease in the number of cells with vegetation (area 2, 3 and 9) while most areas show an increase (area 1, 4, 5, 6, 7 and 8). Figure 31 shows the stacked bar plot of the vegetation for all areas of interest. The largest decrease in vegetated cells is 20% compared to the standard results for area 3. The largest increase in vegetated cells is in area 6 with 15%. Furthermore, for all areas except area 3, there is an increase in the number of cells with low vegetation (0 - 0.1% vegetated). The number of densely vegetated cells (0.3 -1% vegetated) is decreased for all areas.

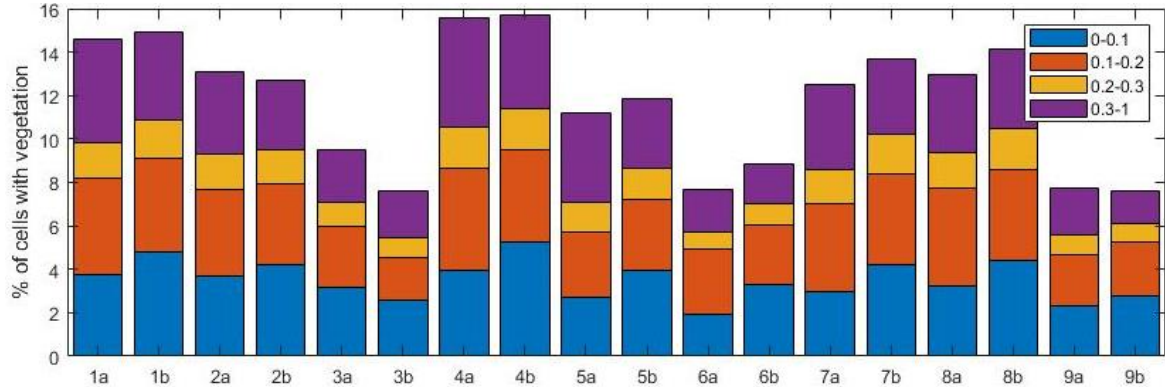


Figure 31, Stacked bar plot with results of the vegetation counting for all areas (1-9). The letter 'a' is the final vegetation for standard model settings and the letter 'b' means the final vegetation for model settings including multidirectional wind.

3.3.2 Beach armouring

In the second model revision, including beach armouring in the DUBEVEG model decreases the probability for aeolian erosion for armoured cells resulting in fewer dunes to develop with larger distances between them (Figure 32 left) and fewer vegetated cells (Figure 32 right). The final topography and vegetation cover including beach armouring is compared with the final topography and vegetation cover without beach armouring.

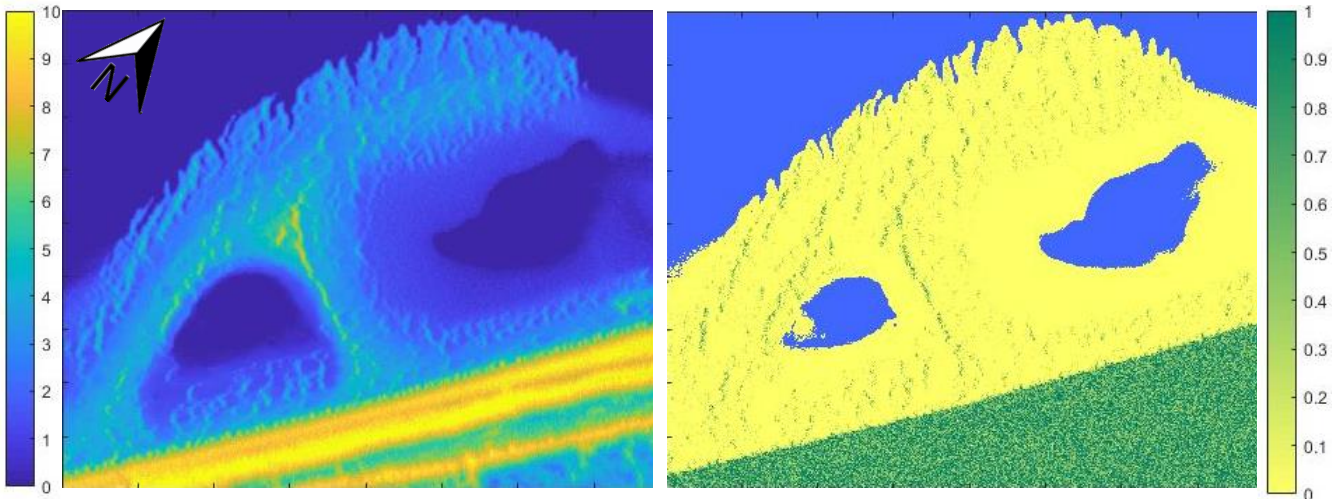


Figure 32, Model elevation results at $t = 6$ years with an armouring layer (left) and the vegetation at $t = 6$ years (right). The blue colour is the area below MSL. Value one (green) means a fully vegetated cell and a value 0 (yellow) means a cell without vegetation.

All areas experience a decrease in the number of cells higher than the threshold when armouring is included. Figure 33 shows the stacked bar plots for all areas of interest as described in chapter 2.4. The largest decrease in cells above the threshold due to armouring is 81% for area 1 and 6 and the smallest decrease, 16%, is for area 2 and 5. Although all areas experience a decrease in the number of cells above the threshold, the number of higher dunes (1.5m and larger) is increasing for the areas 2, 3 and 5.

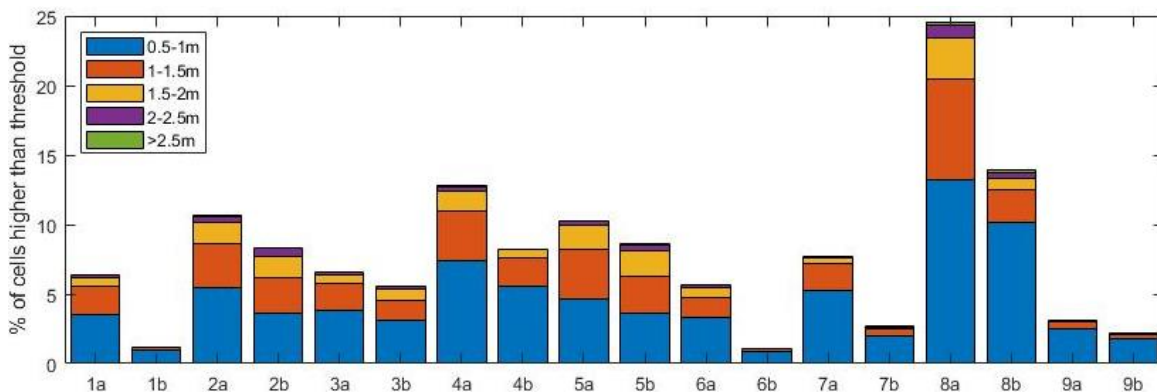


Figure 33, stacked bar plot with results of the dune counting method for all areas (1-9). The letter 'a' is the final topography for standard model settings and the letter 'b' means the final topography for model settings including armouring.

All areas experience a decrease in the number of cells with vegetation on it. Figure 34 shows the stacked bar plot of the vegetation for all areas of interest. The largest decrease in the number of cells with vegetation on it is in area 6 and 8 with 34% and 39% respectively compared to the standard model settings. The area with the lowest decrease in vegetation is area 5 with 12% compared to the standard model settings. Furthermore, all areas, except 3 and 5, have an increasingly low vegetation cover (0 -

0.1) caused by armouring. In all areas, the dense vegetation grade (0.2 and larger) is decreasing due to armouring.

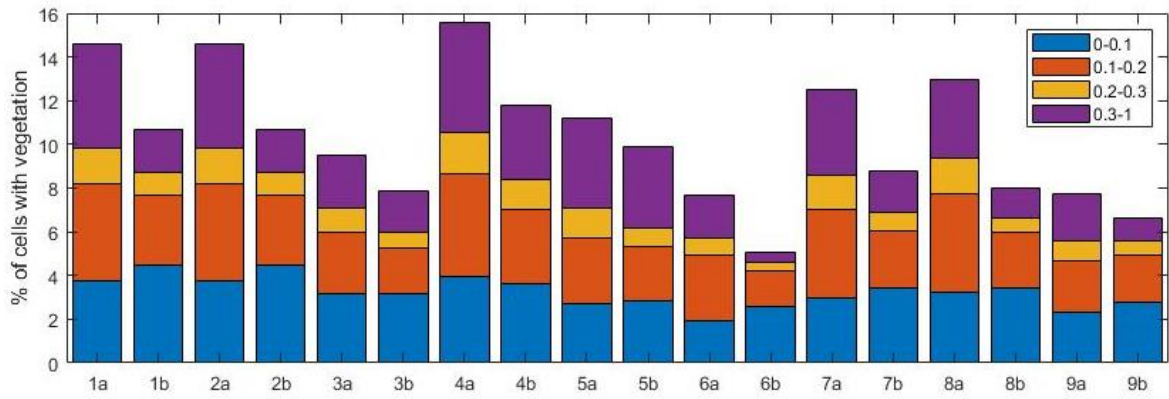


Figure 34, Boxplots with results of the vegetation counting for all areas (1-9). The letter 'a' is the final vegetation for standard model settings and the letter 'b' means the final vegetation for model settings including armouring.

4 Discussion

In this chapter, the results of the model adapted for an out-of-equilibrium anthropogenic shore are discussed followed by the results of the sensitivity analysis and the inclusion of additional physical processes to the model. The term out-of-equilibrium is discussed followed by the applicability of the DUBEVEG model for other shores. Furthermore, a discussion is added about the conclusions and model choices.

4.1 Discussion of the model adapted for an out-of-equilibrium anthropogenic shore

The Sand Motor area is not comparable with normal coastlines and shows a totally different morphological development (Hoonhout & de Vries, 2017a).

The foredune and the lake are lower elevated than the LIDAR measurements while the lagoon has a similar elevation. In the model, the lagoon receives sediment from aeolian transport but is forced to change by the hydrodynamic erosion and deposition conform to the reference surface, while the lake and foredunes only receive sediment from aeolian transport (Hoonhout & de Vries, 2017a).

A reason for the low sediment transport to the lake and foredunes is that the sediment does not travel as far as in the real situation. Consequently, the aeolian sediment source of the modelled dunes is always within the surrounding of the dune (Silva et al., 2017). For this reason, the size of the dunes in the model results is much larger than the observed dunes on the Sand Motor.

Another reason the model simulates large rows of dunes is the absence of beach armouring in the model. The sediment, which the Sand Motor is made off, is dredged offshore including non-erodible materials like shells, pebbles, cobbles and other materials (Hoonhout & de Vries, 2017b). These non-erodible materials can create a beach armouring when regular flooding is absent, causing a significant decrease in available sediment for aeolian transport (Hoonhout & de Vries, 2017a; Nolet et al., 2017). Beach armouring covers parts of the Sand Motor because a large part of the Sand Motor is elevated above the flooding level. If the armouring should not be on the Sand Motor, up to six times larger dunes should arise (Hoonhout & de Vries, 2017a).

Next to the dune development, there is less vegetation observed at the Sand Motor than simulated in the model. On normal beaches, without a lake, lagoon or elevated area higher than the water level, seeds and rhizomes are transported by wind and hydrodynamics (Hesp, 1989; Puijtenbroek, 2017). The largest part of the Sand Motor area cannot be reached by hydrodynamics resulting in vegetation expansion only by wind transport. Despite the lack of hydrodynamic transport of seeds and rhizomes in large parts of the Sand Motor, the probability of new pioneer species to arise is equal for the whole model area. Another reason for the overprediction of vegetation in the model is that people might destroy vegetation (Jackson & Nordstrom, 2013; Puijtenbroek, 2017). In the Sand Motor's design, recreation is taken into account (De Schipper et al., 2016). The areas De Hors and Terschelling, where Silva et al. (2017, 2018) and Keijsers et al. (2016) performed their DUBEVEG model, are less crowded with people compared to the Sand Motor but used the same vegetation parameters.

Next to dune development and vegetation cover, the hydrodynamic erosion simulated by the model is slower than observed in the real situation because only cells that are reached by the maximum water level including wave run-up are able to erode hydrodynamically. This process of hydrodynamic erosion is developed for dune erosion while the coastline of the Sand Motor is constantly eroding hydrodynamically and not only during storms. Nevertheless, this principle is used to force the coastline change of the Sand Motor in the model. To erode the high elevated area, the neighbouring cell(s) need to be eroded below the threshold for avalanching (more than three sand slabs difference with the neighbouring cell for unvegetated cells). After sufficient slabs have avalanched to the lower cells, the

previous cell, which was higher elevated than the water level, can now be reached by the hydrodynamics and can erode to the reference surface. This process is shown in Figure 35.

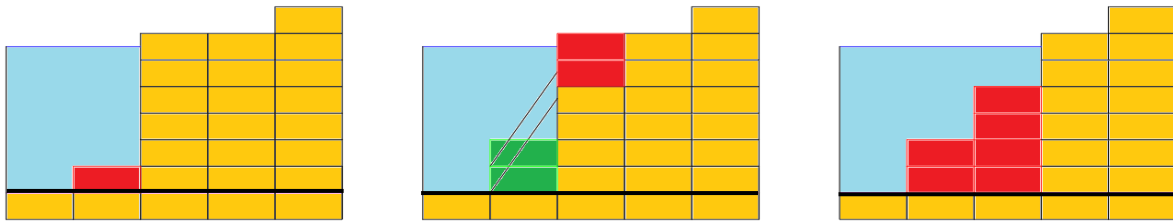


Figure 35, hydrodynamically erosion of cells elevated above the maximum water level including wave runup. The height of the sand slabs is multiplied five times for visibility. Left, the red sand slab is eroded by the hydrodynamics and forced to the reference surface level (thick black line). Middle, the elevation difference exceeds the threshold (three sand slabs) and avalanches to the lowest neighbouring cell. Right, the previous cell, which was elevated above the maximum water level, and the avalanched material erodes to the reference surface.

Furthermore, the number of iterations of the marine and avalanching model limit spatially the speed of the hydrodynamical erosion. Figure 36 shows the 0m-contour of the final results of model runs with a different number of marine iterations (calls of the hydrodynamic module) per model year. The model results are generated for 25, 50 and 100 marine iterations per model year which are compared with the LIDAR measurements. The LIDAR is the final topography observed in the field. The more marine iterations the closer the 0 m-contour in the model equals the LIDAR 0m-contour. By increasing the number of marine iterations from 25 to 100, the calculation time increases four times and still the LIDAR 0m-contour is not reached. The lagoon changes slower than the offshore side of the Sand Motor and shows at 25 marine iteration good equality with the LIDAR. To tackle the problem of the limited speed of hydrodynamic erosion, the areas of interest are chosen further away from the fast-eroding coastline.

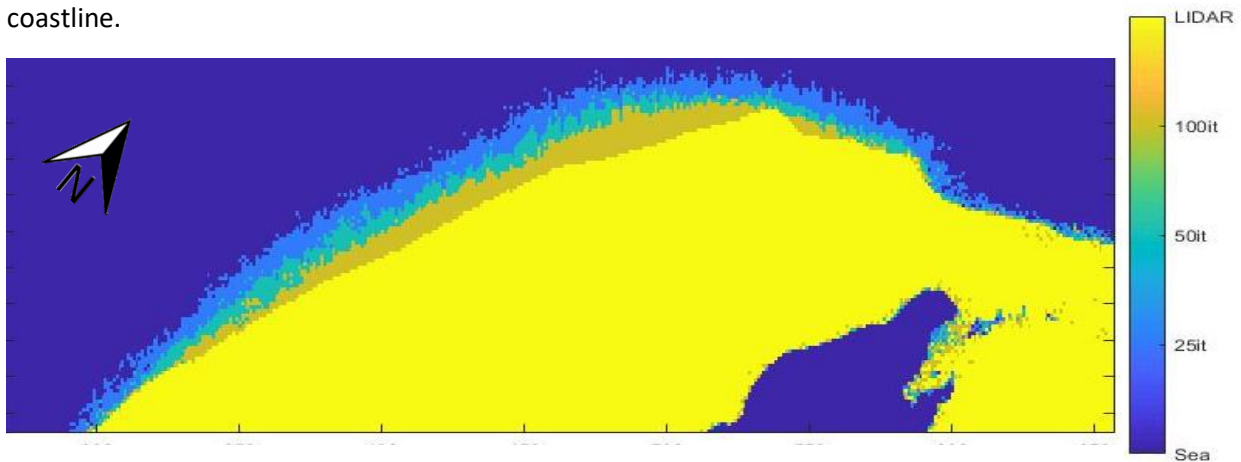


Figure 36, detail image of the most offshore part of the Sand Motor with a grid size of 5·5 m and 25, 50, 50 and 100 aeolian and marine iterations per model year. Colour transitions are at the 0m contour. The difference in 0m contour coastline is visible for each number of iterations. The calculations with this large number of hydraulic iterations are performed with a 5·5 m grid to significantly decrease calculation time compared to a grid of 1.25·1.25 m. It is assumed that the effect on coastline accuracy is similar for the grid size of 1.25·1.25 m.

The Sand Motor does not have a straight coastline but still, it is assumed that the maximum water level counts for the whole area. For a normal beach, like Keijsers et al. (2016), this approach valid. Although the dissipation decreases spatially, the maximum water level is not spatially dependent. The maximum water level consists of the highest water level in 2 weeks time including wave runup. The same value for wave runup is used at the offshore side and in the lagoon area. In real, the tidal forcing in the lagoon is diminished. In 2017, the tidal range was approximately 20 cm inside the lagoon (Hoonhout & de Vries, 2017a). Consequently, in the model, a larger area around the lagoon can be reached by the maximum water level resulting in more hydrodynamic erosion than is observed.

4.2 Discussion of the sensitivity analysis

In this subchapter, the results of the sensitivity analysis are discussed. First, the sensitivity analysis for the probability of erosion and deposition is discussed followed by the sensitivity analysis for the groundwater level and the pioneer vegetation expansion rate.

4.2.1 The probability of aeolian erosion and deposition

All areas of interest, except area 5, have the most cells larger than the threshold when the probability of erosion and deposition ($P_e P_d$) is large (Figure 21). Area 5 experiences maximum dune development at 75% of the $P_e P_d$ as registered by the dune counting described in chapter 2.4. However, the number of dunes increases at increased $P_e P_d$ values (as shown in Figure 37), but some dunes are lower and therefore not all cells with dunes are counted.

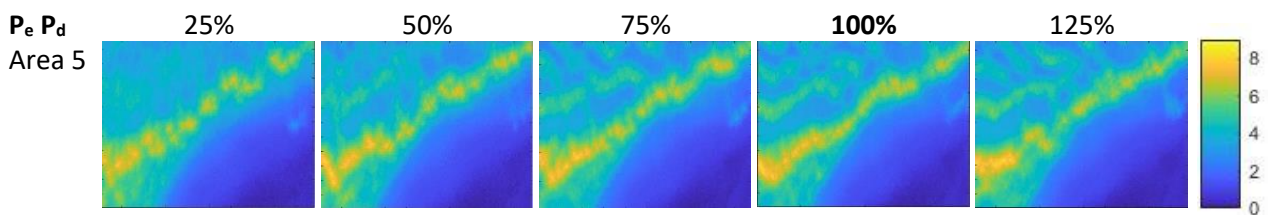


Figure 37, elevation plots of the adapted probability of erosion and deposition ($P_e P_d$) of area 5. These plots are equal to the plots in Appendix B. The percentages above the plots are the $P_e P_d$ values used with a standard value (100%) of P_e of 0.5 and P_d of 0.1.

Furthermore, area 7 shows an increase, decrease, increase and again decrease in the number of dunes above the threshold when increasing the $P_e P_d$ value (Figure 21) which cannot be explained right now. It is unknown whether this pattern is a coincidence due to the stochastic elements in the model or that a combination of processes (erosion/ deposition, vegetation, shadow zones) causes this increasing/ decreasing trend. Multiple model runs of these values need to indicate if this decrease, increase, decrease pattern is coincidence or a combined process that is very sensitive to the erosion/burial rate in this area.

Next to the counting issue of area 5, area 8 is miscalculated as well. The number of cells above the threshold for this area is not correct because the majority of these cells are no dunes. It is known that the hydrodynamic erosion in the DUBEVEG model lags behind the real situation for highly elevated coasts. In area 8, the model predicts dunes, but the smoothed LIDAR map shows that 34% of the area is hydrodynamically eroded and lowered further than the threshold for dunes as shown in Figure 38. The model is counting the cells in the area that are hydrodynamically eroded in the LIDAR but not in the model as dunes if the difference is larger than the threshold.

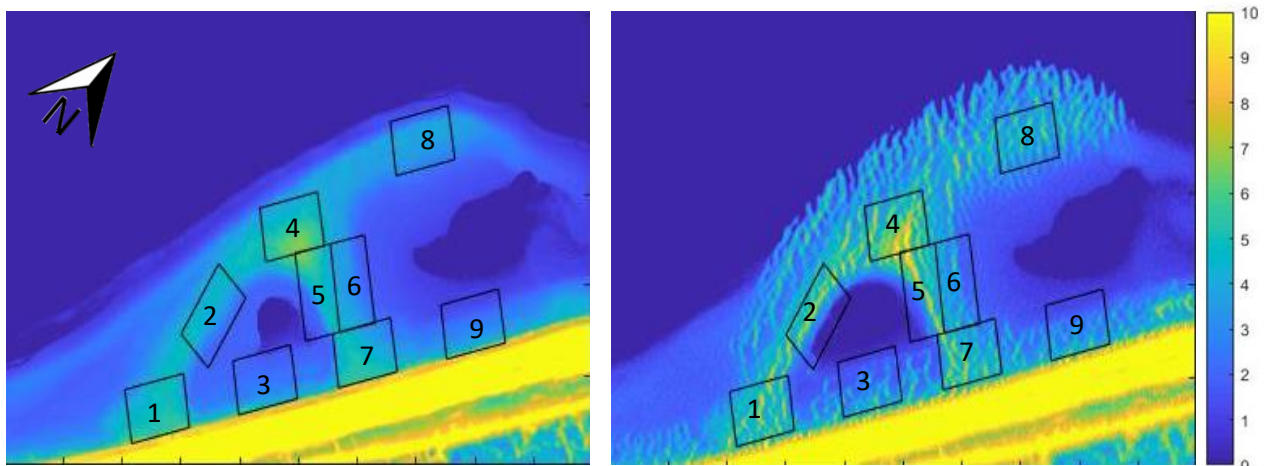


Figure 38, areas of interest at the end of the model time. Results are the LIDAR map (left) and the model results (right).

Next to the counting issues of the model results, the observed elevation in 2017 for areas 1, 3, 7 and 9 have much more cells above the threshold than the other areas. This is caused by the growing foredune at the LIDAR map entering these areas of interest. Figure 38 (left) shows that one boundary line of the areas 1, 3, 7 and 9 is positioned at the foredune while this is not the case in the model results Figure 38 (right). The plots of the foredune entering the areas of interest 1, 3, 7 and 9 are visible in Figure 39.

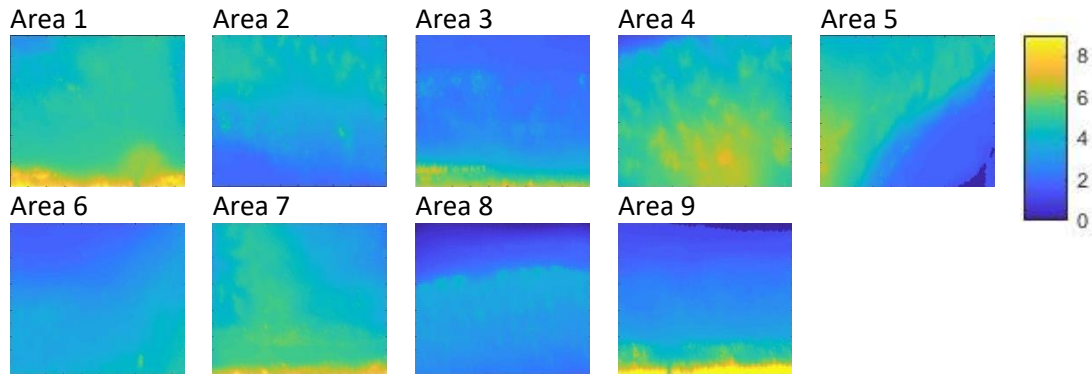


Figure 39, elevation of the areas of interest in February 2017 (equal to the plots of February 2017 in Appendix B). These plots are close-ups of Figure 38 (left)

Additionally to the elevation, the number of vegetated cells is dependent on aeolian sediment input. In general, all areas experience a maximum number of vegetated cells which is caused mainly by the erosion/ burial tolerance of the vegetation based on Keijsers et al. (2016). The higher elevated areas have more vegetation than the lower elevated areas. The groundwater level limits the available sediment for aeolian transport and this effect is higher for low lying areas resulting in less favourable growing conditions for vegetation. Furthermore, area 6 and 9 are subject to hydrodynamical erosion capable of removing vegetation.

4.2.2 The groundwater level

In the model, the number of slabs available for aeolian transport is influenced by the groundwater level as shown in Figure 24. The number of slabs available for aeolian transport is larger in highly elevated areas. The difference in the number of slabs between different groundwater levels is larger for high elevated areas as well. The decrease in the number of cells elevated above the threshold is accelerated for high (0.8 and larger) groundwater levels for the highly elevated areas because larger groundwater levels start to significantly limit the high elevated areas (Figure 40). The lower elevated areas are influenced at lower groundwater levels.

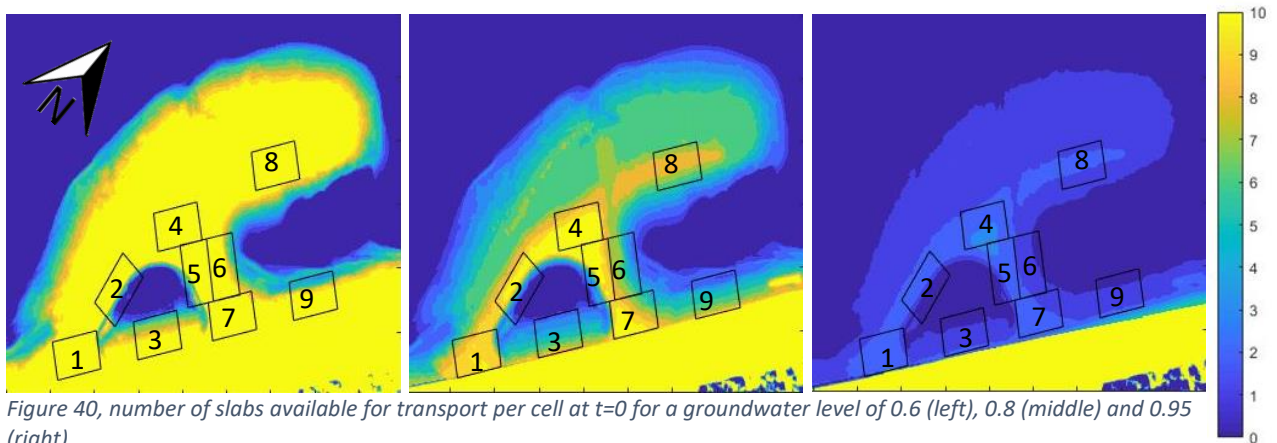


Figure 40, number of slabs available for transport per cell at $t=0$ for a groundwater level of 0.6 (left), 0.8 (middle) and 0.95 (right).

In contradiction with the other areas, area 2 has a similar number of cells above the threshold for all different groundwater levels and an increase in dune height for higher groundwater levels (Figure 41, left). The elevation maps of area 2 in Figure 41, (right) show that at lower groundwater levels more sediment is transported into the lake. The surface below 0m for a groundwater level of 0.6 is 16% and for a groundwater level of 0.9 is 22% of the total surface of the area. The LIDAR map shows that the lake is filling up with sediment and contains no elevation measurements below the 0 m contour in area 2 at the end of the model time. For this area, all sediment that is blown into the lake is not counted as cells above the threshold, because the threshold is higher elevated due to the observed lake infill.

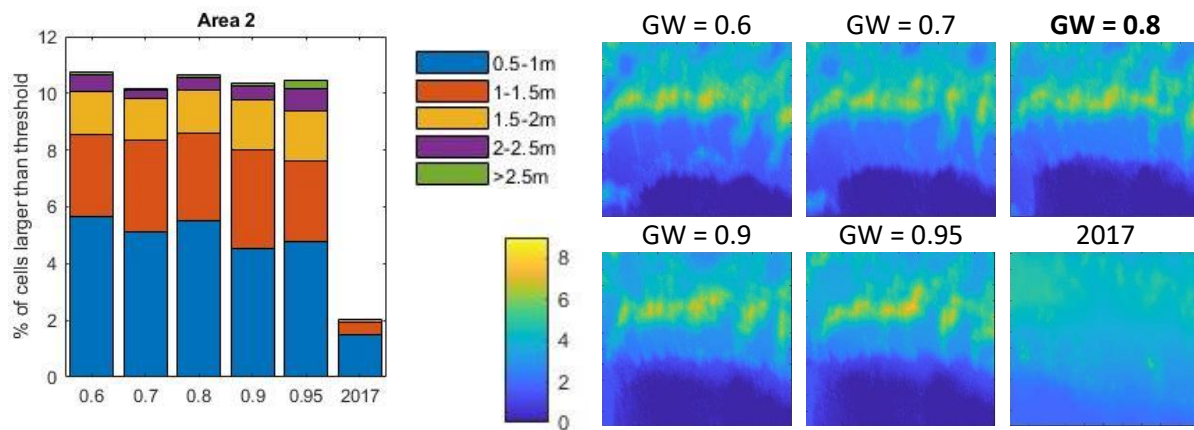


Figure 41, (left) stacked bar plot of the percentage of cells larger than the threshold and (right) six plots of model results of area 2 with different groundwater levels (0.8 is the standard value) and the observed dune development in February 2017. The lowest elevated area at the bottom of every plot is part of the lake. Lower groundwater levels result in more sediment infill in the lake (the dark blue area (0m level) is smaller). The observed lake infill in February 2017 is larger than the model simulates. The plots in this figure are equal to the plots in Appendix D.

Next to the elevation is the vegetation in area 2 responding differently to the groundwater level than other areas (Figure 24, left). Although the total number of cells with vegetation in area 2 decreases, the density of vegetation increases at the high elevated part of this area (Figure 42, left). Figure 42 (right) shows that the area where vegetation is growing withdraws from the lake direction (the bottom of the plots) when the groundwater level is increasing. The density of vegetation is increasing because of a better erosion/ burial ratio for these cells at high groundwater levels. Increased vegetation traps more sediment preventing it from travelling to the lake.

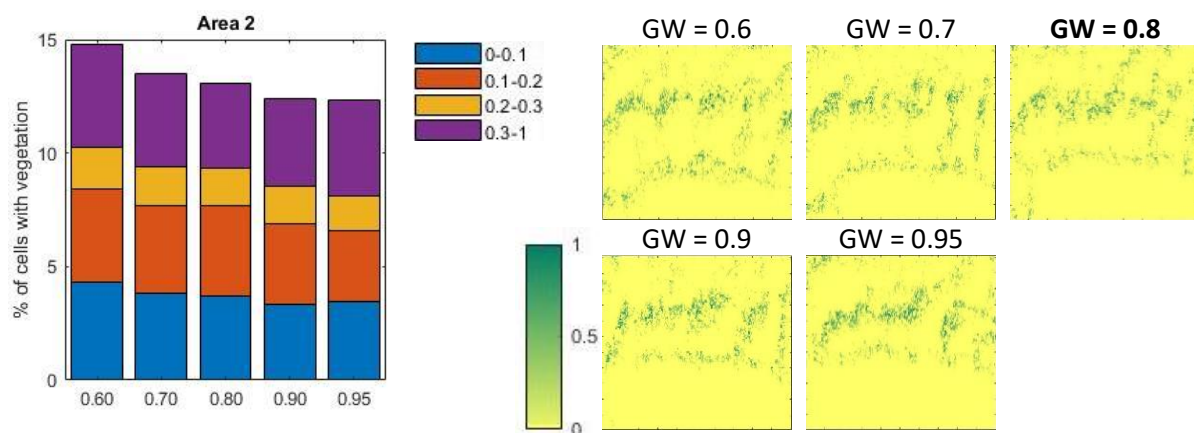


Figure 42, (left) stacked bar plot of the percentage of cells with vegetation larger than the threshold. (right) Five plots of model vegetation results of area 2 with different groundwater levels (0.8 is the standard value). The bottom part of the vegetation plots is the lake area. The plots in this figure are equal to the plots in Appendix E.

4.2.3 The pioneer vegetation expansion rate

At the pioneer vegetation expansion rate ($p_{\text{establish}}$) of 50%, there is a decrease in the number of cells higher than the threshold for area 6, 7, 8 and 9 (Figure 27 and Figure 43). It is unknown if this is a coincidence because of the stochastic parameters in the model or that is a combination of processes decreasing the number of dunes at only this $p_{\text{establish}}$ of 50%. Performing multiple model runs with the $p_{\text{establish}}$ of 50% would clarify if it is a coincidence.

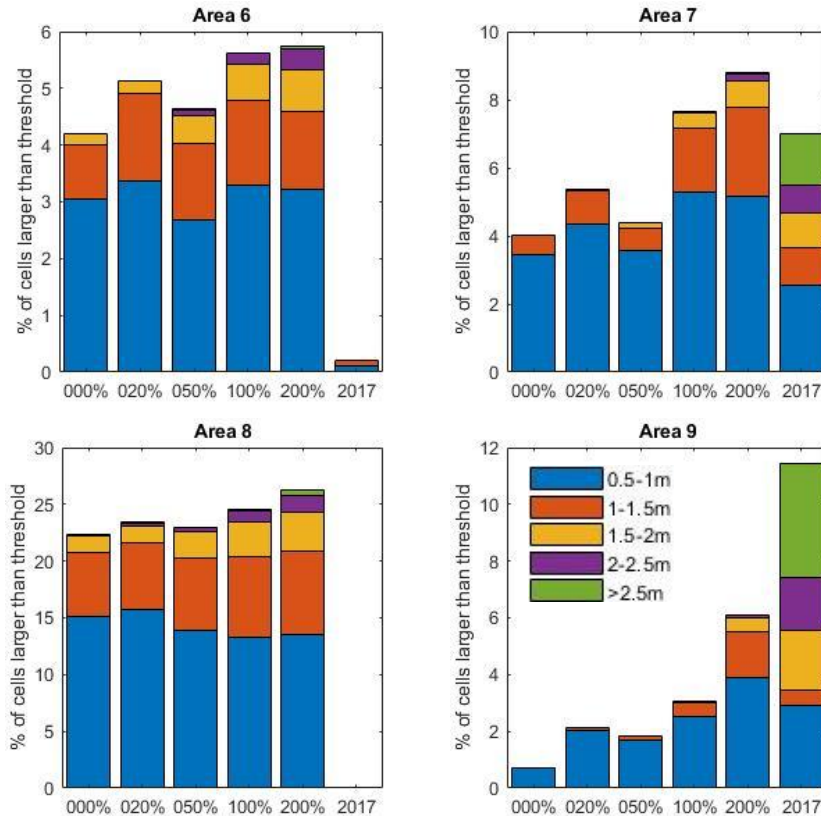


Figure 43, stacked bar plots of area 6, 7, 8 and 9 with a drop in the percentage of cells larger than the threshold at a $p_{\text{establish}}$ of 50%. The plots in this figure are equal to the plots in Appendix F.

4.3 Discussion of including additional model revisions to the model

4.3.1 Multidirectional wind

In the DUBEVEG model, an aeolian eroded slab of sand can only move in a straight line in the direction of the wind. Consequently, in the Sand Motor case, only the slabs of sand eroded below the black line in Figure 44 left are in the model able to reach the foredunes when applying one wind direction because of the almost shore-parallel wind direction. The aeolian eroded slabs of sand above this line are trapped in the lake (only between the grey lines), lagoon or the sea when travelled sufficient distance without depositing. Therefore, a varying wind direction significantly changes the area size that theoretically is able to supply sediment to the foredunes or the lake.

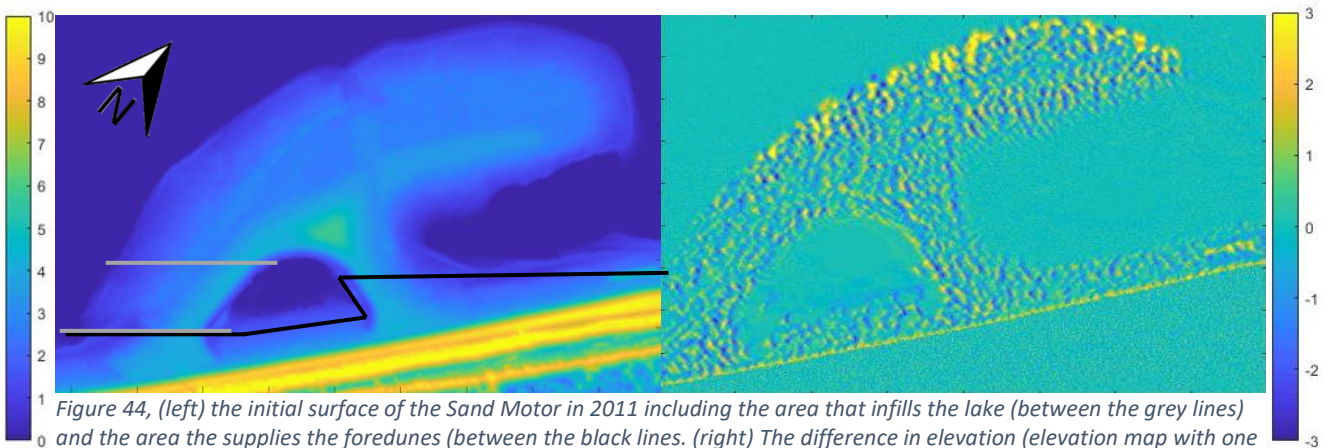


Figure 44, (left) the initial surface of the Sand Motor in 2011 including the area that infills the lake (between the grey lines) and the area that supplies the foredunes (between the black lines). (right) The difference in elevation (elevation map with one wind direction minus the elevation map with two wind directions).

Adding a second wind direction to the model is not the same as rotating the map and using a unidirectional wind in the direction of the average transport of the two wind directions. At a unidirectional wind, dune rows will emerge perpendicular to the wind direction while two wind directions result in shorter and lower dune rows closer to each other in multiple directions. In the Werner model (Werner, 1995), a precursor of the DUBEVEG model, eroded slabs of sand could move in two directions during the same model iteration to mimic a unidirectional wind not parallel or perpendicular to the grid (Nield and Baas, 2008). Test simulations of Nield and Baas (2008) showed that this approach resulted in different dune shapes compared to rotating the map and using one transport direction. It is more realistic that sand transport is in one direction during an iteration. In this research, it is not meant to create a unidirectional wind by adding multiple transport directions, but to discover the difference in dune patterns with two wind directions.

Furthermore, the DECAL algorithm of Nield and Baas (2008) calculates one random cell without replacements at the time for erosion while the DUBEVEG model calculates all cells at once, making it impossible to have multiple transport directions. There has to be an order which slab of sand moves first to deposit at a location, changing the topography including shadow zones for a next slab to be deposited. Areas fulfilling the shadow zone criteria for one wind direction might not fulfil the criteria for another wind direction.

Although there are many assumptions and simplifications made, (for example: neglecting the other quadrant wind measures, averaging the wind measures to a quadrant, not including seasonal/ monthly wind directions) including a second wind direction changes the dune rows in size and orientation which is more realistic in an area where a multidirectional wind is very common.

The lake and lagoon side of the areas do receive less aeolian sediment input at the model simulation with multidirectional wind than the model simulation with the unidirectional wind, decreasing the number of cells with vegetation on it because of less favourable erosion/ burial conditions. Because of the multidirectional wind, the average transport direction of the sediment is rotated more perpendicular to the foredunes. As a consequence, area 3 has the largest sediment input shortage because the lake does not supply aeolian sediment below the MSL. Furthermore, area 9 has an aeolian sediment input shortage because the lagoon is in the direction of the wind. However, the lagoon is forced to fill up according to the reference surface and supports some aeolian sediment for area 9.

Although area 3 and 9 have a decrease in vegetated cells because of the multidirectional wind, most areas experience an increase in the number of vegetated cells. The aeolian sediment is more spread into multiple dunes instead of a few dune rows which results in more locations with an optimal burial/erosion rate for vegetation to grow and therefore, the number of cells with vegetation increases in these areas.

4.3.2 Beach armouring

Although many assumptions are made for including beach armouring in the DUBEVEG, the effect of it on dune development is significant. There are fewer sand slabs moving resulting in fewer dunes to develop due to sediment shortage. This is mostly in the highly elevated areas of interest where armouring occurs more often (Figure 45).

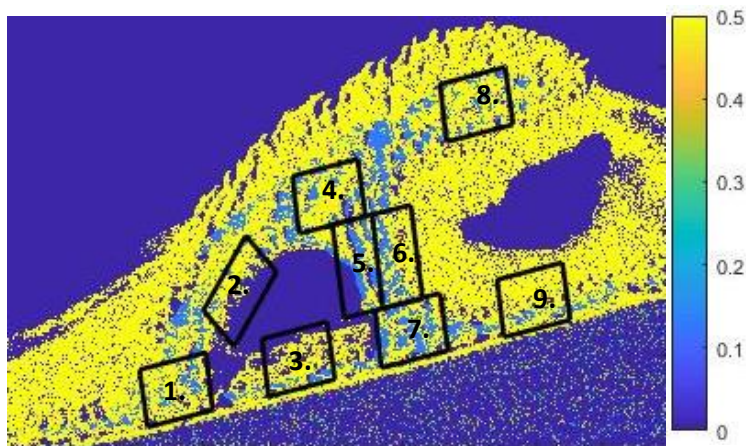


Figure 45, The aeolian erosion probability map at $t = 6$ years including the areas of interest. The maximum probability of erosion is 0.5 and armouring 0.125. Dense vegetated areas or areas below MSL have a decreases probability of aeolian erosion.

4.4 General discussion

The Sand Motor is an out-of-equilibrium coast that transforms over time to an equilibrium coast. An equilibrium coast is a straight coast with a stable beach profile over time. The longshore difference in hydrodynamic erosion and deposition of sediment change the coastline towards an equilibrium. The Dutch coast at the location of the Sand Motor is strictly speaking not in equilibrium because of a receding coastline due to sea level rise. This is the reason that the Sand Motor is built. The change in the coastline of the Sand Motor is significantly faster than the coastline retreat because of sea level rise and therefore the Sand Motor is called 'out-of-equilibrium'.

The applicability of the DUBEVEG model for different (out-of-equilibrium anthropogenic) shores than the Sand Motor depends on requirements. To model out-of-equilibrium shores, measurements of future changes in elevation are needed to create the reference surface. With this surface, the hydrodynamic erosion can force the coastline change in the model. Furthermore, at the moment it is not possible to model (for any shore) hard structures and the corresponding effect on aeolian erosion and deposition.

If someone else would have done this research, he or she would most likely have similar conclusions for the aeolian transport distance, the fast-changing coast that is lagging behind compared to the observed measurements, the effect of multidirectional wind, armouring and the vegetation distribution. First, the parameter used in this research for the probability of aeolian deposition is based on Keijsers et al. (2016) and used by (Silva et al., 2017). Using an unsupported other value for the parameter is not likely. Second, the coastline would definitely lag behind when the hydrodynamic erosion is based on only the storm surges regardless of the number of hydrodynamic iterations used. Third, the effect of multidirectional wind would result in similar dune patterns and not in large dune

rows which were simulated by using unidirectional wind in the model. Fourth, the effect of including armouring would reduce dune development. The severity of the reduction in dune developments might differ significantly based on the assumptions made for the locations and effect of beach armouring. Fifth, the pioneer vegetation distribution is based on Keijsers et al. (2016) and using a different value is unsupported. Based on the sensitivity analysis, the probability for pioneer vegetation expansion does not influence the dune patterns but only the height of the dunes.

Furthermore, someone else could choose another grid size, slab height, differ in the number of aeolian iterations or the wind direction. First, the grid size should not be smaller than 1m because it results in a fundamental change in the dynamics of the vegetation growth and individual vegetation elements resulting in different unexpected landforms (Nield & Baas, 2008). A grid size of 1.44 is the maximum grid size with the parameters used for sediment flux, aeolian erosion and deposition, the minimum number of aeolian iterations and still fulfilling the slab height conform (Nield & Baas, 2008) as described in 2.3.1. Second, the number of aeolian iterations could be increased, increasing the calculation time, but it did not result in different dune patterns during the test for the number of hydraulic and aeolian iterations at 5.5 m grid size. Third, a different wind direction might be chosen based on the amount of measured sediment transport in a direction instead of the time of the wind direction. Consequently, when applying unidirectional wind the dune rows that are simulated are perpendicular to the chosen wind direction.

5 Conclusions

The goal of the research is 'To assess and improve the applicability of the DUBEVEG model for an out-of-equilibrium anthropogenic shore. Three research questions are formed to guide the study towards the objective. The conclusion will be given per research question and for the objective.

5.1 The extent that the observed dune formation patterns at an out-of-equilibrium anthropogenic shore like the Sand Motor can be simulated by the model

The cellular automata model DUBEVEG (DUne BEach VEGetation) is applied for the out-of-equilibrium anthropogenic shore the Sand Motor. The model results show different dune development, aeolian deposition locations and vegetation locations compared to the LIDAR measurements of actual dune development. The model simulates rows of dunes perpendicular to the wind direction while the LIDAR measurements do not show these dune patterns. The observed vegetation occurs mainly near the foredune and around the lake, while the model simulates vegetation all over the Sand Motor.

Furthermore, the aeolian transport distance in the model is low and for this reason, the aeolian sediment source of the modelled dunes is always within the surroundings of the dune. Consequently, the lake, lagoon and foredunes receive less aeolian sediment compared to the LIDAR measurements.

The hydrodynamic erosion in the model is slower than in the observed situation. In the model, the change in coastline is forced by hydrodynamic erosion based on the highest water level in two weeks (storm surges). However, the coastline of the Sand Motor is subject to constant hydrodynamic erosion and not only erosion by storm surges because the coast is out-of-equilibrium. A spatial difference in longshore erosion and deposition causing the Sand Motor to return to the equilibrium coast, a straight coastline.

5.2 The dominant parameters explaining modelled dune formation patterns at the Sand Motor

A sensitivity analysis is performed to get an understanding of the dominant parameters influencing dune development. The parameters that are used in the sensitivity analysis are the combined probability of aeolian erosion and deposition ($P_e P_d$), the groundwater level and the pioneer vegetation expansion rate. The sensitivity analysis for the combined $P_e P_d$ shows that more dunes, but of similar elevation, develop at a higher $P_e P_d$. The effect of $P_e P_d$ for the number of dunes is relatively small compared to the groundwater level. The sensitivity analysis for the groundwater level shows that increasing the groundwater level results in a decrease in the number and elevation of dunes. The dune development of low elevated areas is more influenced by the groundwater level because the sediment available for aeolian transport is limited. The effect on dune elevation is relatively small compared to the pioneer vegetation expansion rate. The sensitivity analysis for the pioneer vegetation expansion rate shows that increasing the pioneer vegetation expansion rate results in an increase in the height of the dunes but the locations of these dunes are similar and not influenced. Vegetation decreases the probability of aeolian erosion, increases the aeolian deposition and stabilises the sediment by allowing steeper angles of repose. For this reason, the simulated dunes can increase in height.

5.3 Conclusions of including additional physical processes to the model

Two model revisions are tested for their influence on the dune development on the Sand Motor. The first model revision is multidirectional wind and the second model revision is beach armouring. In the standard model, unidirectional wind (one aeolian transport direction) is applied. Beach armouring is relevant for this area because large parts of the Sand Motor are elevated above the storm surge level. The lack of hydrodynamic erosion causes the beach armouring to limit the sediment supply available for aeolian erosion.

In the first model revision, including multidirectional wind in the DUBEVEG model (two aeolian transport directions) results in different dune patterns and vegetation that is more spread over the Sand Motor area compared to simulation with the unidirectional wind. The dunes, simulated by the model with the multidirectional wind, are smaller and closer together compared to the model results with the unidirectional wind. The results of the simulation with multidirectional wind are more realistic because the dune patterns are closer to observations than the rows of dunes simulated by the model with the unidirectional wind.

In the second model revision, including beach armouring in the DUBEVEG model decreases the probability for aeolian erosion for armoured cells. In the model, beach armouring occurs only at the high elevated areas of the Sand Motor resulting in fewer dunes to develop on these highly elevated areas with larger distances between the dunes and fewer vegetated cells.

5.4 The applicability of the DUBEVEG model for out-of-equilibrium anthropogenic shores like the Sand Motor

This research shows that it is possible to implement a forced coastline by hydrodynamics, beach armouring and multidirectional wind in the DUBEVEG model, but improvements can be made in future research. The DUBEVEG model in the current form is not applicable for the out-of-equilibrium anthropogenic shores like the Sand Motor because processes are missing. However, including multidirectional wind (aeolian transport directions) and beach armouring in the model result in a better approach to the observed dunes. Assumed is that improvements in these processes would further increase the approach of the observed dune patterns and increase the applicability of the DUBEVEG model for out-of-equilibrium anthropogenic shores.

Advances of the DUBEVEG model is that complex processes (hydrodynamic erosion, aeolian sediment transport and vegetation development) are partly replaced by stochastic parameters decreasing the computation time significantly compared to computational fluid dynamic (CFD) models. The DUBEVEG is very flexible since many rules in the model can be easily adapted which is needed for implementing out-of-equilibrium anthropogenic shores.

6 Recommendations

This research shows that it is possible to implement a forced coastline by hydrodynamics, beach armouring and multidirectional wind in the DUBEVEG model, but improvements can be made in future research. First, the aeolian transport distance of sediment needs attention because the sediment is not transported far enough, similar to Silva et al. (2017). Second, continuous hydrodynamic erosion needs to be implemented to erode an out-of-equilibrium coast constantly instead of only with storm surges. Third, details for groundwater and armouring need to be implemented in the model to increase the accuracy of dune development. Currently, there is no difference between aeolian erosion of sediment close above or far above the groundwater level while sediment close to the groundwater level is more likely to be wet and harder to erode (Silva et al., 2017). Furthermore, the armouring simulated in this research is based on multiple assumptions while field measurements of the locations, time and effect of armouring would increase the accuracy of modelling the spatial probability of aeolian erosion.

Thinkable improvements in the hydrodynamic adaptations to model an out-of-equilibrium anthropogenic shore are to the hydrodynamic erosion and the water levels. First, if the elevation value of a cell in the reference surface is below the MSL, the cell is forced to that value. This might solve the problem of cells elevated above the maximum water level that cannot erode directly, but only indirectly by avalanching. However, the hydrodynamic erosion probability in the model should not change for dunes. A second thinkable improvement is about water levels. Spatially difference in water levels including wave runup would result in more accuracy in the area that is exposed to hydrodynamic erosion. This might be achieved by spatially combining wave dissipation and wave runup.

No model simulations are performed in this study with both beach armouring and multidirectional wind. Assumed is that combine those processes would increase the approach of the observed dune formations.

References

- Arriaga, J., Rutten, J., Ribas, F., Falqués, A., & Ruessink, G. (2017). Modeling the long-term diffusion and feeding capability of a mega-nourishment. *Coastal Engineering*, *121*, 1-13.
- Baas, A. C. (2002). Chaos, fractals and self-organization in coastal geomorphology: simulating dune landscapes in vegetated environments. *Geomorphology*, *48*(1-3), 309-328.
- De Schipper, M. A., De Vries, S., Ruessink, G., De Zeeuw, R. C., Rutten, J., Van Gelder-Maas, C., & Stive, M. J. (2016). Initial spreading of a mega feeder nourishment: Observations of the Sand Engine pilot project. *Coastal Engineering*, *111*, 23-38.
- Dean, R. G. (1984). Water wave mechanics for engineers and scientists. *Advanced series on ocean engineering*, *2*, 353.
- Du Pont, S. C. (2015). Dune morphodynamics. *Comptes Rendus Physique*, *16*(1), 118-138.
- Durán, O., & Herrmann, H. J. (2006). Vegetation against dune mobility. *Physical review letters*, *97*(18), 188001.
- Essink, G. H. O., & Bierkens, M. F. (2016). Fresh groundwater resources in a large sand replenishment. *Hydrology and Earth System Sciences*, *20*(8), 3149.
- Hesp, P. A. (1989). A review of biological and geomorphological processes involved in the initiation and development of incipient foredunes. *Proceedings of the Royal Society of Edinburgh, Section B: Biological Sciences*, *96*, 181-201.
- Hoonhout, B., & de Vries, S. (2017a). Aeolian sediment supply at a mega nourishment. *Coastal Engineering*, *123*, 11-20.
- Hoonhout, B., & de Vries, S. (2017b). Field measurements on spatial variations in aeolian sediment availability at the Sand Motor mega nourishment. *Aeolian Research*, *24*, 93-104.
- Jackson, N. L., & Nordstrom, K. F. (2013). Aeolian sediment transport and morphologic change on a managed and an unmanaged foredune. *Earth Surface Processes and Landforms*, *38*(4), 413-420.
- Keijsers, J., De Groot, A., & Riksen, M. (2016). Modeling the biogeomorphic evolution of coastal dunes in response to climate change. *Journal of Geophysical Research: Earth Surface*, *121*(6), 1161-1181.
- Luijendijk, A. P., Ranasinghe, R., de Schipper, M. A., Huisman, B. A., Swinkels, C. M., Walstra, D. J., & Stive, M. J. (2017). The initial morphological response of the Sand Engine: A process-based modelling study. *Coastal Engineering*, *119*, 1-14.
- Mulder, J. P., & Tonnon, P. K. (2011). "Sand Engine": Background and design of a mega-nourishment pilot in the Netherlands. *Coastal Engineering Proceedings*, *1*(32), 35.
- Nield, J. M., & Baas, A. C. (2008). Investigating parabolic and nekha dune formation using a cellular automaton modelling approach. *Earth Surface Processes and Landforms*, *33*(5), 724-740.
- Nolet, C., van Puijenbroek, M., Suomalainen, J., Limpens, J., & Riksen, M. (2017). UAV-imaging to model growth response of marram grass to sand burial: Implications for coastal dune development. *Aeolian Research*.
- Nordstrom, K. F., Jackson, N. L., Korotky, K. H., & Puleo, J. A. (2011). Aeolian transport rates across raked and unraked beaches on a developed coast. *Earth Surface Processes and Landforms*, *36*(6), 779-789.
- Oceanservice. (2013, January 22, 2013). LIDAR-light Detection and Ranging- is a remote sensing method used to examine the surface of the Earth.
- Puijenbroek, M. E. B. v. (2017). *Dunes above and beyond. The interaction between ecological and geomorphological processes during early dune development.* (PhD thesis), Wageningen University, Wageningen, The Netherlands.
- Rijkswaterstaat. (2016). *LIDAR Elevation, Coast.*
- Ryu, W., & Sherman, D. J. (2014). Fore dune texture: Landscape metrics and climate. *Annals of the Association of American Geographers*, *104*(5), 903-921.
- Shoremonitoring. (2017). *Zandmotor Topographic Survey, actual surveyed path.*

- Silva, F. G., Wijnberg, K. M., de Groot, A. V., & Hulscher, S. J. (2017). On the importance of tidal inlet processes for coastal dune development.
- Silva, F. G., Wijnberg, K. M., de Groot, A. V., & Hulscher, S. J. (2018). The influence of groundwater depth on coastal dune development at sand flats close to inlets. *Ocean Dynamics*, 1-13.
- Stive, M., De Schipper, M., Luijendijk, A., Ranasinghe, R., Van Thiel De Vries, J., Aarninkhof, S., . . . Marx, S. (2013). *The sand engine: A solution for vulnerable deltas in the 21st century?* Paper presented at the Coastal Dynamics 2013: 7th International Conference on Coastal Dynamics, Arcachon, France, 24-28 June 2013.
- Stockdon, H. F., Holman, R. A., Howd, P. A., & Sallenger Jr, A. H. (2006). Empirical parameterization of setup, swash, and runup. *Coastal Engineering*, 53(7), 573-588.
- Tonnon, P., Huisman, B., Stam, G., & van Rijn, L. (2018). Numerical modelling of erosion rates, life span and maintenance volumes of mega nourishments. *Coastal Engineering*, 131, 51-69.
- Van der Weerd, A. J., & Wijnberg, K. M. (2016). Aeolian sediment flux derived from a natural sand trap. *Journal of coastal research*, 75(sp1), 338-342.
- Werner, B. (1995). Eolian dunes: computer simulations and attractor interpretation. *Geology*, 23(12), 1107-1110.
- Zandmotor (2016). The Sand Motor Five years of Building with Nature [Youtube]. In *a*. <https://www.youtube.com/watch?v=1ASvcZdrO5A&t=1s1>: b.

Appendix A: An extensive description of the calculation steps in the DUBEVEG model.

A.1. Aeolian transport module

In this subchapter, the processes regarding aeolian transport are described with the help of flowcharts. First, the shadow zones are described followed by the aeolian erosion map and the aeolian deposition map. With this information, the change in elevation and the actual elevation including avalanching can be calculated.

First of all, the flowchart (Figure 46) shows how the DUBEVEG model builds a shadow map. A threshold step limit between neighbouring cells is calculated based on the shadow angle and cell size. There is no need for a step limit for diagonal cells because the sand slabs are transported in one direction (direction of the wind) and are not influenced by diagonal cells. The grey box in the flowchart is the logical question if the step limit is larger than the allowed step limit. When this is the case the cell is in a shadow zone (resulting in a value 1) and if the question is negative the cell is not in the shade (resulting in a value 0).

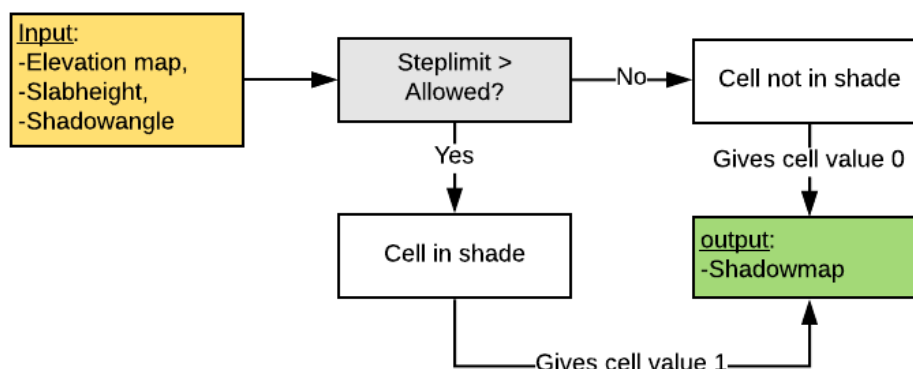


Figure 46, a flowchart of how the model locates the shadow zones.

Second, the flowchart in Figure 47 shows how the aeolian erosion map is determined. Vegetation cover captures sand particles with its root system (Durán & Herrmann, 2006). When a certain vegetation grade (C_{lim}) is present in an area this area cannot erode (Keijsers et al., 2016). A value 0 means no vegetation at all and a value 1 means fully vegetated. Furthermore, sand slabs cannot erode when located in a shadow zone defined in the shadow map. Aeolian transport on the beach decreases when the level of moisture is higher (Nolet et al., 2017; Nordstrom, Jackson, Korotky, & Puleo, 2011). In the model, aeolian erosion cannot take place below sea level or below the groundwater level (Silva et al., 2017). The groundwater level is defined in the model as an elevation to the reference surface (Silva et al., 2017). If the area fulfils all requirements the probability of erosion is calculated by the erosion probability (defined in chapter 2.3.1) multiplied by one minus the vegetation effectiveness. This results in an erosion probability map ranging from zero (no erosion) to the maximum erosion probability (P_e).

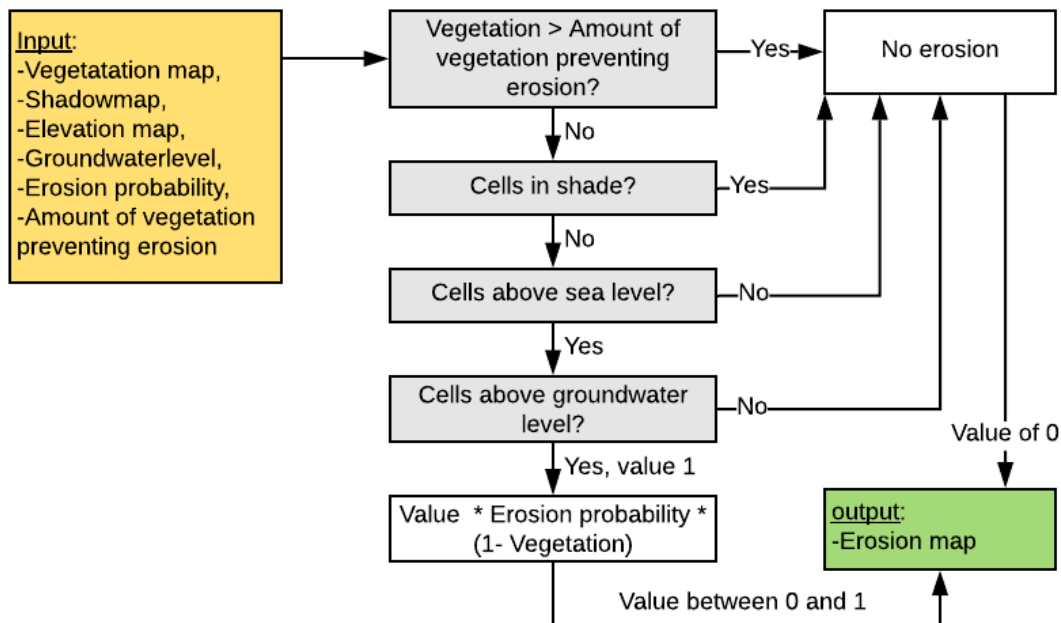


Figure 47, a flowchart of how the model obtains the erosion probability map.

Third, aeolian sedimentation is described as a wind speed reduction reducing the forcing effects on the particles in movement causing them to settle. The flowchart in Figure 48 describes how the model builds a deposition probability (P_d) map. Wind speed in an area is reduced by obstacles causing a wind shelter behind them called shadow zones. (Hesp, 1989). In the model, the shadow zones are defined by the shadow map resulting in a deposition probability of one for cells in the shade. Next to the elevation, the vegetation is an important factor for the probability of deposition. Vegetation is an obstacle for aeolian transport because the plants themselves reduce the wind speed (Hesp, 1989; Puijenbroek, 2017; Ryu & Sherman, 2014). The higher and denser the plants the larger the effect of the wind speed reduction around them (Puijenbroek, 2017). In the model, a denser vegetated area increases the deposition probability. This probability is calculated by one minus the probability of deposition times the vegetation plus the probability of deposition.

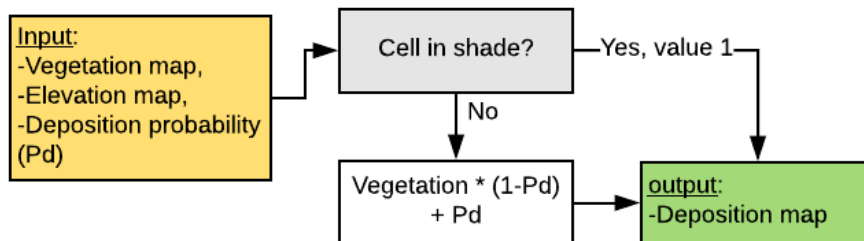


Figure 48, a flowchart of how the model builds a deposition probability map.

Fourth, the aeolian erosion and deposition probability maps are described and are used to calculate the change in elevation. The slab jump length (J), the number of cells a sand slab moves each time, and a random field between zero and one are needed to calculate the change in elevation as shown in Figure 49.

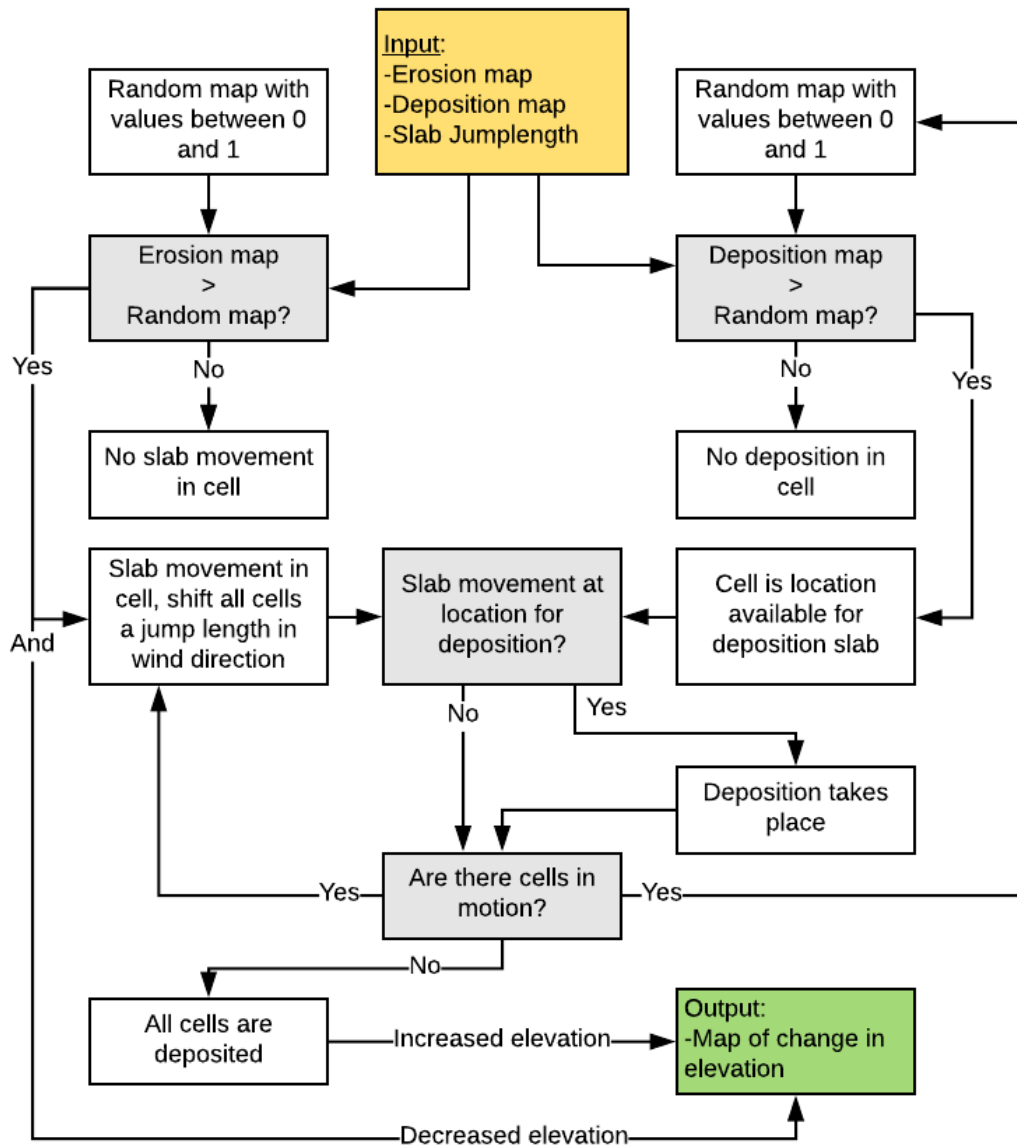


Figure 49, a flowchart of how the model calculates the aeolian change in elevation.

The first logical question is to determine in which areas (cells) the deposition/ erosion is larger than the random values. If the random number for a certain cell is larger than the predefined probability no slab deposition/ movement takes place in that cell. If the random erosion value is larger than the predefined probability there is slab movement, which means that the sand slab is transported one jump length in the wind direction. Physically, this can be seen as moving particles in saltation or creeping motion. Next to the movement, the decrease in elevation in the cell where the slab is transported is reported in the output map of change in elevation. If the deposition map has in an area a higher value than the random map, this cell is a location suitable for a slab to deposit. The next logical question is if there is a slab movement at a location for deposition. A positive answer leads to deposition of a slab of sand in that cell. A negative answer leads to (I) again the steps of creating a random map and the logical question if the predefined deposition probability is higher than the random map and (II) the slab movement of one jump length in the wind direction followed by the logical question if the moved slab has reached a location to deposit. This continues until all slabs have been deposited which results in a map of change in elevation.

Fifth, aeolian transport and hydrodynamic erosion can transform the elevation in an area such that the angle of repose is exceeded (θ_b for unvegetated cells and θ_v for sufficiently vegetated cells), causing an avalanche. The angle of repose is determined in chapter 2.3.2. The avalanche module in the DUBEVEG model is shown in the flowchart in Figure 50.

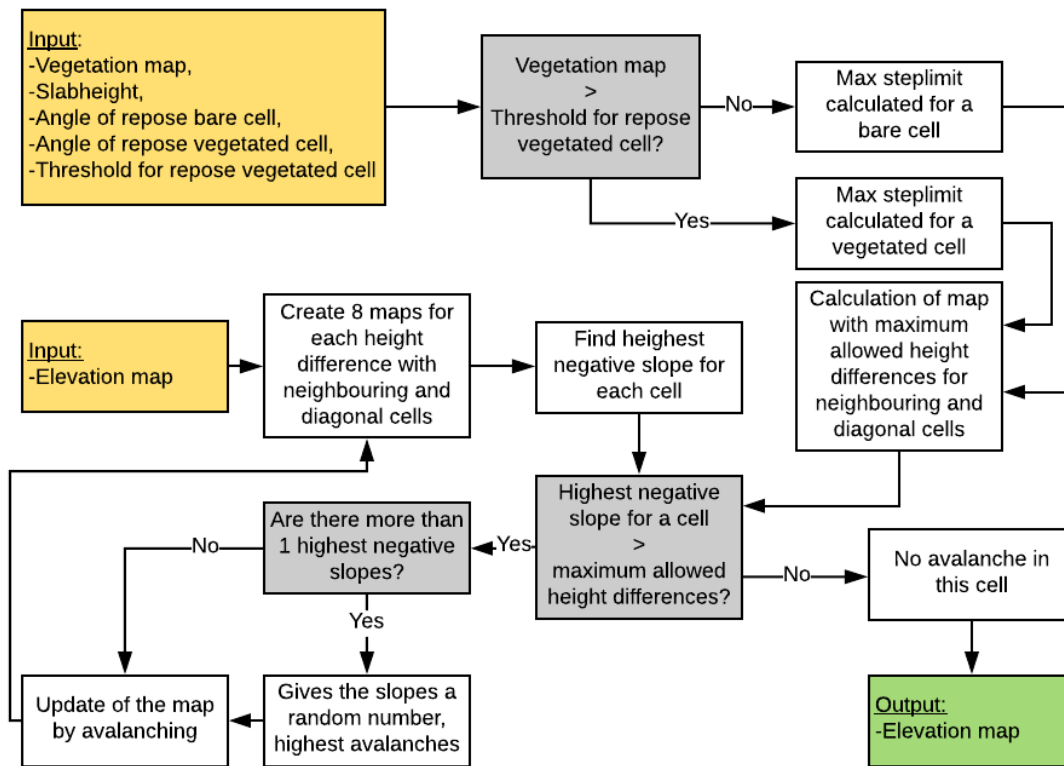


Figure 50, a flowchart of how the model determines the new elevation map due to avalanching.

The first logical question is if the vegetation effectiveness in a cell is larger than the threshold. Due to the vegetation establishment the stability of the sand increases which allows steeper slopes (Keijsers et al., 2016). This is incorporated in the model by a steeper angle of repose for cells with vegetation effectiveness larger than the threshold (T_{veg}). After the determination of which angle of repose is used for a cell, the maximum allowed elevation difference between neighbouring cells and diagonal cells is calculated. Then, for each cell, the elevation difference for neighbouring and diagonal cells are determined and the highest negative slope is selected. The logical question for each cell is if the highest negative slope for the cell is larger than the maximum allowed height differences. When this is not the case no avalanching will happen. At a positive answer, the following question is if there are more than one highest negative slopes. A negative answer leads to avalanching from the current cell to the lowest neighbouring or diagonal cell. When there are more the same steepest slopes, a random number chooses which one receives the avalanching material. After the avalanching again the height differences for neighbouring cells and diagonal cells is determined followed by the question is the slopes are too steep. This continues until all slopes are smaller than the allowed maximum slope resulting in an update of the elevation map. This avalanching process is exactly the same after the marine process.

A.2. Hydrodynamic module

In this subchapter, the processes regarding hydrodynamics are described with the help of flowcharts. First, the formula for wave runup is described followed by the formula for the dissipation, wave strength and probability of erosion due to waves. The probability of hydrodynamic erosion combined with the minimum probability of erosion is calculated followed by the probability for hydrodynamic beach update resulting in a new elevation map.

First, for calculating the maximum water level the highest water level recorded in this period is used in the model (Keijsers et al., 2016) combined with the wave runup based on Stockdon et al. (2006). The formula is used for calculating the 2% exceedance value of wave runup peaks on all natural beaches under extreme dissipative conditions:

$$\text{Wave runup} = 0.043\sqrt{(H_0L_0)} \quad (2.1)$$

wherein H_0 is the deep-water wave height and L_0 is the deep-water wavelength (Stockdon et al., 2006). This formula (2.1) is used when the beach is subject to extreme dissipative conditions when the Iribarren number (ξ) is smaller than 0.3 (Stockdon et al., 2006):

$$\xi > b\sqrt{(H_0/L_0)} \quad (2.2)$$

wherein b is the foreshore slope, which is 1:50 in the Sand Motor area (De Schipper et al., 2016).

Second, in the model, the dissipation is the only factor that brings a difference in hydrodynamic erosion probabilities for inundated areas. Without the dissipation factor in the probabilities of erosion, the complete inundated area should always erode. The formula for calculating the dissipation in the model is:

$$\text{Dissipation} = \frac{L}{h} - \frac{L}{h_0} \quad (2.3)$$

Wherein L is the cell size, h the water depth in the current cell and h_0 is the offshore water depth which depends on the deep-water wave length. This formula is valid at values larger than zero because for water depths greater than the offshore water depth the dissipation is zero. Dissipation starts when the wave has interaction (energy loss) with the bottom which happens when the offshore wave leaves the deep water region and enters the intermediate water depth region. The intermediate depth starts at the wave length divided by 2 (Dean, 1984).

Third, with the total dissipation values calculated, the wave strength is calculated with the following formula:

$$\text{Wave strength} = 0.012 * h \quad (2.4)$$

Wherein h is the water depth. The probability of erosion due to a wave (P_{wave}) is calculated with the formula:

$$P_{\text{wave}} = (h_{\text{max}} - 0.012 * \text{Total dissipation}) \text{ Wave strength} \quad (2.5)$$

Wherein h_{max} is the maximum erosive strength of waves. In this formula values smaller than zero are set to zero. The total dissipation for each cell and the wave strength are calculated above.

Fourth, due to very shallow water depths near de beaches and in the lagoon the dissipation strength is very high resulting in zero erosion change in these areas. Hydrodynamic erosion or deposition does happen in these areas because the topography is changing over time caused by hydrodynamic forces. To adapt the model a minimum erosive strength of waves ($P_{\text{wave_min}}$) is added for areas that (I) have a

smaller probability of erosion due to waves (P_{wave}) than the P_{wave_min} and (II) have a lower elevation than the maximum water level and (III) are not sheltered (as shown in the flowchart in Figure 51). The P_{wave_min} value has overwritten the P_{wave} values in the areas near the beach and the Hydrodynamic erosion now is possible in these areas.

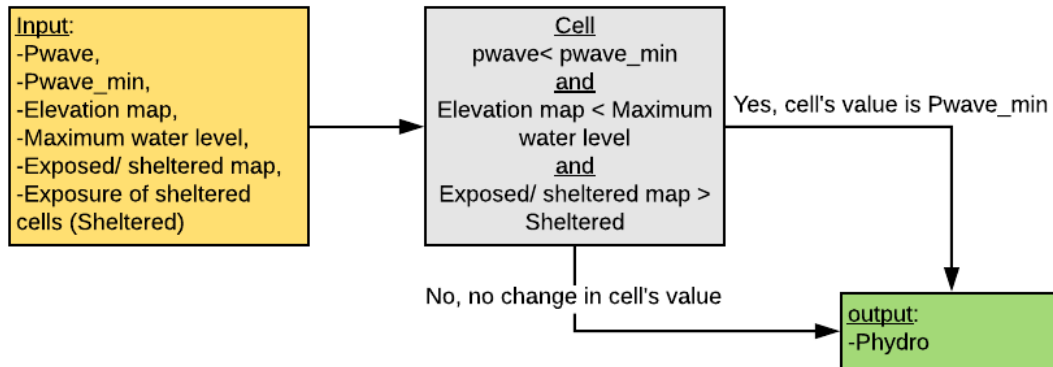


Figure 51, a flowchart of how the model calculates the probability of hydrodynamic erosion ($Phydro$).

Fifth, to update the beach in the model three maps are used, namely the $P_{exposed}$ map (described in chapter (2.2.4, Figure 9), the P_{hydro} map and a map for the effectiveness of vegetation against erosion (P_{veg}). The P_{veg} is calculated with the formula:

$$P_{veg} = 1 - 0.5 * \text{Effective vegetation map} \quad (2.6)$$

This formula gives a map with probabilities of erosion with a maximum of one (no vegetation effect) and the value of the vegetation resistance for hydrodynamics (see chapter 2.3.2) for a complete vegetated cell. The probability map of hydrodynamic beach update ($P_{beachupdate}$) is calculated with the formula:

$$P_{beachupdate} = P_{veg} * Phydro * P_{exposed} \quad (2.7)$$

Sixth, to update the beach elevation profile due to hydrodynamic erosion or accretion four maps are needed. The first map needed is the elevation map which is in the first model iteration a LIDAR map of the area (the initial profile) and after that the elevation map of the previous model iteration. The second map needed is the probability map of hydrodynamic beach update ($P_{beachupdate}$). The third map needed is the reference surface elevation map described in chapter 2.2.2. Finally, a map of random values is needed to stochastically update the beach elevation. In the flowchart in Figure 52 is described how the model determines the new beach elevation level. The first logical question is if the random cell is smaller than the same cell in the $P_{beachupdate}$ map. A negative answer leads to no change in elevation and a positive answer leads to an elevation update in that cell. This update is done by setting the elevation of the cell to the elevation of the reference surface. The process mimics the erosion or accretion of the sea. After the beach elevation update, the avalanching module is called.

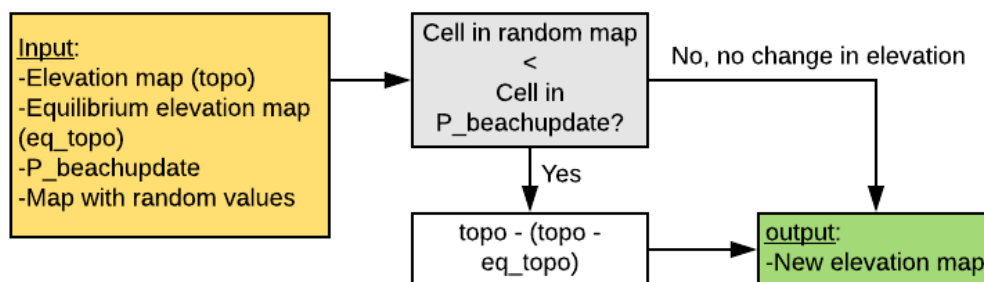


Figure 52, a flowchart of how the model determines the new elevation.

A.3. Biotic module

In this subchapter, the model processes regarding vegetation are described with the help of flowcharts. First, the flowchart of how the model determines lateral expansion followed by lateral expansions and final vegetation growth.

First, the flowchart in Figure 53 explains how the model determines lateral expansion. All possible locations for lateral expansion ($p_{lateral}$) are determined which are all four neighbouring cells of an already vegetated cell. All cells suitable for lateral expansion are given the probability value for lateral expansion. If in a cell the probability for lateral expansion is larger than the random value obtained from a random map, lateral expansion in this cell is possible.

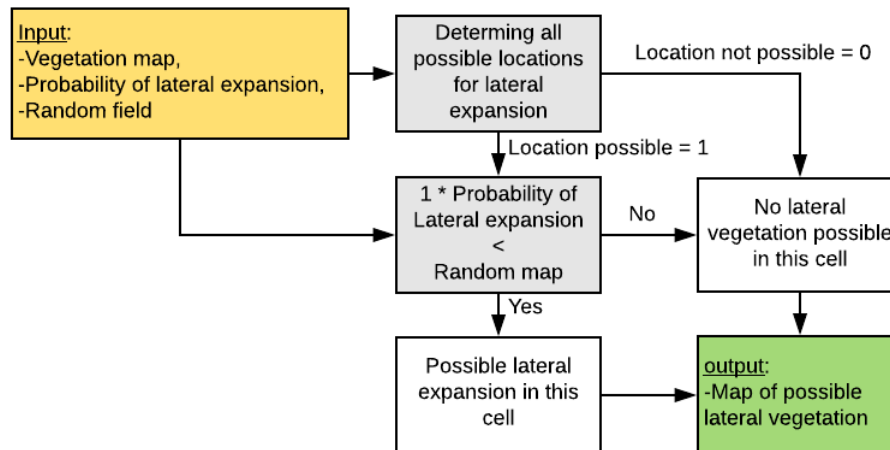


Figure 53, Flowchart of how the model determines the lateral expansion of vegetation

Second to the lateral expansion, the pioneer species in the model can expand as a pioneer as well ($p_{establish}$). This mimics the expansion of vegetation by seeds or rhizomes transported by wind or sea. In the flowchart in Figure 54 is explained how the model determines pioneer vegetation. Pioneer vegetation cannot settle in low lying areas below sea level (for example the lake or lagoon). The pioneer location is stochastically determined with the help of random values. If the random value in a cell is smaller than the probability of expansion there is a possible location for pioneer vegetation.

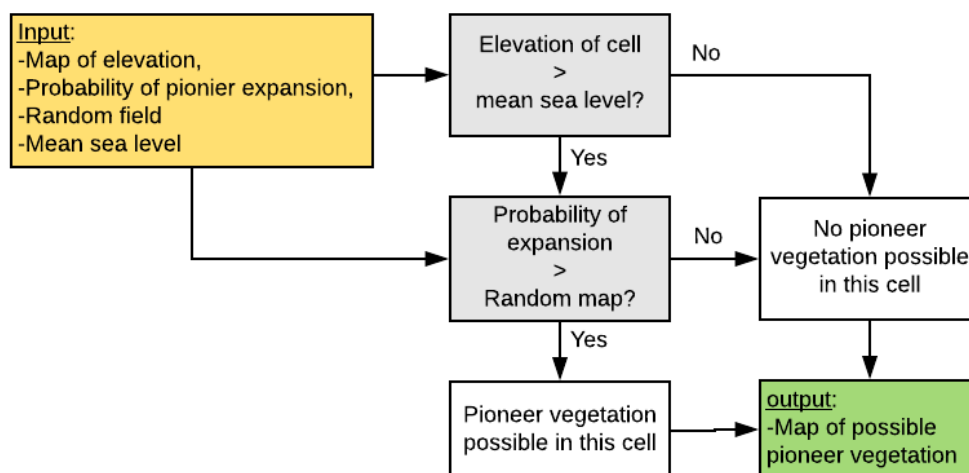


Figure 54, a flowchart of how the model determines the pioneer vegetation.

Third, the flowchart of how the model determines vegetated growth or decay of one species is shown in Figure 55. First, the growth rate of vegetation in each cell in the area is determined based on the growth curves and the sedimentation/ erosion rate. For the vegetation loss, the negative growth is

subtracted from the previous vegetation. Vegetation growth depends on the locations of lateral and pioneer expansions and the previous vegetated. If a cell is already fully vegetated the vegetation cannot increase. Second, the new vegetation density in a cell for one species is the previous vegetation plus the vegetation growth minus the vegetation loss. The vegetation density is then multiplied with the probability of hydrodynamical erosion to give the final new vegetation density of one species.

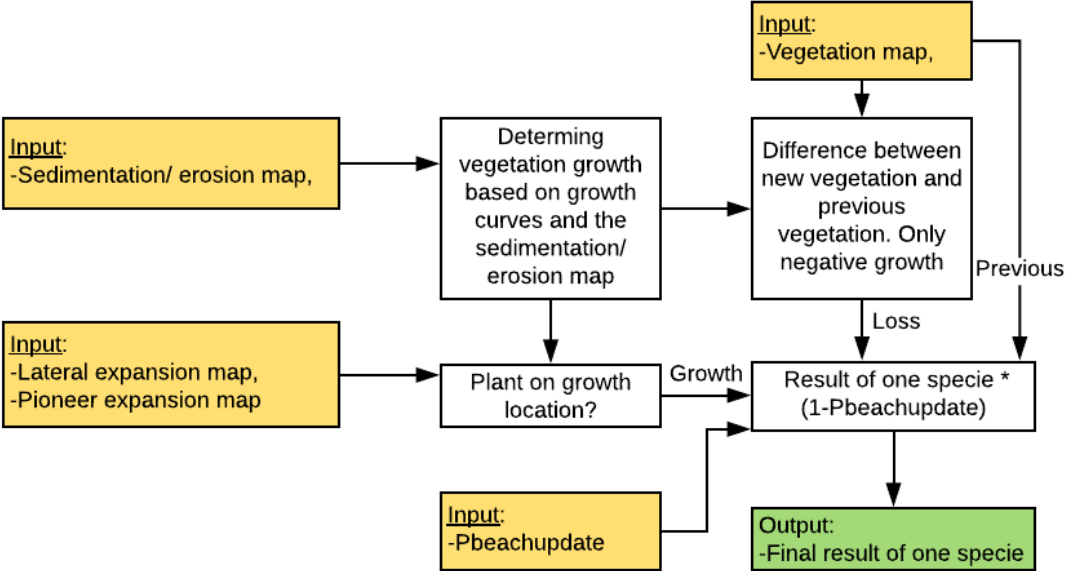


Figure 55, a flowchart of how the model determines growth or decay of one species.

Previous steps are done for both vegetation species. Each species cannot have a higher vegetation density than one and not a lower vegetation density than zero. The density of both species is added and, if necessary, reduced to the maximum density value of one.

Appendix B: Elevation plots and stacked bar plots of the adapted probability of erosion and deposition ($P_e P_d$)

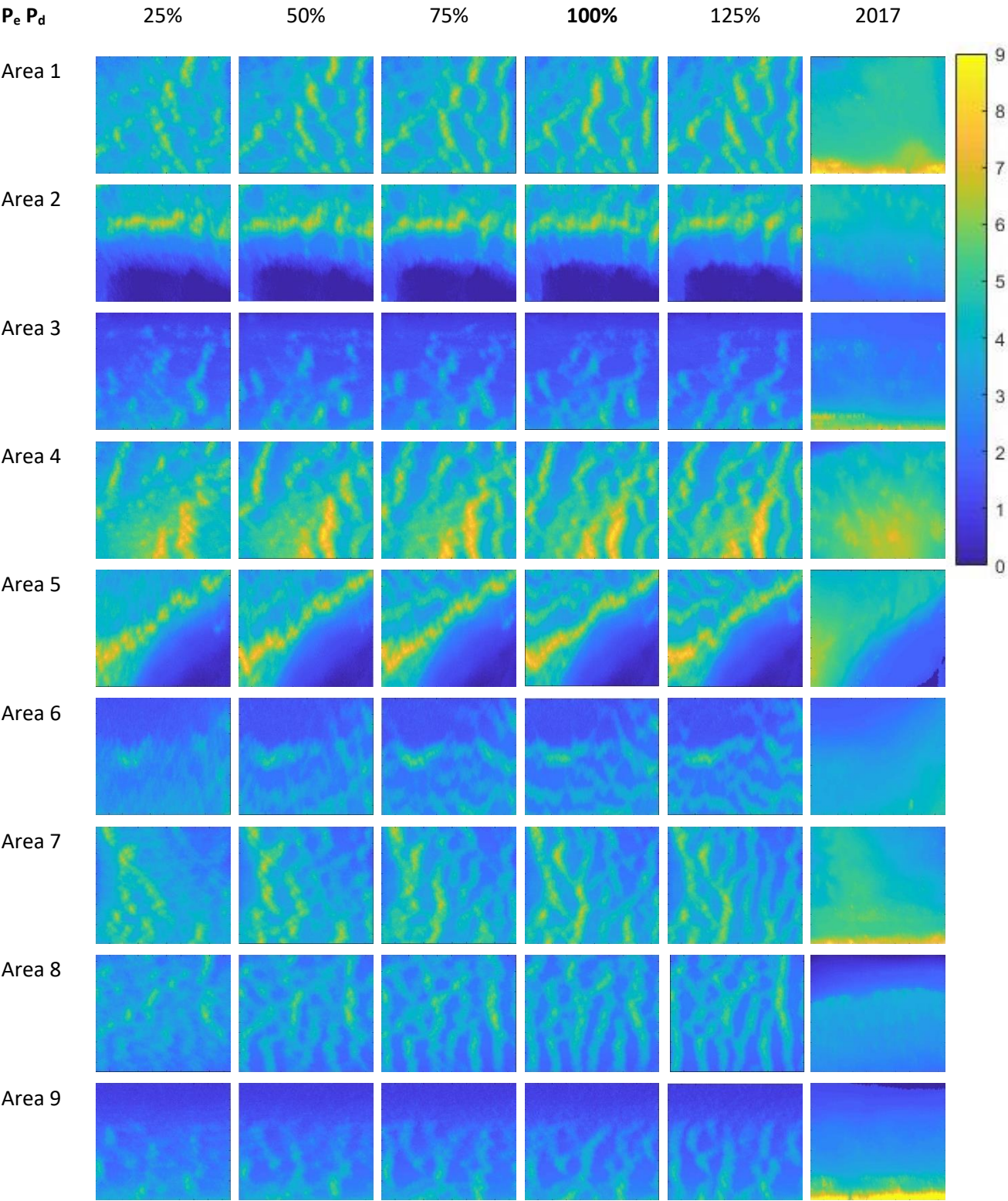
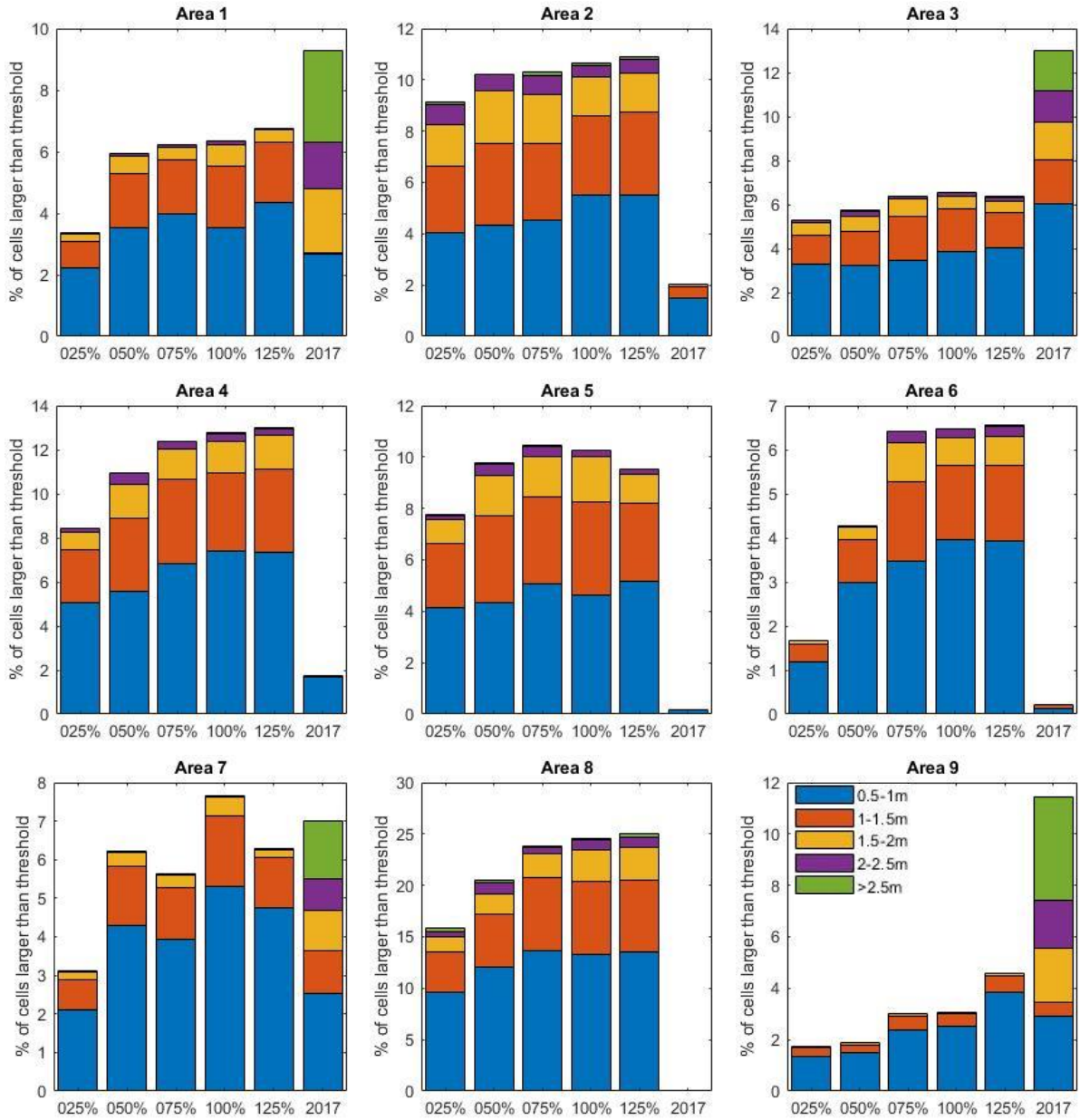
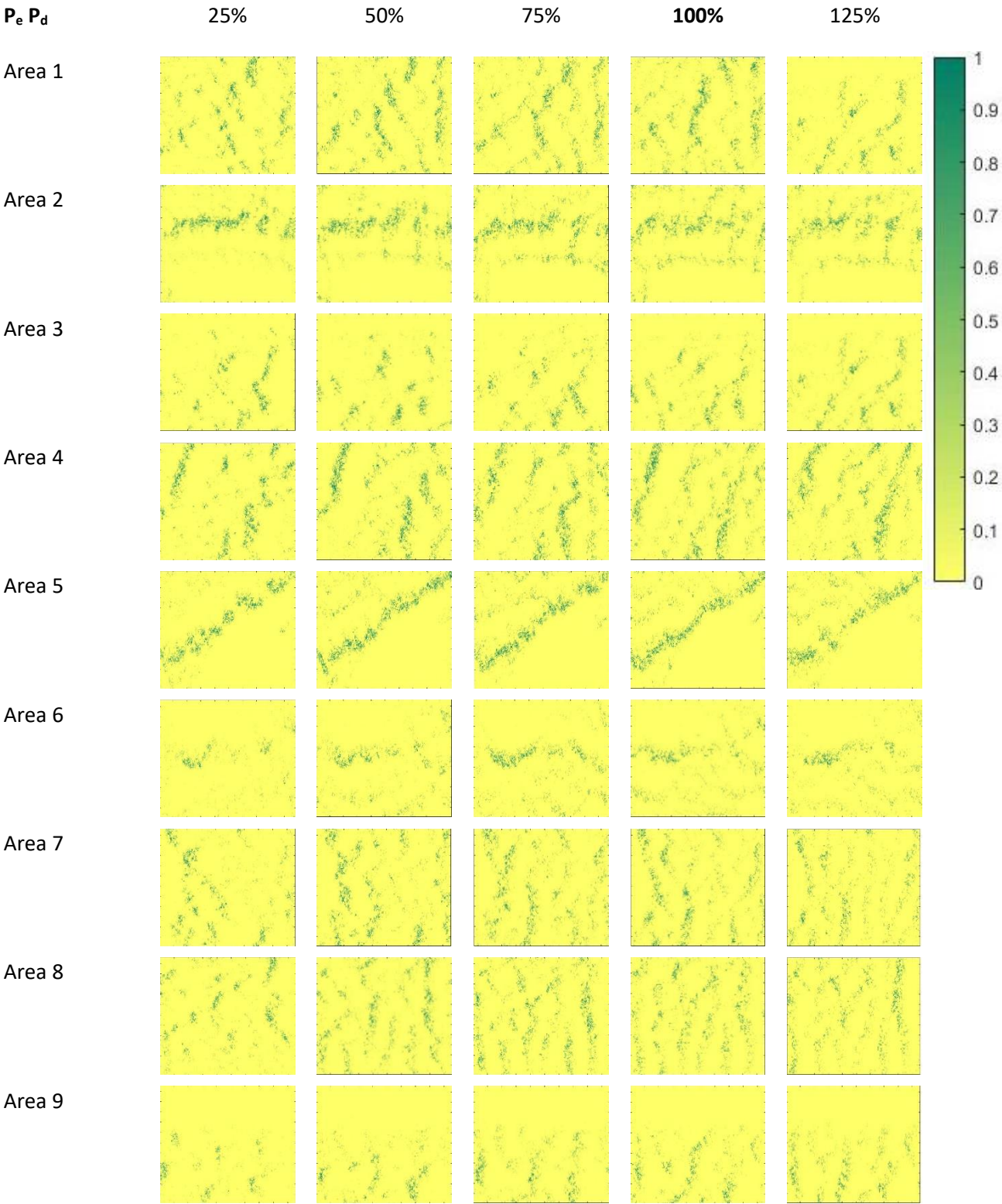
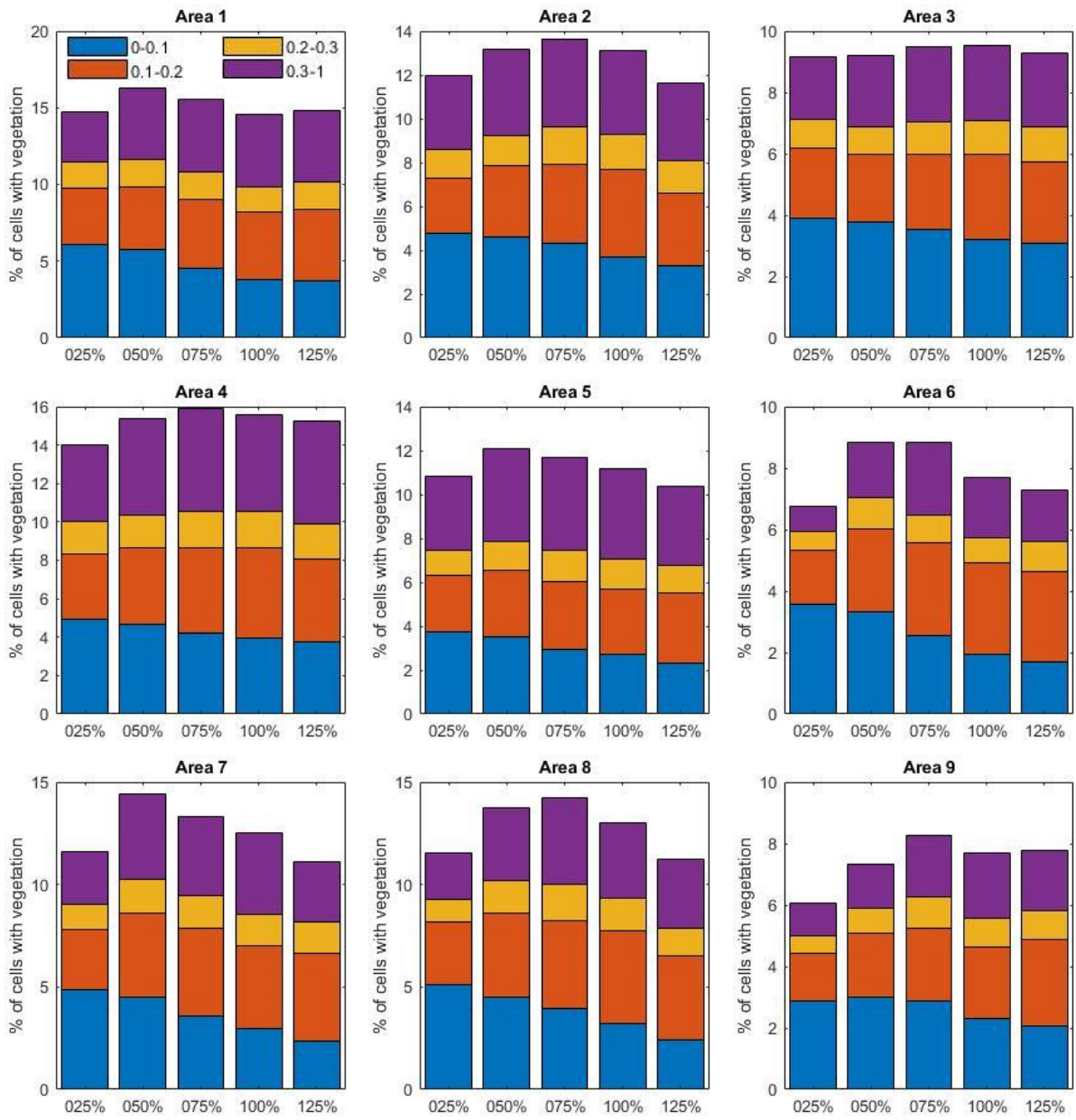


Figure 56

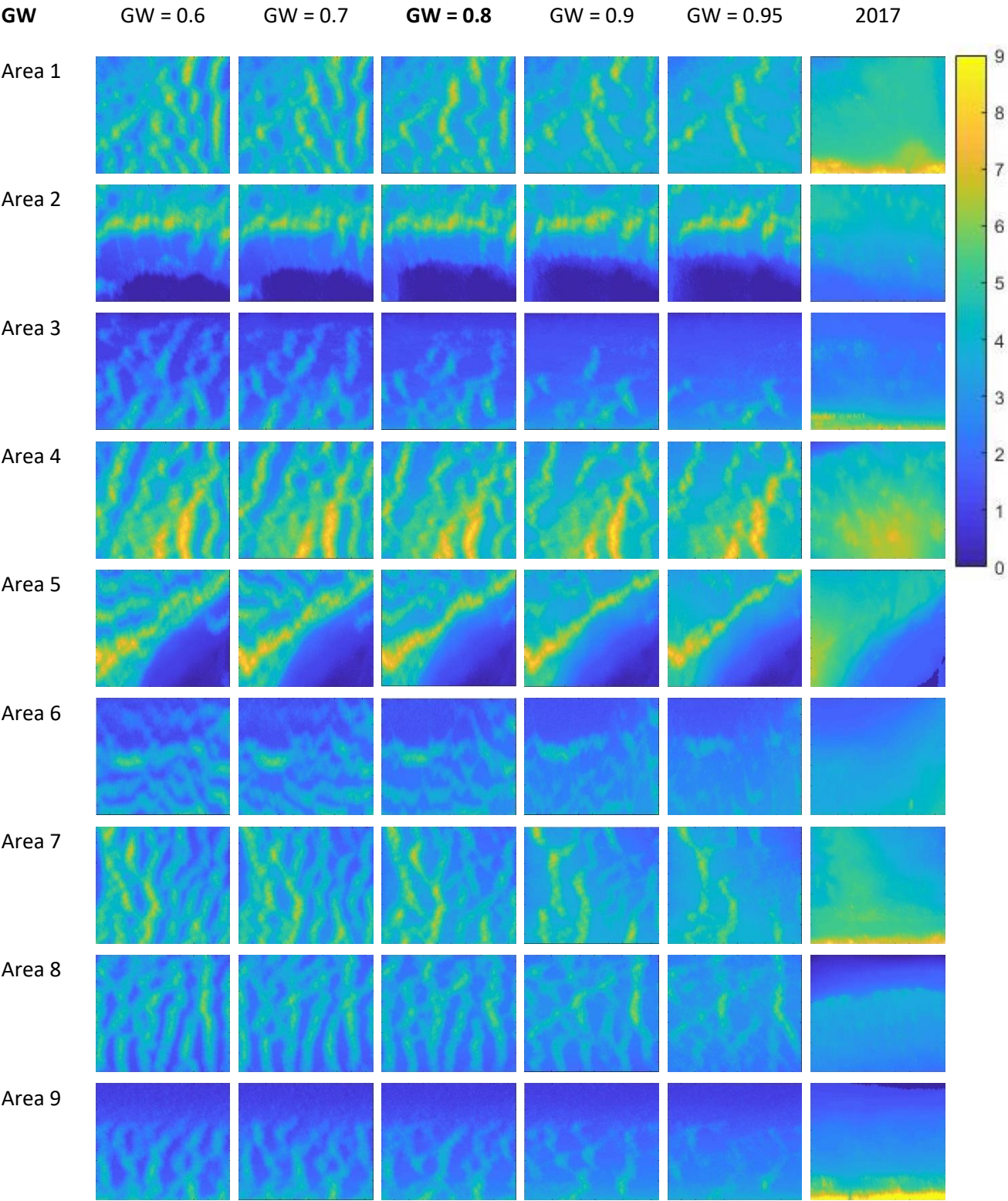


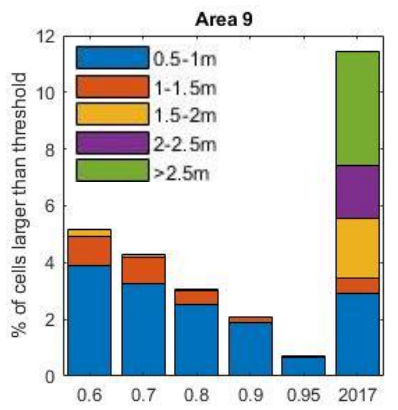
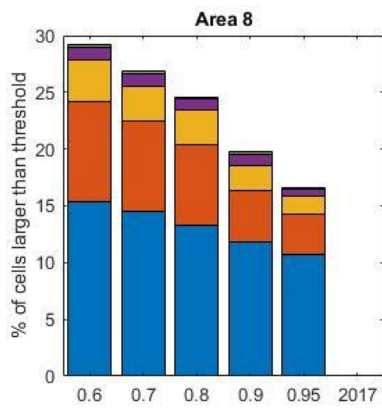
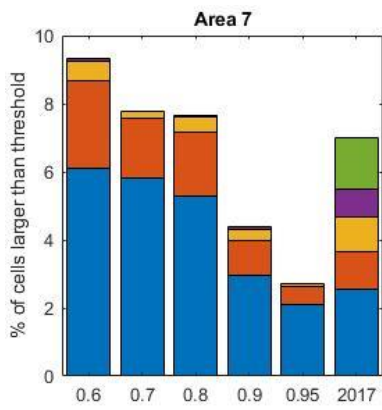
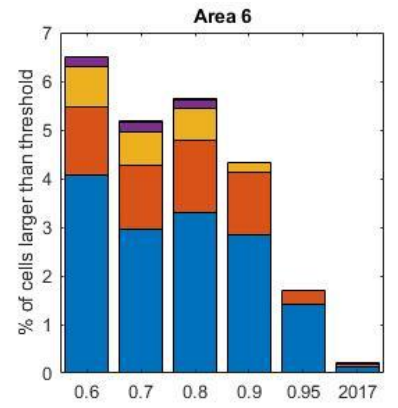
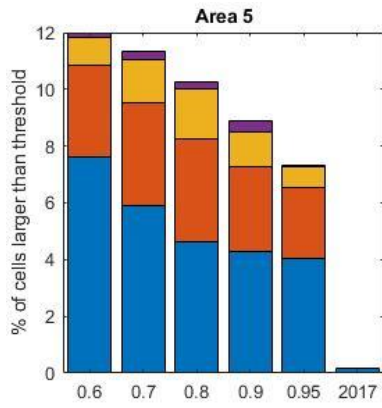
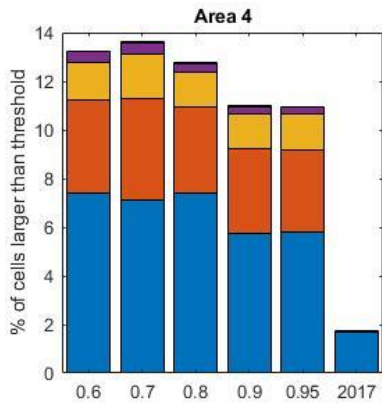
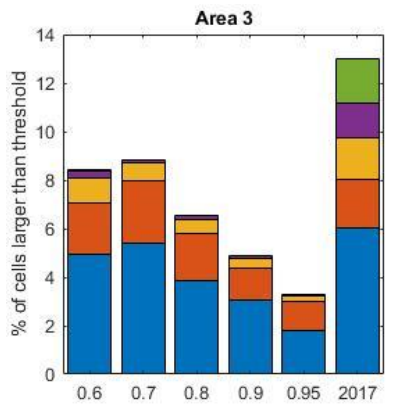
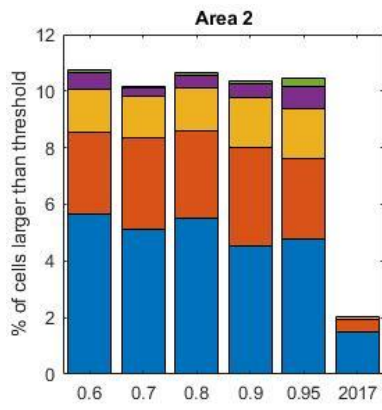
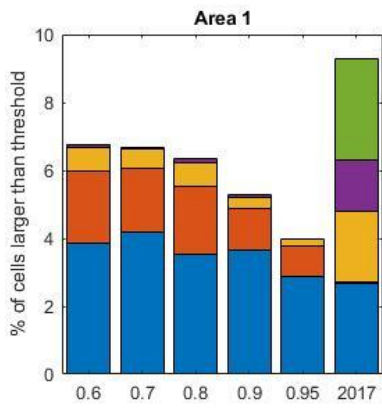
Appendix C: Vegetation plots and stacked bar plots of the adapted probability of erosion and deposition ($P_e P_d$)



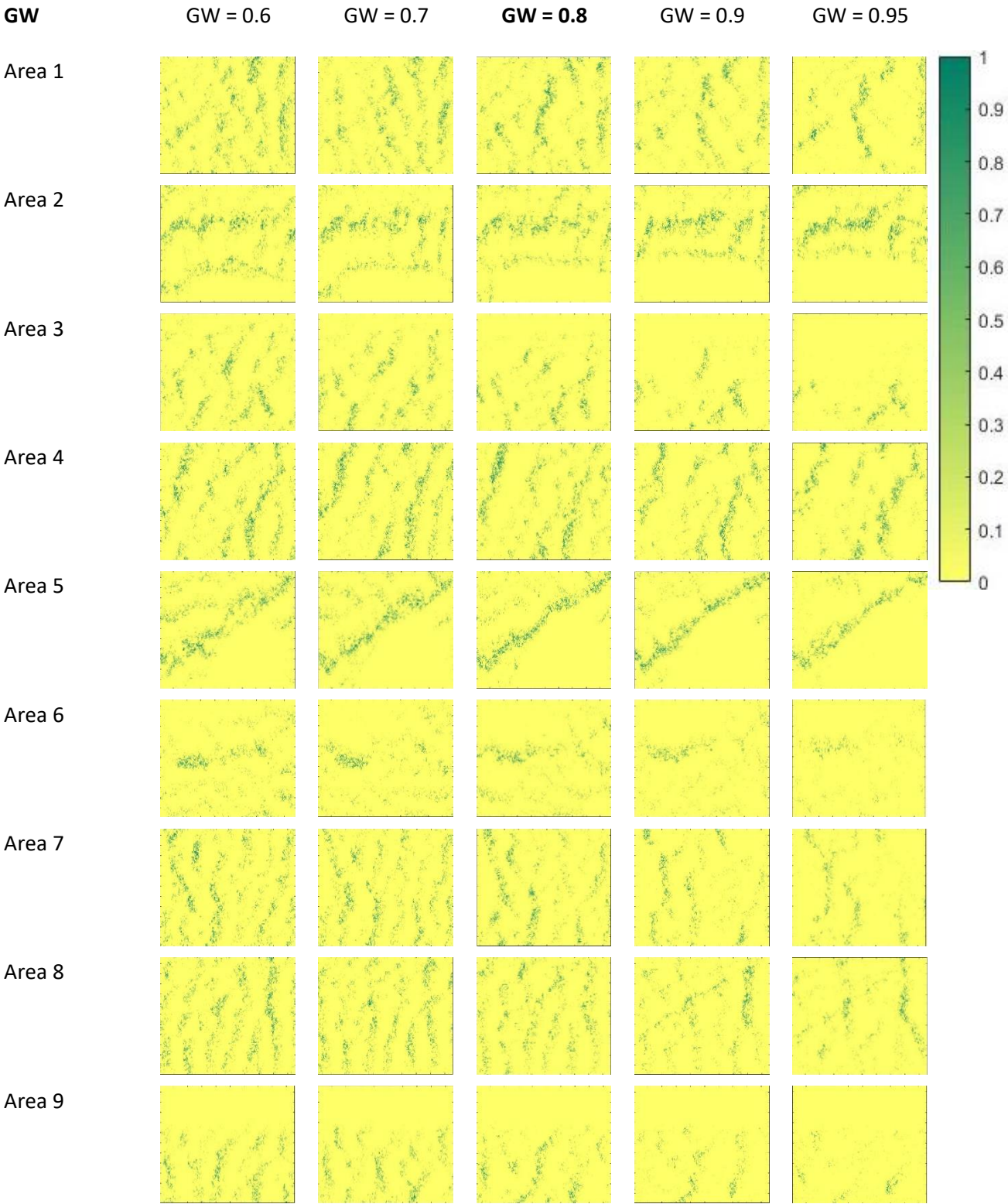


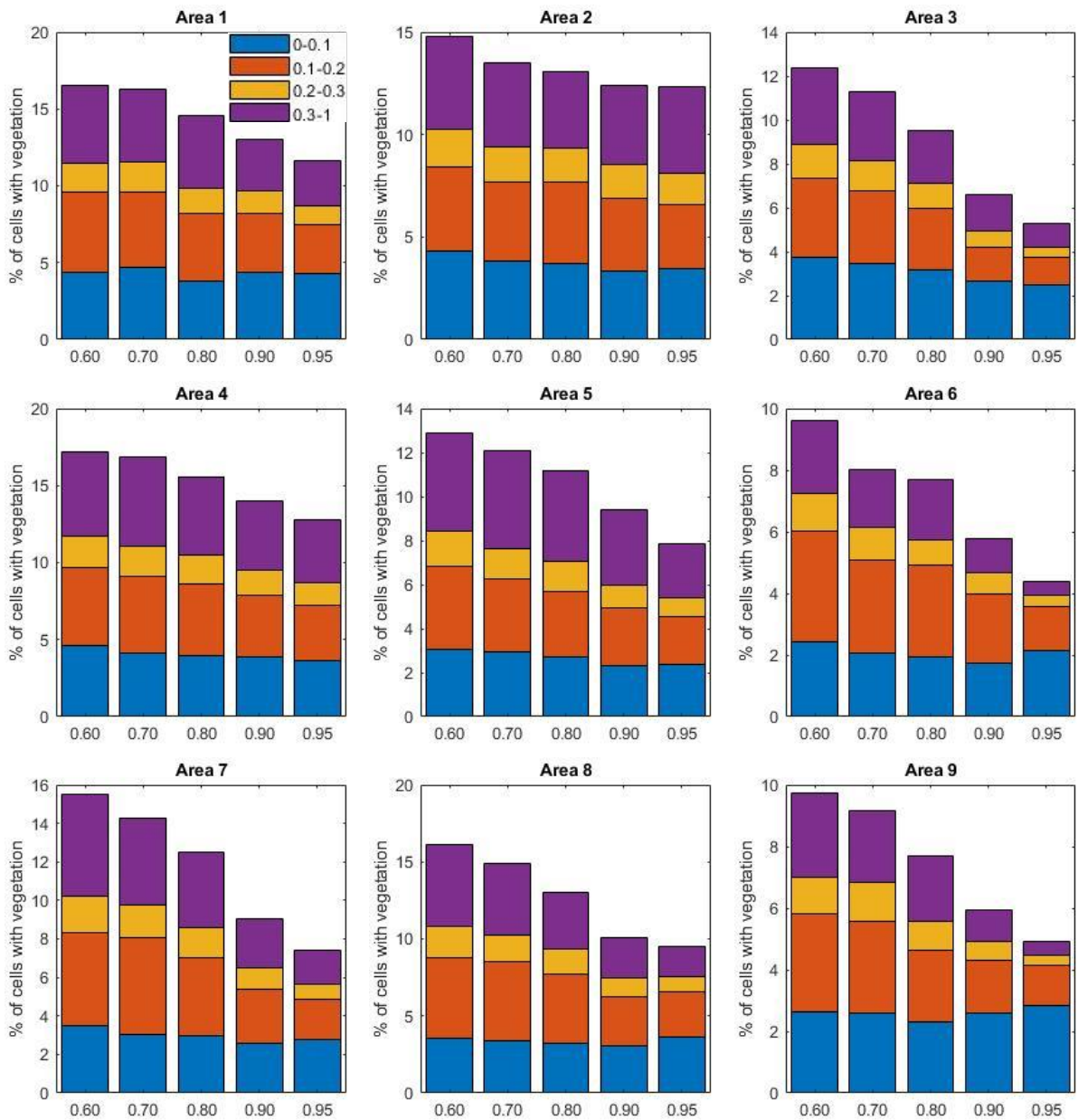
Appendix D: Elevation plots and stacked bar plots of the adapted groundwater level (GW)



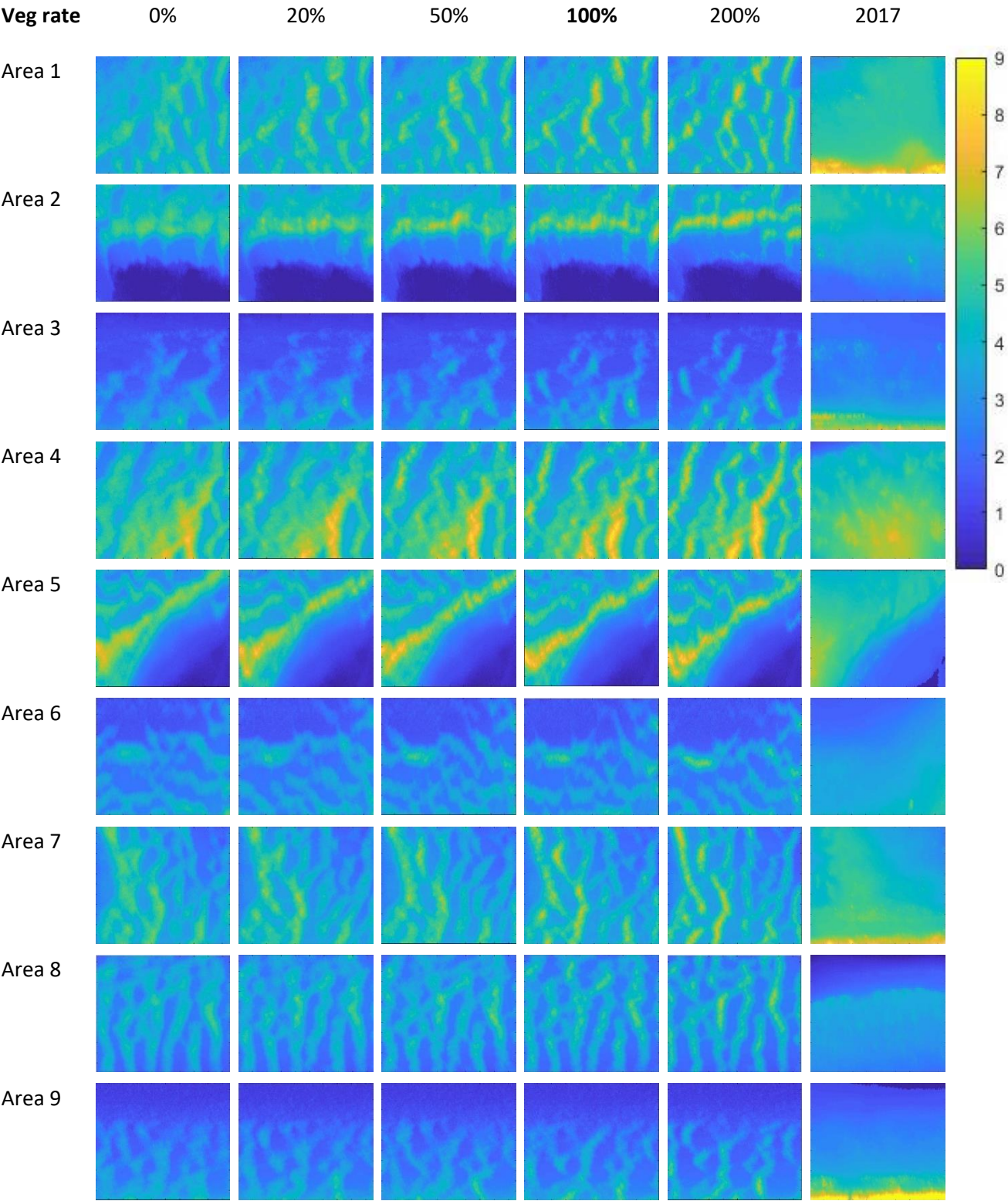


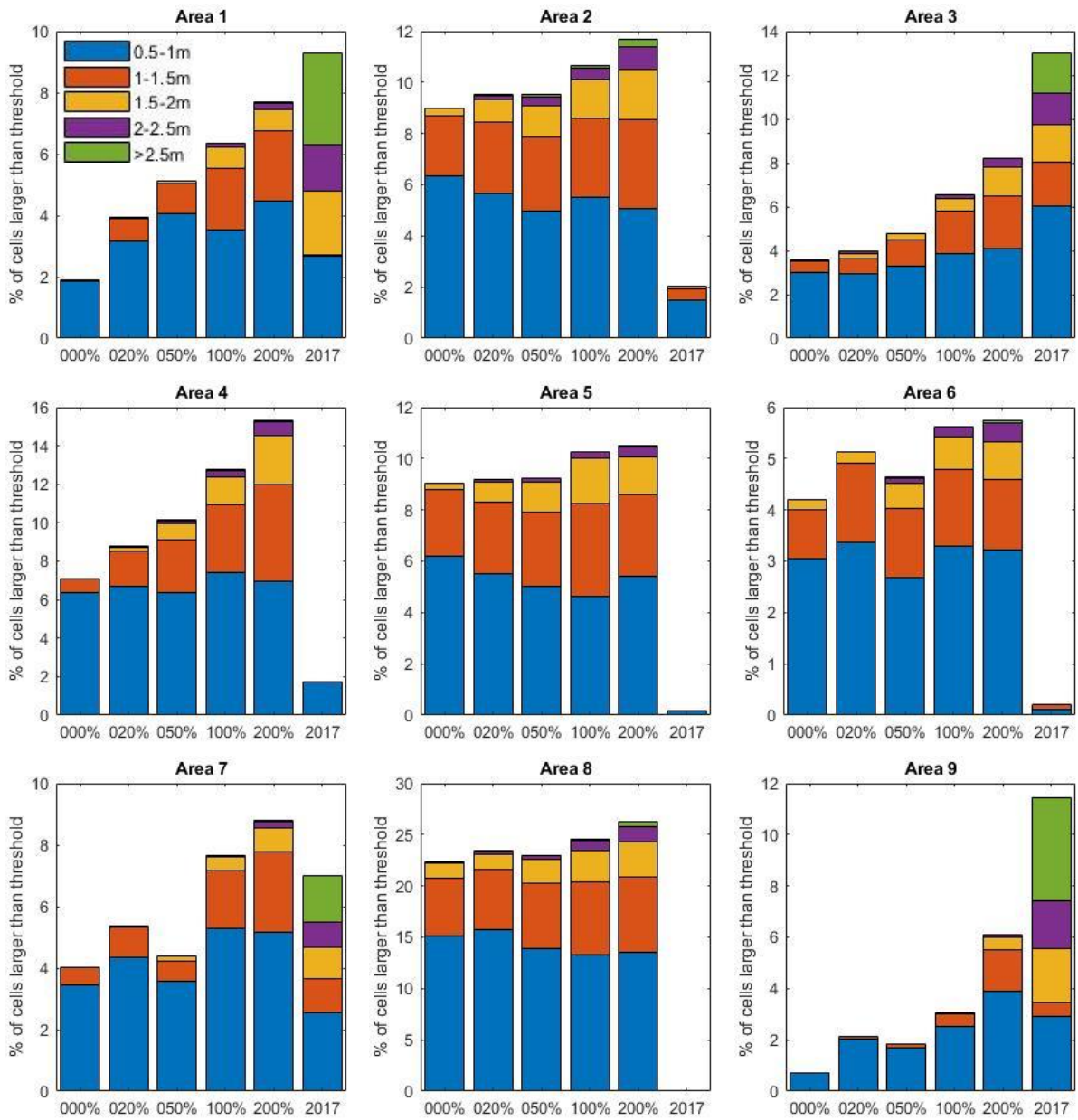
Appendix E: Vegetation plots and stacked bar plots of the adapted groundwater level (GW)





Appendix F: Elevation plots and stacked bar plots of the adapted vegetation expansion rates (Veg rate)





Appendix G: Vegetation plots and stacked bar plots of adapted vegetation expansion rates (Veg rate)

